NEURAL NETWORKS DURING JOINT PIANO PLAYING

Characterization of Hyperbrain Networks During Joint Piano Playing Using a Complex Dynamics Framework

By Hector D Orozco Perez, BSc

A Thesis Submitted to the School of Graduate Studies in Partial Fulfilment of the Requirements for the Degree Master of Science

McMaster University

Master of Science (2019)

Hamilton, Ontario (Department of Psychology, Neuroscience, and Behaviour)

TITLE: Characterization of Hyperbrain Networks During Joint Piano Playing Using a Complex Dynamics Framework

AUTHOR: Hector D Orozco Perez (McMaster University)

SUPERVISOR: Dr. Laurel Trainor

SUPERVISORY COMMITTEE: Dr. Jim Reilly, Dr. Ian Bruce, Dr. Louis Schmidt

NUMBER OF PAGES: 1, 113

Abstract

Social interaction is essential for human life, but we have little understanding of the neural mechanisms supporting it. Recent research has shown correlated activity between the brains of individuals (Goldstein et al. 2018; Müller et al. 2018; Dikker et al. 2017; Toppi et al. 2016) using the novel technique of Electroencephalography Hyperscanning, which allows us to record multiple persons' electrical brain activity at the same time. Interpretation of this data, however, is still unclear: does common activity reflect social interaction or is it just a by-product of shared perception? Furthermore, there is no unifying framework on how to analyze these novel data. Although we did not find evidence for synchronous brain activity between pianists playing duets using a complex dynamics framework, we were able to differentiate music pieces with ambiguous leadership roles from those with clear leadership roles using multivariate statistical approaches (graph theory). Furthermore, ambiguous leadership network characteristics correlated with participants' perceptions of the quality of their performances. This thesis also contributes to this field by expanding previously proposed frameworks (Duan et al. 2015) to include a complex dynamics approach and thoroughly discussing issues in hyperbrain analysis. By standardizing the protocols, interpretations, and data analysis approaches of data from EEG hyperscanning, we can better elucidate what this synchrony means, effectively helping us move the field of single-person social neuroscience towards a two person neuroscience (Dumas 2011; Schilbach et al. 2013). This has profound implications at several levels, including the quantification of high level social constructs, such as empathy or joint attention, to clinical research, where these statistics can be used as diagnosis tools for the socially impaired brain.

Acknowledgements

I moved to Hamilton in 2016 to start this degree. Now, two years and a half later, I find myself at a loss of words to describe how grateful I feel. To "Team A(&W)", thank you for always being there for me. For all the board games, the support, and the growth. To "The Staircase" and my troupe "You Got Males!", for without them my time in Hamilton would've been duller and boring-er. Thanks for the lessons, the love, the tummy-ache-inducing laughs. To Hamilton's queer community, thank you for making the rainbow shine during the gray days. To my supervisor, thank you for the mentoring, the guidance, and all the amazing support. To my labmates, thank you for creating such a welcoming and friendly environment from day 1. I want to thank my parents and siblings, too. Without your unconditional love and support (both emotional and financial), I would not have been able to engage in the projects that ultimately led me to transition from Academia to Industry. Los llevo en mi corazón donde quiera que vaya, siempre. I would not be the Hector I am today had it not been for the love, support, and influence I received from the people I met during my time in Hamilton. And for this, I will be forever grateful.

This work was made possible by the facilities of the Shared Hierarchical Academic Research Computing Network (SHARCNET) and Compute Canada. Finally, I would like to thank NSERC for the NSERC-CREATE in Complex Dynamics graduate fellowship I received from them.

Contents

List of Figures

List of Tables

Declaration of Authorship

I, Hector D Orozco Perez, declare that this thesis titled, "Characterization of Hyperbrain Networks During Joint Piano Playing Using a Complex Dynamics Framework" and the work presented in it are my own. I confirm that I designed the study, collected the data, analyzed the data and wrote this document with advice from my supervisor and supervisory committee.

"*How can a three-pound mass of jelly that you can hold in your palm imagine angels, contemplate the meaning of infinity, and even question its own place in the cosmos? Especially awe inspiring is the fact that any single brain, including yours, is made up of atoms that were forged in the hearts of countless, far-flung stars billions of years ago. These particles drifted for eons and light-years until gravity and change brought them together here, now. These atoms now form a conglomerate- your brain- that can not only ponder the very stars that gave it birth but can also think about its own ability to think and wonder about its own ability to wonder. With the arrival of humans, it has been said, the universe has suddenly become conscious of itself. This, truly, it the greatest mystery of all.*"

V.S. Ramachandran

Chapter 1

Introduction

Coordinated social interaction is essential for human life (Sänger et al. 2011; Dumas et al. 2014)). Whether helping a friend lift a heavy piece of furniture, jamming with colleagues on a Friday afternoon, or even engaging in a seemingly trivial conversation with your neighbor, our brains constantly integrate sensory information to meet the coordinative demands of our daily lives. Recently, there has been a surge of studies in which researchers scan two or more people at the same time (referred to as hyperscanning; Montague et al. 2002) to characterize hyperbrain networks, or networks with nodes shared between different brains (Tognoli et al. 2007; Hari and Kujala 2009; Babiloni and Astolfi 2014; Wang et al. 2018). These studies aim to move the field of neuroscience towards a *two person neuroscience*, under the premise that social cognition is different when interacting with others compared to being shown videos of others in an fMRI scanner (Dumas 2011; Schilbach et al. 2013; Dumas et al. 2014). Studying real interactions present particular challenges, such as reconciling ecological validity with tight experimental control, and the complexity of statistical models and analysis to determine connectivity in hyperbrain networks. Furthermore, whether inter-brain synchrony reflects functional similarity in common tasks (i.e., the similar task hypothesis) or if it reflects interpersonal interaction (i.e., the cooperative interaction hypothesis) is

still unclear (Liu et al. 2018; Hu et al. 2018). To address these fundamental methodological questions, we measured electroencephalography (EEG) in pianists playing duets together to characterize hyperbrain networks as indexed by brain oscillations using a complex dynamics framework (Dumas et al. 2014) that combines advanced signal decomposition techniques (Limpiti et al. 2006), information theory (Staniek and Lehnertz 2008), and graph theory (Bullmore and Sporns 2009).

Hyperscanning refers to the practice of performing multiple person electrophysiology and/or neuroimaging in order to understand how co-variations of neural activity (characterized as Hyperbrain networks) are influenced by the social interactions between the subjects (Montague et al. 2002; Mu et al. 2018). Duane and Behrendt (1965) were the first researchers to use this paradigm to study social interaction. Unfortunately, their area of interest was extrasensory communication between twins. EEG technology at the time had scarce spatial resolution, and the choices of statistical and data analysis of this report were suboptimal (Duane and Behrendt 1965). Following this, EEG hyperscanning was forgotten by the scientific community for many years. Recently, however, multiple person electrophysiology has seen a rise in popularity in fields such as social neuroscience and the study of brain oscillations (Babiloni and Astolfi 2014; Mu et al. 2018; Liu et al. 2018). Dumas et al. (2010) published one of the earliest reports using EEG hyperscanning to show interbrain synchrony in a social task. Participants either led or imitated each other through hand gestures. Hyperbrain networks formed between modelers and imitators at different frequency bands, suggesting functional purposes (i.e., possibly reflecting modulations related to leadership during the interaction) of these synchronies between brains (Dumas et al. 2010).

Two competing hypotheses try to explain these synchronies: the cooperative interaction hypothesis and the similar task hypothesis (Hu et al. 2018; Mu et al. 2018). The

cooperative interaction hypothesis posits that hyperbrain networks represent neural activity related to social interaction and are dependent on factors such as cooperation (Balconi et al. 2018), perceived human-to-human interactions (Hu et al. 2018), and the interplay of systems such as "self-other entrainment" and "co-representation" (Novembre et al. 2016). The similar task hypothesis (related to the "common input problem") posits that hyperbrain networks are just a by-product of similarity in tasks, perceptions, and sensorimotor activity as two people interact. To tease these two apart, several studies have used different ecologically valid settings, such as social games (Hu et al. 2018; Balconi et al. 2018), real-world interactions (Hirsch et al. 2017; Goldstein et al. 2018), and music ensembles (Novembre et al. 2016; Sänger et al. 2013; Babiloni et al. 2012). These situations require participants to be tightly coordinated with each other at different levels, from low-level sensorimotor coordination all the way to higher representations of the objective at hand (Sänger et al. 2011).

Interpersonal coordination occurs when individuals synchronize their attention, actions, and mental states with each other to engage in social activities that have a common objective (Ackerman and Bargh 2010). There are two broad types of interpersonal coordination: matching/mimicry and interactional synchrony (Mu et al. 2018; Dumas 2011). For the purposes of this thesis, we were mainly interested in interactional synchrony. Human social behaviour is assumed to have cyclical and rhythmic properties. Behavioural rhythms, like other physiological cycles—such as circadian rhythms and hormone cycles—have entrainment properties that allow them to synchronize with another "time giver" (i.e., a driver; for example, circadian rhythms entrain to the day-night cycle). In the case of social situations, this "time giver" can be another human. Interactional synchrony is thus defined as the degree of congruence between the behavioural cycles of two or more people (Bernieri and Rosenthal 1991).

Interactional synchrony requires the perception, representation, and anticipation of

one's own and the partners' actions (Sänger et al. 2011). To do this, the brain needs a mechanism that must meet three constraints (Sänger et al. 2011):

1. Be fast enough to permit the fluidity and precision of social interaction (Roelfsema et al. 1997)

2. Integrate and bind spatially distributed but functionally related neural information (Varela et al. 2001)

3. Support both perception and motor function (Sanes and Donoghue 1993)

As originally proposed by (Lindenberger et al. 2009), brain oscillations satisfy these constraints. Brain oscillations are fast and bind spatially distributed but functionally related information at the level of individual neurons, cell assemblies, and cortical areas (Ben-Ari 2001). Hyperbrain networks could reflect interactional synchrony and its neural substrates. Furthermore, most of the brain regions involved in this activity seem to derive from two broad systems: the Mirror Neuron System (MNS) and the Mentalizing System (MS) (Mu et al. 2018).

The Mirror Neuron System (MNS), along with the Mentalizing System (MS), seem to support human interactional synchrony (Wang et al. 2018). Most work suggests that both systems work in a complimentary and synchronous fashion within individuals (Van Overwalle and Baetens 2009), though some work suggests that the Mirror Neuron System might be subservient to the Mentalizing System (Frith and Frith 2006). The MNS includes neurons in the inferior frontal gyrus, inferior parietal lobule (which is related to language, motor and sensory detection), the superior temporal gyrus (which can provide additional visual information inputs as well as being an auditory processing hub), the intraparietal and superior temporal sulcus, and premotor cortex (Rizzolatti and Craighero 2004; Iacoboni and Dapretto 2006). It is associated with sensing other people's goals based on low-level behavioural input (limited to familiar executed actions; Iacoboni

et al. 1999; Van Overwalle and Baetens 2009). Newman and Girvan (2004) expanded the traditional conception of the MNS by proposing that it not only serves to mimic other's actions, but rather, at least two thirds of these neurons respond when performing contextualized complimentary actions. Furthermore, Molenberghs et al. (2012) propose that the MNS goes beyond the cerebral regions usually attributed to it and may even include areas recruited during auditory, somatosensory, and affective tasks.

While the MNS serves a role in the preparation of one's own actions and simulating other's actions, the MS involves the anticipation of other's intentions and the ability to infer other's mental states (Sperduti et al. 2014; Frith and Frith 2006). The temporo-parietal junction (TPJ) and the medial prefrontal cortex (mPFC) work together to form the mentalizing system (Van Overwalle 2011; Saxe 2006). The TPJ is associated with short-time estimates of intentions, desires, and goals related to other people (Van Overwalle and Baetens 2009). The medial prefrontal cortex makes critical contributions to the neural basis of mentalizing and the social self (Babiloni et al. 2007; Schilbach et al. 2010; Funane et al. 2011; Amodio and Frith 2006), as well as to cooperation (Decety et al. 2004). Indeed, in the context of hyperscanning, several fMRI and fNIRS (imaging modalities with superior spatial resolution) studies have revealed interbrain synchrony at the right inferior frontal gyrus (Saito et al. 2010; Koike et al. 2016; Cheng et al. 2015) and the temporo-parietal junction (Bilek et al. 2015; Tang et al. 2015; Dai et al. 2018). However, compared to fMRI and fNIRS, hyperscanning EEG methods offer both a superior temporal resolution (in the order of milliseconds) and portability that could further the characterization of these hyperbrain networks in more naturalistic environments (Mu et al. 2018).

EEG is one of the most powerful techniques to explore neural oscillations in a non-invasive manner (Cohen 2017). Its sub-millisecond temporal resolution and portability

allow us to study social interactions in natural scenarios, reconciling ecological validity with experimental control (Cohen 2014; Wang et al. 2018). Dikker et al. (2017) recorded students' EEG during normal classes and determined that brain-to-brain synchrony predicts both student engagement and social dynamics. The authors interpret brain-to-brain synchrony as shared attention that modulates synchrony by "tuning" neural oscillations to the temporal structure ("rhythm") of the incoming perceptual stream. They emphasize that brain-to-brain synchrony is not a mechanism in itself, but rather, a way to operationalize the underlying neural computations that support the psychological processes under investigation.

Goldstein et al. (2018) measured hyperscanning EEG in heterosexual romantic couples during pain administration to the female partner. They found that social touch during pain conditions increased brain-to-brain coupling in hyperbrain networks at alpha-mu frequencies. These networks showed associations between the central regions of the pain receiver and the right hemisphere of the pain observer. Furthermore, clusters in these networks (as indexed by a hierarchical clustering analysis) correlated with both the pain alleviation effect (i.e., analgesia magnitude) and the observer's empathy accuracy.

Toppi et al. (2016) recruited civil pilots and measured their simultaneous EEG's during a simulated flight, where they introduced artificial "malfunctions" to manipulate hierarchical roles (Captain vs. First Officer). They showed that brain-to-brain connectivity differentiated phases of the flight (e.g., denser patterns of interbrain connectivity at both alpha and theta during landing after an artificially introduced electrical malfunction) and these connections highlighted the role of different cortical areas involved in cooperative behaviour (mostly parietal-central-frontal areas). Most importantly, this paper highlights how hyperscanning methodologies are superior to single-brain analyses, which failed to differentiate flight phases and levels of interaction.

Of particular interest to us is the study of music ensembles as a model of human

interaction (D'Ausilio et al. 2015). Building on previous studies (Lindenberger et al. 2009; Sänger et al. 2013), we propose to study interactional synchrony in piano duos. Music has distinct features that make it a promising avenue for social cognition research, such as ecological validity (it serves a very explicit social function by conveying group and individual emotions), generalizability (musicality is a wide-spread human capacity), and a formal description of the interaction (the music score resembles a script; Merriam and Merriam 1964; Hargreaves and North 1999; D'Ausilio et al. 2015). Previous work (Lindenberger et al. 2009; Sänger et al. 2011; Sänger et al. 2013; Müller et al. 2018) has determined that, indeed, it is possible to use music ensembles to study the neural substrates of interpersonal action coordination.

Precursors to our work have used EEG and fNIRS hyperscanning to study saxophone quartets, dyads engaged in joint singing, and guitar ensembles (from duos to quartets). Babiloni and Astolfi (2014) found that alpha desynchronization in the right inferior prefrontal gyrus (as indexed by an sLORETA solution) correlated with musicians' empathy quotient test scores only in conditions in which the quartet observed a video of themselves playing music (as opposed to a resting condition, a playing condition, and a control condition). This results suggest that alpha rhythms in these regions reflect "emotional" empathy in musicians observing their own performance. They did not, however, try to characterize hyperbrain networks. Osaka et al. (2015) used fNIRS hyperscanning to investigate cooperative singing and humming. The left inferior frontal cortices of the singing dyads synchronized more for both singing and humming compared to both singing alone and scrambled pairs. The right inferior frontal cortex also synchronized between dyads in humming conditions, possibly due to more dependence on musical processing in the absence of words. Lindenberger et al. (2009), Sänger et al. (2011), Sänger et al. (2013), and Müller et al. (2018) found synchronicities between guitarists' EEG recordings in terms of phase couplings. Furthermore, they found hyperbrain networks between the brains of guitar players with small-world properties——an

optimal architecture for information processing where the nodes of a network are both functionally integrated but segregated. In their most recent article (Müller et al. 2018), they used EEG hyperscanning to characterize hyperbrain networks in a guitar quartet. Using an adaptive phase locking index paired with a sliding window procedure, they showed that interactions between brains are characterized by dynamic changes, such that strength statistics and modular structures are non-stationary and change as a function of frequency and time, reflecting the musical situation and other interactional synchrony requirements.

These experiments, however, had a number of shortcomings. The guitar ensembles studies focused on theta and delta frequency bands (which are known to be prone to spurious connectivity, specially when measured by phase-based statistics Lindenberger et al. 2009; Burgess 2013), rather than mu and alpha frequency bands, which have been traditionally associated with activity from the mirror neuron system (Bernier et al. 2007; Tognoli et al. 2007; Ahn et al. 2018; Astolfi et al. 2011); the lack of non-linear cross-frequency analysis; the lack of correlation between specific observed behaviours and the EEG activity (as suggested by Babiloni and Astolfi 2014); and the lack of systematic manipulation of music pieces with different roles and motor demands for each participant. In sum, none of the studies present a thorough characterization of hyperbrain networks combining source modeling with non-linear multivariate statistics, a systematic manipulation of music pieces, self-reports, and proper statistical control (both a baseline and a shuffled participant analysis). The paradigm we employed aims to both replicate these findings and extend them by addressing most of these shortcomings.

As a cautionary note, we are not suggesting that the existence of significant correlations or covariances between different brain oscillations means a physical "communication channel" between multiple brains. As Dikker et al. (2017) emphasizes, we propose that this synchrony is not a mechanism itself, but rather an indication of an indirect chain of

events that starts from a particular cerebral region of one person and ends in the cerebral processes elicited in the brain of a second person. Such indirect relationships may be mediated by behaviour, perception, and internal predictive models. The computational links we are investigating in the EEG brain oscillations are a form of spatio-temporal map of the multiple cerebral regions involved in joint music playing and, more generally, interactional synchrony (Babiloni and Astolfi 2014).

Using brain oscillations as a neural marker of interactional synchrony has its caveats. Notably, finding synchronous EEG activity across brains could be due to the similarity in the perception stream impacting both brains (i.e., the similar task hypothesis). To get around this, we propose a complex dynamics framework paired up with a leader-follower manipulation to study hyperbrain networks (Sporns 2011; Wibral et al. 2014). Complex dynamics science investigates entities (in this case, brain regions) where the global system behaviour (i.e., interactional synchrony) is a non-trivial (i.e., non-linear) result of interactions between local agents (i.e., cortical areas; Lizier n.d.; Duan et al. 2015). Specifically, we use permutation-based information theory statistics (Staniek and Lehnertz 2008). These statistics offer several advantages, such as being model-free, handling stochastic dynamics quite well, and capturing non-linear relationships (Lizier n.d.).

We decided to use two types of piano duos: homophonic and polyphonic duos. In homophonic duos, there is a clear melody (Piano I) and accompaniment (Piano II), thus ecologically introducing a leadership situation without verbal instruction. On the other hand, polyphonic duos are pieces where there is no clear melody and accompaniment, or there are multiple melodies—such as in a Canon or a Fugue. These two manipulations allow us to compare two different contexts: *leadership* and *no leadership*. By manipulating this variable, we can start to make inferences about how the direction of information flow is influenced by context.

We modelled the pianists' brains as dynamical, non-linear systems (Boker 1996), where each agent of the system (in this case, macro-cortical regions) simultaneously stores, transfers, and modifies information in variable amounts (Wibral et al. 2014; Ciaramidaro et al. 2018). For the purposes of this thesis, we focused on the description of information flow between these cortical areas. Information in this sense refers to a draw at a given time point from a stochastic system (Shannon 1948). We did this modeling in a three stage process:

1. We decomposed the scalp EEG into 12 macro-cortical regions of interest using a novel cortical patch model paired with a linearly constrained minimum variance beamformer inverse solution (Limpiti et al. 2006). See Section 2.7.1 for details.

2. We determined effective connectivity (i.e., information flow) between these cortical regions using Symbolic Transfer Entropy (at all possible traditional frequency band interactions between theta, delta, alpha, beta, and gamma; Staniek and Lehnertz 2008). Effective connectivity describes the set of causal effects of one system over another one (Garofalo et al. 2009). In this context, causality is defined as Wiener's "observational causality principle", where process X is causal to process Y if Y is better predicted by incorporating past information of X than by using only past information of Y (Wiener 2013).

3. We determined the hyperbrain networks' characteristics using graph theory statistics (Bullmore and Sporns 2009).

4. We used appropriate control conditions for statistical testing (both baseline and scrambled pairs as suggested by Mu et al. 2018).

We used this framework to answer the question: "is information transfer between cortical areas, as indexed by brain oscillations, related to interactional synchrony? Or, is it just a by-product of shared perception and similarity of movements?". We hypothesized

that information would flow between participants' frontal, temporal, and parietal areas specially at alpha/mu frequencies (Tognoli et al. 2007; Lindenberger et al. 2009; Sänger et al. 2013; Wang et al. 2018). We also hypothesized that information would flow more from leaders to followers than vice versa, especially during homophonic duets (Toppi et al. 2016). Ultimately, we hypothesized that hyperbrain networks are not just a by-product of shared perception and similarity in movements, but rather a correlate of interactional synchrony while musicians play piano duets.

Chapter 2

Methods

We aimed to characterize hyperbrain networks while pianists play together using advanced signal processing techniques, information theory, and graph theory.

2.1 Ethics

The experimental procedures conformed to the World Medical Association's Declaration of Helsinki and were approved by the McMaster Research Ethics Board. All participants gave their informed consent by signing a form and each of them received a $100.00 honorarium.

2.2 Participants

Twelve classical pianists (six female, mean age 24.8±5.6) participated in the experiment after providing written informed consent. Participants had had on average 13.7±2.5 years of formal piano training and 7.6±4.7 years of music ensemble training (as accompanists, playing chamber music, etc.). Exclusion criteria by self-report included neurological damage or abnormalities, hearing loss, and left-handedness. Participants

were recruited from music programs in several different institutions by both email and word-of-mouth.

2.3 Stimuli

We chose the piano pieces based on four criteria:

1. Music style (all were classical in the popular sense with written musical scores)
2. That they were clearly either polyphonic (no dominant melody nor accompaniment) or homophonic (embedded social roles—leader follower; clear melody and accompaniment dynamic)
3. That they were explicitly written for 2 pianos (a duo) and not a transcription
4. That they contained a salient moment (which we dubbed a synch point) in which synchronization between the pianists could be particularly difficult (e.g., fermata or ritardando/accelerando).

From these pieces, we chose 40s excerpts in which either the polyphonic or the homophonic characteristics were evident (either one piano lead the other or no clear leader at all). In 2 cases (see Table 2.1), synch points were not explicit in the score, and were added with the aid of a professional pianist (Erika Reiman, PhD).

We began with a pool of 15 pieces, ranging in styles (from Baroque to Romantic). From this pool, and with the aid of a professional pianist (Erika Reiman, PhD) we chose four pieces (see Table 2.1 and Appendix B). Most of these pieces were written in the late romantic, early impressionist style. These pieces most clearly met the criteria listed

above; and this specific music style is associated with increased expressiveness and emotion in the music (Beard and Gloag 2004), reflected as expressive tempo markings that required the participants to listen to each other in order to be synchronized throughout.

Table 2.1: Music Pieces

Duo Type	**Pieces**	**Tempo**	**Bars**
Polyphonic	Kanon, from Sonata for 2 Pianos (3rd Movement Kanon, Hindemith)	Slow	Bars 21-32 (added fermata at bar 26)
Polyphonic	Entre Cloches, from Sites Auriculaires (Ravel)	Allégrement	Bars 1-14
Homophonic	Caprice Mélancolique (Hahn)	Andantino Poétique	Bars 1-30 (Added a rit. at bar 9, added tonic at bar 30)
Homophonic	Valse from Suite No 1 Op. 15 (Arensky)	Allegro	Bars 1-49

2.4 Music duo pairings

We paired the pianists ahead of time based on five factors: age, years of piano experience, if they had conservatory education or not, if they currently worked as professional pianists or not, and if they were currently playing in an ensemble (Sänger et al. 2013; see Table 2.2). Pianists in a same duet had never played music together and had never met each other before (except in one duet, in which pianists reported knowing each other but having neutral feelings for each other).

Table 2.2: Duo pairings

	Age		**Music Training**		**Ensemble Training**		**Cons Education**		**Prof. musician**		**Ensemble**	
1	23	20	15	12	10	8	Y	Y	N	Y	Y	N
2	29	32	10	10	7	5	Y	Y	N	N	N	N
3	20	18	10	15	6	4	Y	Y	N	N	Y	Y
4	21	24	15	15	4	8	Y	Y	Y	N	N	N
5	38	28	15	15	20	13	Y	Y	N	Y	N	N
6	21	23	14	18	4	2	Y	Y	Y	Y	Y	N
Diff	**3.8±2.8**		**2±2.1**		**3.2±1.9**		**6/6**		**3/6**		**4/6**	

2.5 Experimental procedure

We used a leader follower manipulation with one experimental factor (duo type: homophonic or polyphonic). We first contacted participants through email so they could answer a screening questionnaire inquiring about the exclusion criteria (Appendix A). We paired them up in advance using the criteria mentioned in the last section.

The experiment took place in the LIVELab, a unique 106-seat Research Performance Hall designed to investigate the experience of music, dance, multimedia presentations, and human interaction (McMaster University, Hamilton, Ontario, Canada). Four to six weeks before their scheduled appointment, each participant was sent sheet music for the four excerpts (see Appendix B and Section 2.3) and they were asked to familiarize themselves with both parts of the duets (Piano I and Piano II). They were asked to have a good night sleep before they came in (to minimize artifactual alpha activity) and to bring in their glasses instead of their contacts (to minimize blinking artifact in the EEG signal).

On the scheduled day, participants came in and were introduced to each other. From that moment on, we explicitly forbid them to communicate verbally with each other. We measured their heads to choose an appropriate EEG cap size, and then digitized each

participants' electrode positions (Polhemus Fastrak) prior to data recording. After that, participants were taken to the main stage in the LIVELab (see Appendix D for diagram of the setup), where they filled out a number of questionnaires (see below; importantly, they filled out the "Music Affiliation Questionnaire", Appendix C, before and after the experiment) while we applied conductive gel to the electrodes in the cap. After this, a 3 minute baseline was recorded in which participants sat still at the piano, and then the participants underwent four experimental blocks, one per excerpt. The order of blocks (excerpts) was pseudorandomized across participants. Participants played the Piano 1 and Piano 2 parts of each excerpt on different trials, and the order of leadership assignment was always counterbalanced within each piano dyad.

To determine the pseudorandomized orders of excerpts across participants, we first calculated all possible permutation of the four excerpts (total of 24). Then, we randomized them using Python's *random()* function. One experimental block consisted of one "dummy" trial (a "warm-up") followed by four trials: one participant played the Piano I part for two trials, and then they switched parts for the last two trials. Thus, each piece was performed 1 + 4 times in total. After each performance, participants filled out the "Perception of Music Performance Questionnaire" (adapted from Pesquita et al. 2014; Appendix E).

When all trials were done, participants were paid a $100.00 honorarium and were debriefed that the purpose of the experiment was to examine how they interacted. On their way out, they filled out for a second time the "Music Affiliation Questionnaire" (Appendix C) and then answered two short questions: (1) What do you think the purpose of this study was? (2) When doing it, did you have any thoughts as to why we were asking certain things?

2.6 Data Acquisition

2.6.1 Personality questionnaires

Psychometric questionnaires were delivered as online surveys using Google Forms. Participants filled out 6 online questionnaires using Google Forms. Before the experiment, they filled out:

1. Demographic and general music abilities questionnaire (Appendix F)
2. Goldsmiths Musical Sophistication Index (Müllensiefen et al. 2014)
3. Ten-Item Personality Inventory (Gosling et al. 2003)
4. Interpersonal Reactivity Index (Davis et al. 1980)
5. Music Affiliation Questionnaire (MAQ) (Appendix C)

At the end of the experiment, the participants filled out the MAQ a second time. Questionnaire responses were downloaded from Google Forms as a csv and imported to Python for further processing.

2.6.2 EEG

We recorded EEG at 2048 Hz using 64 active sintered Ag/AgCl ring wet electrodes (g.SCARABEO; g.tec medical engineering GmbH, Austria) placed on a g.GAMMAcap2 based on the international 10-10 system. Impedances were kept bellow 10kΩ. Two g.HIamp biosignal amplifiers were used for data recording. Recordings were made with 24-bit precision, relying on oversampling to reduce noise by averaging samples. Data were recorded using the g.Recorder software, referenced to the average of both earlobes and with the ground at Cz, and stored for offline analysis.

2.6.3 MIDI

We recorded MIDI files of all performances by interfacing two FP-80 Roland Digital Pianos (Roland Corporation, Japan) with a USB audio interface (Scarlett Focusrite, Focusrite plc, England) using a Digital Audio Workstation (Reaper, Cockos Incorporated, USA).

2.6.4 Video

We recorded the performances using a SONY PXW-X70 XDCAM camcorder. Display resolution of the camera is 1920x1080 and the resolution of the videos is 1920x1090. Videos were recorded at a frame rate of 59.940059 frames per second using the H264-MPEG-4 AVC codec (part 10) (h264).

2.6.5 Trigger latency and data Synchronization

EEG, MIDI, and video data were synchronized using an in-house device consisting of an Arduino board interfaced with 2 female DB25, a BNC connector, and a female 6.35mm TRS (see Fig. 2.1 for the basic circuit diagram; find all the details here: https://github.com/neurohazardous/hyperSynch). A button was connected to the Arduino board through BNC. When pressed, three 50ms TTL pulses (with 500ms between them) were sent through the female parallel ports to each g.HIamp (through parallel ports) and to both an audio interface and the video camera (through a split TRS connector).

Using an Oscilloscope, we concluded that the latency of the triggers between both EEG systems was 5μs and the latency between the EEG systems and the video/MIDI

recording was of 10μs. These latencies are negligible as the EEG system samples every half millisecond (2048 Hz).

To align the data, we visually inspected the MIDI recordings and determined when, and for how long, participants played together with respect to the onset of the third pulse. We quantified this time and trimmed the data around this window.

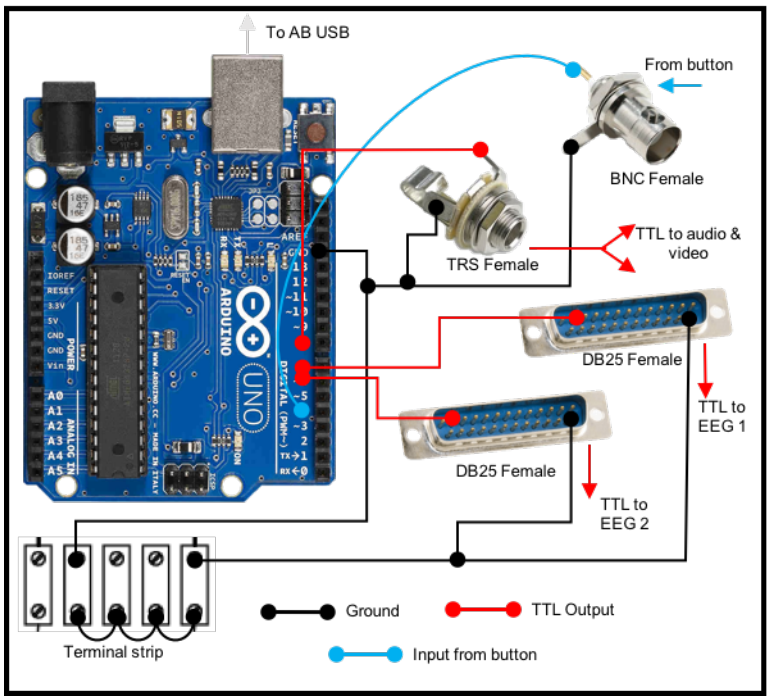

Figure 2.1: Diagram of in-house device used to synchronize EEG data with both video and MIDI.

2.7 Data Analysis

For the purposes of the this thesis, we only analyzed and processed EEG data, and data from the MAQ and the PMPQ.

2.7.1 EEG Data: Preprocessing

Data were preprocessed in MATLAB using a combination of EEGLAB (Delorme and Makeig 2004), FieldTrip (Oostenveld et al. 2011), and in-house developed scripts. The preprocessing consisted of three grand steps: artifact correction and preprocessing, template-electrode alignment, and source decomposition. We first imported data (20 trials + baseline per experimental subject) to EEGLAB (*pop_loadhdf5()* plugin), high pass filtered it at 0.5Hz using a zero-phase hamming window FIR filter (*pop_eegfiltnew()*), loaded channel's information and digital locations (*pop_chanedit()*), trimmed data starting at piano play onset plus three seconds both at the beginning and at the end of the playing time period (adding 3s padding takes care of filter and Hilbert Transform artifacts), and used two of EEGLAB's plugins to correct artifacts: *CleanLine()* and *clean_rawdata()*. *CleanLine()* takes out line noise in the signal by running a spectral regression of a 60 Hz sinusoid (of unknown phase and amplitude) and then subtracts it from the data (Bigdely-Shamlo et al. 2015). Because we wanted to keep the experimental conditions as ecologically valid as possible, participants were able to move as much as they wanted. To prune the data from high variance artifacts (e.g., motion artifacts, eye-movement) we used EEGLAB's *clean_rawdata()* function, which runs an electrode rejection algorithm and Artifact Subspace Reconstruction (Mullen et al. 2013). First, we rejected (1) electrodes that had a correlation of 0.75 or less with their neighbouring electrodes, (2) electrodes with activity that was at least 8 standard deviations away from the other electrodes, and (3) electrodes that saturated (i.e., flat lined) for more than 5 seconds. Then, Artifact Subspace Reconstruction extracted clean data from the recording, got calibration statistics, and used a sliding window Principal Component Analysis to reject high variance components. After this, we ran a spherical interpolation (*pop_interp()*), and re-referenced to common average (*fullRankAveRef()*).

The remaining two steps (template-electrode alignment and source decomposition)

were run in FieldTrip combined with in-house scripts. Because we did not have individual MRI T1w scans, we decided to use the ICBM152 template. Specifically, we used the symmetric, 0.5mm resolution template, which represents an unbiased non-linear average of the MNI152 database that combines the features of both high-spatial resolution and signal-to-noise while not being subject to variations in individual brains (Fonov et al. 2011). In addition, the ICBM152 is one of the most common templates used: FSL—a comprehensive library of analysis tools for fMRI, MRI and DTI brain imaging data—comes with a large set of atlases, all geared towards the ICBM152. We started by reading off the MRI template (*ft_read_mri()*) and adding the fiducial locations (naison, left and right pre-auricular points) taken from (Cutini et al. 2011). We then segmented (i.e. separated) it into three tissues: brain, skull, and scalp (*ft_volumesegment()*). To create a conductive headmodel using the boundary element method (BEM), we need to take the volume information and transform it into surface information (main assumption: electricity flows within the same kind of tissue in a uniform fashion, so we only need to account for tissue changes). We did this by modelling the surfaces of the three tissues as points (vertices) connected in a triangular way using FieldTrip's *ft_prepare_mesh()* function. We used 1000 vertices per tissue (see Fig. 2.2). From the geometric description of each tissue, we created a volume conduction model using FieldTrip's "dipoli" implementation (Oostendorp and Van Oosterom 1989). The headmodel was created once and was used for each individual subject. Before decomposing the EEG data into sources, we aligned each individual's electrodes to the headmodel. We did so in two steps: a first, automatic pass using FieldTrip's *ft_electroderealign()* function (aligns the template's and electrode's fiducials) and a second interactive pass (using the same function with different parameters). Note that this interactive pass includes three kinds of transformations: translation, rotation, and linear scaling. After this, we prepared the leadfield matrix by discretizing the cortical volume into a 1cm grid. The leadfield matrix describes how each dipole along this discrete grid in our headmodel projects to the scalp. We created

this model by using FieldTrip's *ft_prepare_leadfield()*. Once we had the leadfield and individually aligned electrodes, we created the forward model.

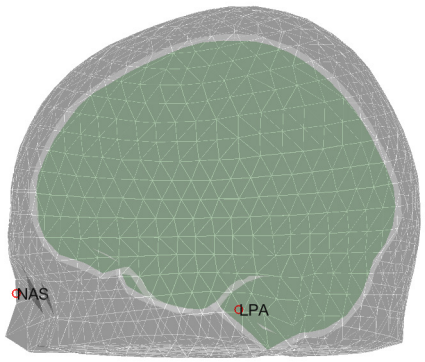

Figure 2.2: The geometry of the volume conduction model. All surfaces (scalp: gray, skull: white, brain: green) plotted together. From this view, two fiducials are visible: nasion (NAS) and Left pre-auricular point (LPA)

Table 2.3: Cortical parcellation after spatial downsampling. Bolded patches were not included in Symbolic Transfer Entropy Analysis.

Cortical Patches		
Prefrontal Left	Prefrontal Right	Motor Left
Motor Right	**Basal Ganglia Left**	**Basal Ganglia Right**
Insula Left	Insula Right	Parietal Left
Parietal Right	Temporal Left	Temporal Right
Occipital Left	Occipital Right	**Limbic Left**
Limbic Right	**Cerebellum Left**	**Cerebellum Right**
	Cerebellum Mid	

We decided to implement a cortical patch basis model (see Limpiti et al. 2006) that describes arbitrary spatially distributed activity within each cortical patch using a set of local basis functions. Because this model does not assume activity distribution within the cortical patches, it can describe both focal and spatially distributed activity. We started off with the Automated Anatomical Labeling (AAL) atlas (Tzourio-Mazoyer et

al. 2002), one of the most commonly used atlases in the imaging literature (Soares et al. 2016). Associating the ICBM152 template with the AAL atlas allowed us to localize designated anatomical features in coordinate space, as well as to associate functional results to identified anatomical regions (Soares et al. 2016). Because EEG does not offer the same resolution as MRI, we decided to pool anatomically relevant regions, essentially doing a spatial downsampling, going from 116 regions to 13 (see Table 2.3; note deep brain structures were not included in further analysis because current dissipates as a function of the square distance, making it difficult to obtain reliable data from these regions). For each cortical patch, we determined the leadfield points (or dipole sources) located in it (based on the downsampled AAL atlas). We modeled the signal coming from the each patch as

$$S_{k,j}(t) \approx H_k a_{k,j}(t) \tag{2.1}$$

where $S_{k,j}(t)$ is the signal originating from the kth patch during the jth epoch at time t; H_k is a rectangular matrix with dimensions (number of channels) by 3 (number of dipoles inside the patch). This setup corresponds to an unconstrained model because the dipole moment orientations are unknown (i.e., we do not have individual T1w MRI scans so we do not know each person's individual anatomy); and $a_{k,j}(t)$ is a 3 (number of dipoles inside the patch) by 1 vector whose entries represent the three components ($x-$, $y-$, and $z-$coordinate directions) of the dipole amplitude at each point of the dipole grid. The problem here is twofold: q_k can be quite large even for modest sized patches (resulting in a very large number of unknown parameters when doing the inverse solution) and the columns of H_k can be linearly dependent (because of volume conduction). Consequently, we did a low-rank approximation of H_k by minimizing the normalized mean-squared error between the approximated signal within the patch ($\hat{s}_{k,j}(t)$) and the actual signal ($s_{k,j}(t)$). This minimization is done by choosing p_k left singular vectors of H_k corresponding to

the p_k largest value (these are obtained by a singular value decomposition). Limpiti et al. (2006) define the **mean representation accuracy statistic (γ_k)** to choose an appropriate p_k. The number of bases (p_k) chosen for each patch determines a trade-off between representation accuracy and the ability to differentiate between distinct patches. We chose a γ_k of 0.85. With this, we get the basis function that describes activity for each patch. This is the forward model (for a more in depth description of the process, see Limpiti et al. 2006).

With the forward model in hand, we decided to use a linearly constrained minimum variance (LCMV) inverse solution (Van Veen et al. 1997). The LCMV criterion designs a spatial filter to minimize the output power subject to a unit response constraint to a location of interest, in our case, to each patch. So, for each patch, Limpiti et al. (2006) define the LCMV problem for the patch basis model as:

$$\min_{w_k} w_k^T R_x w_k \quad subject \quad to \quad w_k^T U_k v_k = 1, \tag{2.2}$$

where w_k is the weights of the spatial filter, R_x is the covariance matrix of the data, and, in our case of unknown moment orientations, v_k is chosen to be the eigenvector corresponding to the smallest eigenvalue of $U_k^T R_x^{-1} U_k$, where U_k is the low rank (p_k) approximation of the leadfield matrix. The spatial filter is given by:

$$w_k = [v_k^T U_k^T R_x^{-1} U_k v_k]^{-1} R_x^{-1} U_k v_k. \tag{2.3}$$

The amplitude of the patch's signal for each epoch is then estimated by applying the spatial filter of 2.3 to the actual data $x_j(t)$

$$\hat{G}_{k,j} = w_k^T x_j(t). \tag{2.4}$$

Once the spatial filters for each cortical patch were applied to all the data, these were exported to Python for further analysis. Both time frequency and symbolic transfer entropy analyses were carried out in Compute Canada's Graham cluster using a serial farm. We created a base Python script that intakes 6 parameters (subject a, subject b, pair name, source frequency band, target frequency band, and delay). This heavily optimized computation time.

2.7.2 EEG Data: Time-frequency decomposition

Preprocessed data were imported to Python and frequency bands were isolated using a zero-phase Blackman windowed sinc FIR filter (Delta: 1 – 3 Hz; Theta: 4 – 7 Hz, Alpha: 8 – 12 Hz, Beta: 13 – 28 Hz, Gamma: 30 – 45 Hz). We chose a Blackmann window to minimize spectral leakage across frequency bands. Using Numerical Python (Oliphant 2006) and Scientific Python (Oliphant 2007), we calculated the power at each frequency band (the squared magnitude of the analytic signal; i.e., Hilbert transform). We performed a baseline normalization (percentage change from baseline; see Eq. 2.5) to (1) disentangle background dynamics from actual task-related oscillations and (2) to ensure our data were normally distributed (Cohen 2014). The equation used was as follows

$$\%\text{change}_{tf} = 100\frac{\text{activity}_{tf} - \overline{\text{baseline}_\text{f}}}{\overline{\text{baseline}}_f}, \tag{2.5}$$

where activity_{tf} is a specific time-frequency point and $\overline{\text{baseline}}_f$ is the average activity across time at a given frequency band (Cohen 2014). The units of these data are %

change from baseline. After normalizing with respect to baseline, we got rid of the 3s padding at the beginning and end of each trial and decimated by a factor of 16 (from 2400Hz to 150 Hz; see next section).

2.7.3 EEG Data: Symbolic Transfer Entropy

Symbolic Transfer Entropy (STE) can be interpreted as a non-linear extension of Granger Causality (Lee et al. 2015). It is based on the concept of Entropy, first developed by Claude Shannon in 1948, as a means to quantify information in a random process (Shannon 2001). It quantifies how much new information a series of messages is conveying by taking a weighted average of the probability mass function for the process of its possible outcomes (see Eq. 2.6).

$$S = -\sum_{i} P_i log_2(P_i). \tag{2.6}$$

To infer information transfer between two processes, Schreiber (2000) proposed the concept of transfer entropy. Given a source signal X and a target signal Y, transfer entropy quantifies how much information is flowing from process X to process Y based on the influences the state of X has on the n^{th} transition probabilities of system Y. It is important to note that Transfer Entropy is asymmetrical because of the conditioning on the transition probabilities. The basic idea is to model both time series as two separate Markov process: one including only the target signal, and the other including both the target and the source signals. The deviation between both distributions is then estimated. If both signals are completely independent, or if they are completely synchronized, transfer entropy tends to 0 (Schreiber 2000). Studying time series with this approach, however, becomes problematic because collapsing a time series into a probability distribution requires the choice of several parameters (frequency distribution

bins, method of approximation, etc.). To get around this, Staniek and Lehnertz (2008) proposed Symbolic Transfer Entropy, a particular implementation from the *permutation entropy* approaches (Bandt and Pompe 2002).

$$T^{S}_{X\to Y} = \sum p(\hat{y}_i, \hat{y}_{i-1}, \hat{x}_{i-\delta}) log_2 \frac{p(\hat{y}_i|\hat{y}_{i-1}, \hat{x}_{i-\delta})}{p(\hat{y}_i|\hat{y}_{i-1})} \tag{2.7}$$

This approach to calculating transfer entropy starts with a symbolization process that restricts the user input in the algorithm to three parameters: an embedding dimension (m), a sample lag between the symbolized points (l, which is closely related to the process of decimating), and the lag between the past points of the source signal x used to predict the future points of signal y (δ). Symbols are defined by reordering the amplitude values of both signals x_i and y_i (i indicating the ith sample). For a given i, m (or the embedding dimension) amplitude values $X_i = \{x(i), x(i+l), ..., x(i+(m-1)l\}$ are arranged in an ascending order $\{x(i+(k_{i1}-1)l) \leq x(i+(k_{i2}-1)l) \leq ... \leq x(i+(k_{im}-1)l)$. This way, every X_i is uniquely mapped onto one of the $m!$ possible permutations. A symbol is then defined as $\hat{x}_i \equiv k_{i1}, k_{i2}, ..., k_{i3}$ and with the relative frequency of symbols we estimate joint and conditional probabilities of the sequence of permutation indices.

Eq. 2.7 shows a slightly modified version from the originally proposed method. Here, we only delayed the source signal, as opposed to both the source signal and the target signal. We did this for several reasons:

1. Delaying only the target signal is one less parameter to deal with (instead of delaying both signal and source), rendering our model simpler. Occam's razor tells us that when two models are compatible with a set of observations, we should always go for the simpler model (for a more in depth description, see Chapter 28 of MacKay and Mac Kay 2003).

2. As outlined by Wibral et al. (2013), this delay conditioning represents an actual causal relationship; it also properly eliminates any information storage from the past of Y that could otherwise be mistaken as information transfer from X. Finally, this allows us to take a dynamical systems view of the *state transition* $Y_{t-1} \to Y_t$, and consider the TE as measuring how much information $X_{t-\delta}$ provides about the state transition.

3. It aligns with the Wiener principle of causality (Wiener 2013).

4. It takes a while for current to travel from cortical patch X to cortical patch Y, but neurons in Y have their own intrinsic dynamics that act much faster than the $X \to Y$ transmission. In this case, delaying both signals is likely to underestimate relevant information in the target's past, and therefore overestimate STE and inflate false positives.

All in all, Symbolic Transfer Entropy is a convenient, robust, and computationally fast method that allows us to quantify the preferred direction of information flow between time series from observed data.

2.7.4 Symbolic Transfer Entropy: Parameters and calculation

Instead of manipulating the sample lag parameter l, we decided to decimate the data by a factor of 16. We chose an embedding dimension of 3, i.e. creating symbols by taking three samples back as suggested by Staniek and Lehnertz (2007), and we explored three different delays: 20ms, 200ms, and 1000ms. These parameters give us a resolution of 20ms per symbol; in other words, we use 20ms worth of data to predict a future 20ms delayed either by 20ms, 200ms, or 1000 ms. We chose these delays for the following reasons:

1. Testing different delays allows us to correctly interpret information transfer revealed by any analysis of directed interactions across brain structures; simulations show that Transfer Entropy will be maximal at the system's delay. Transfer Entropy increases as we approach the true delay, and it also detects bidirectional interactions. Despite this, we acknowledge that testing only three delays is not sufficient to completely characterize the range of dynamics the human brain exhibits (Wibral et al. 2013).

2. The relevant timescale at which information flows in both within and between networks is an empirical question by itself, so we chose three delays: short, mid, and long. We hypothesized that shorter and medium delays were relevant for within networks, while medium and long delays were relevant for between networks (Honey et al. 2007; Varela et al. 2001).

3. Most of the work done so far only uses one delay (Lungarella and Sporns 2006; Buehlmann and Deco 2010), mostly because of limited computational resources. Simulation studies have shown that delayed transfer entropy identifies synapses at a better performance than other algorithms (Ito et al. 2011). Though we are looking at oscillating cortical activity, these results are encouraging.

2.7.5 Grand Hyperbrain Networks

Using Numerical Python (Oliphant 2006) and Scientific Python (Oliphant 2007), we calculated, per delay, STE scores for each region pair (including self-interactions), across both subjects (within-person and between-person networks), at each frequency pair (both within and cross frequencies). We ended up with a "Grand" Hyperbrain Network for each delay, which are non-symmetrical square matrices with 14,400 entries (12 brain regions, 2 roles [piano 1, piano 2], 5 frequency bands; see Chapter 3 for examples of these). The

first question we sought to answer was: can we identify **between**-person connections that are significantly different from both baseline and noise while participants are playing with each other? To answer this, we performed two statistical tests. First, we averaged both homophonic and polyphonic networks to obtain one *playing* matrix per duet pair. From this *playing* matrices, we averaged all pairs together to determine the top .33% between-person connections at each delay (i.e. 48 connections per delay, a total of 143). Once we identified these, we went back to the data for each duet pair, and compared them to two other values: a baseline value and a scrambled pairs value. To estimate the baselines we determined the Grand Hyperbrain Networks per pair per delay for the 3 minute recordings taken prior to playing. For the scrambled comparison, we scrambled the participant pairs and determined scrambled Grand Hyperbrain Networks (for this step, we kept experimental structure consistent, i.e., subject 3A's Entre Cloche trial when they were Piano I was analyzed with subject's 5B trial of the same piece when they were Piano II). To compare both baseline and scrambled values to those obtained while they were playing the duets for the 143 top-valued connections, we performed permutation-based, paired t-tests (Ernst et al. 2004). The process is as follows:

1. Get the ordered vectors (a 6 by 2 matrix where each row represents one pair) of data containing the playing statistic and either the corresponding baseline or scrambled values.

2. Get the experimental (paired) t-statistic from these two vectors.

3. The null hypothesis is: the only difference between these two vectors is the label, so we permute the data. Because this is a paired test, we keep the ordering of the data (i.e., we only permute the values in the rows, not in the columns to keep the ordering of the pairs). This leaves us with 64 permutations.

4. Construct the distribution of the paired statistic. Because this is a one tailed test,

we calculate the p-value as the ratio of permuted t-statistics that are larger than the experimental one.

5. Perform an FDR (BH) procedure to control for multiple comparisons at each delay (Groppe et al. 2011; Benjamini and Hochberg 1995), setting the significance level at $\alpha = 0.05$.

We considered the between connections to be significant if they were statistically higher than both the baseline and the noise (scrambled) threshold. Connections that were significant were then correlated (Pearson correlation coefficient) at the trial level with the trial average (both subjects) of the first three PMPQ scales: synergy, quality, and synchrony (see Appendix E) using SciPy's *pearsonr()* function. It evaluates the significance of these correlations by estimating the probability of an uncorrelated system producing data sets that have a Pearson correlation at least as extreme as the one computed from the actual data.

2.7.6 Music Affiliation Questionnaire

To determine how affiliated participants felt before and after the experiment, we administered the Music Affiliation Questionnaire (Appendix C). We compared pre and post answers of questions 4 through 6 to determine if participants reported greater affiliation then before the experimental session. To evaluate the statistical significance of this, we used a permutation-based paired t-test (see section 2.7.5).

2.7.7 Graph Theory

The second question we sought to answer was: "Are there differences between Homophonic and Polyphonic pieces?" To tackle this, we used Graph Theory Statistics to

compare the Grand Hyperbrain Networks from each experimental factor. Graph Theory is the branch of mathematics that deals with the description and analysis of graphs. A graph is an abstract representation of a system's elements and its dyadic interactions, and it is defined as a set of nodes (vertices) linked by connections (edges; Bullmore and Sporns 2009; Sporns 2011). In our case, these graphs are the hyperbrain grand matrices: the vertices are the cortical patches and the edges are the directed Symbolic Transfer Entropy scores. Because of this, the graphs we analyzed are considered to be both directed (because they are not symmetrical) and weighted (because the connections are not binary).

We obtained two hyperbrain networks per pair (see Section 2.7.5 for details) by averaging all the homophonic pieces and the polyphonic pieces. From this, we derived four graph theory statistics using a Python implementation of MATLAB's Brain Connectivity Toolbox (LaPlante 2018):

1. Average Clustering Coefficient (weighted, directed), which quantifies (in average) the "intensity" of triangles around a node

2. Average Node Strength (directed), which quantifies the sum of weights (STE) of links connected to the node

3. Characteristic Path Length, the average shortest path length in the network

4. Global efficiency, the average inverse shortest path length in the network

After we obtained these statistics, we compared Homophonic and Polyphonic duos using a permutation-based, paired t-tests and an FDR procedure to control for multiple comparisons (see Section 2.7.5) at each delay. In this case, because it was a two-tailed test, we compared the absolute value of the statistic to the absolute value of the permutation distribution. After this, we correlated these four statistics at the trial level with

the trial average (across subjects) of the first three PMPQ scales: synergy, quality, and synchrony (see Appendix E) using SciPy's *pearsonr()* function. To correct for multiple comparisons, we used an FDR procedure.

2.7.8 Small-world properties as a function of time

The third and last question we sought to answer was: "do these networks exhibit increasing small world properties as a function of time?". The Small world property of networks combines high levels of local clustering among nodes of a network (cliques, so to speak) and short paths that globally link all nodes of the network (Bullmore and Sporns 2009). These networks were first described in the context of social networks (Travers and Milgram 1967). These networks exhibit optimized architectures where all nodes of a large system are linked through relatively few intermediate steps, even when most nodes are only connected to their own neighborhood.

To determine the trial-level small world coefficient, we calculated the ratio between the Average Clustering Coefficient and the Characteristic Path Length. Then, we averaged all the trials for each block (i.e., the five repetitions of one piece) for each duet pair (these were consistent within pairs but differed between pairs—each experimental block consisted of one piece but the pieces were pseudorandomized). Then, we calculated the correlation between this score and the position of the block in the experiment to determine if the small-world properties of the networks evolved as a function of time over the experiment. Our hypothesis was that, because this was the first time participants played with each other, the more they played with each other the more optimized the hyperbrain networks would become. We corrected for multiple comparisons using an FDR procedure.

2.7.9 Small-world coefficient and music affiliation questionnaire

As an final analysis, we compared the evolution of small-world coefficients across the blocks with the change of affiliation before and after playing together. We first obtained the slope of the line going from the first experimental block of the small-world coefficients to the fourth (last) experimental block. We then obtained the difference of the MAQ scores between the pre and post experiment questionnaires. Finally, we correlated these two measurements. Given that we had only 6 pairs, these results should be taken as exploratory, and as a guide for future studies. Again, we corrected for multiple comparisons using an FDR procedure.

Chapter 3

Results

3.1 Music Affiliation Questionnaire

Subjects report higher affiliation after the experiment (paired t-statistic = 3.11, permuted p value < 0.05; see Fig. 3.1).This is particularly interesting as these people never played together before, and that we explicitly forbade them to talk to each other for the duration of the experiment.

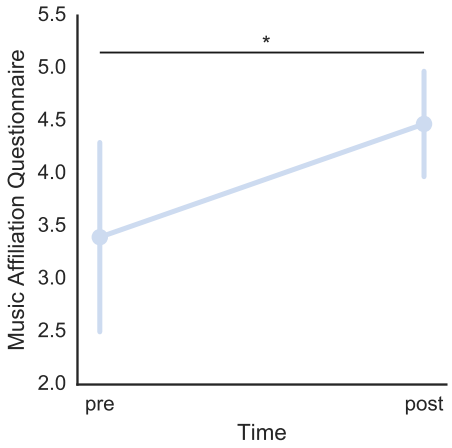

FIGURE 3.1: Average of the scores from questions 4 - 7 of the Music Affiliation Questionnaire (see Appendix C). Error bars represent 95% confidence intervals. An asterisk signifies the difference is statistically significant at $\alpha = 0.05$

3.2 Grand Hyperbrain Networks

3.2.1 Hyperbrain networks: Full Characterization

To characterize hyperbrain networks while pianists play with each other we initially averaged all the pieces together. These matrices are not symmetrical and they have not been thresholded in any way. For the purposes of this thesis, we were mainly interested in the between-person networks, but the within-person connections are interesting and will be discussed briefly.

At a timescale of 20ms (see Fig. 3.2), we see that the strongest connections are within the cortical patches (feedback loops) at the highest frequencies (beta and gamma). Most connections appear to be bidirectional (i.e. $X \rightarrow Y \approx Y \rightarrow X$), and the most prominent connections appear similar across frequencies are: (1) a bidirectional loop between the temporal and insula patch (both left and right), (2) a bidirectional loop between prefrontal and insula (mostly on the right side), and (3) a bidirectional loop between the motor and prefrontal areas (both left and right). Note that we see no cross-frequency interactions at this timescale.

At a timescale of 200ms (see Fig. 3.3), we see again that the strongest connections are between within-person cortical patches (feedback loops), but this time at lower frequencies (theta, delta, and alpha). Again, most connections appear to be bidirectional (i.e. $X \rightarrow Y \approx Y \rightarrow X$), and even though we see more complex patterns of connectivity than at the early delay, the most prominent connections are (specially at lower frequencies): (1) a bidirectional loop between the temporal and insula cortical patches (both left and right), (2) a bidirectional loop between prefrontal and insula (mostly on the right side), and (3) a bidirectional loop between the motor and prefrontal areas (both left and right). In addition, the bidirectional relationship between both occipital left and right

cortical patches is more prominent than at 20 ms. Once again, please note that we see no cross-frequency interactions at this timescale.

At a timescale of 1000ms (see Fig. 3.4), no clear brain connectivity patterns are visible. Please note that the three graphs at different delays use different scales for STE, and that the scores at 1000ms are about half of those from the 200ms delay, and about one order of magnitude smaller than those at the earliest (20ms) delay. At 1000 ms, there is, however, a pattern at the level of frequency interactions: if this is actually relevant to brain functioning or not remains to be tested.

3.2.2 Hyperbrain Networks: Between Connections

After characterizing the full Hyperbrain networks, examined the between connections in more detail (see Figs 3.5, 3.6, and 3.7). All of the top 1% connections (i.e., 48 connections per delay) were significantly different from baseline, but none of them were significantly different from the values obtained by scrambling the pairs (for specific connections and statistical values, see Appendix G), suggesting that there was no significant STE present. Because none of the values were significant, we did not proceed to correlate any of these values with the PMPQ results.

3.3 Graph Theory Statistics

In the next series of analyses, we aimed to examine differences between the grand hyperbrain networks at the level of one of our experimental manipulations: homophonic versus polyphonic musical structure. We see that at all delays, and for all graph theory statistics, homophonic and polyphonic music gave rise to different network properties: polyphonic duos had larger average clustering coefficients, average node strength, and

efficiency, whereas homophonic duos had greater characteristic path length (see Fig. 3.8). For a detailed description of the statistical values, see Appendix H.

Because we found significant differences related to our experimental manipulation of musical structure, we decided to correlate the trial level values of the graph theory statistics with the first three scales of the PMPQ (see Appendix E), namely synergy, synchrony, and quality. After correcting for multiple comparisons using an FDR procedure, all the Polyphonic graph theory statistics correlated with the self reports on quality at the trial level (see Fig. 3.9). Average clustering coefficient, average node strength, and characteristic path length correlated positively, while efficiency correlated negatively with quality. Please note that, regardless of delay, these correlations remained significant. For a detailed description of the statistical values, see Appendix H.

3.4 Small-world coefficient

As a final analysis, we examined the small world properties of the hyperbrain networks as a function of both time and affiliation. We found no significant correlation between time block (i.e., experimental block 1, 2, 3, or 4) and the pieces position (i.e., the 5 repetitions of the piece averaged together) in the experiment (see Fig. 3.10 **a, b, c**) nor a significant correlation between the change in affiliation and the slope of the change between the first piece and last piece's small world coefficient for each pair of performers (see Fig. 3.10 **d, e, f**). The latter results might reflect our sample size (6 pairs). For a detailed description of the statistical values, see Appendix I.

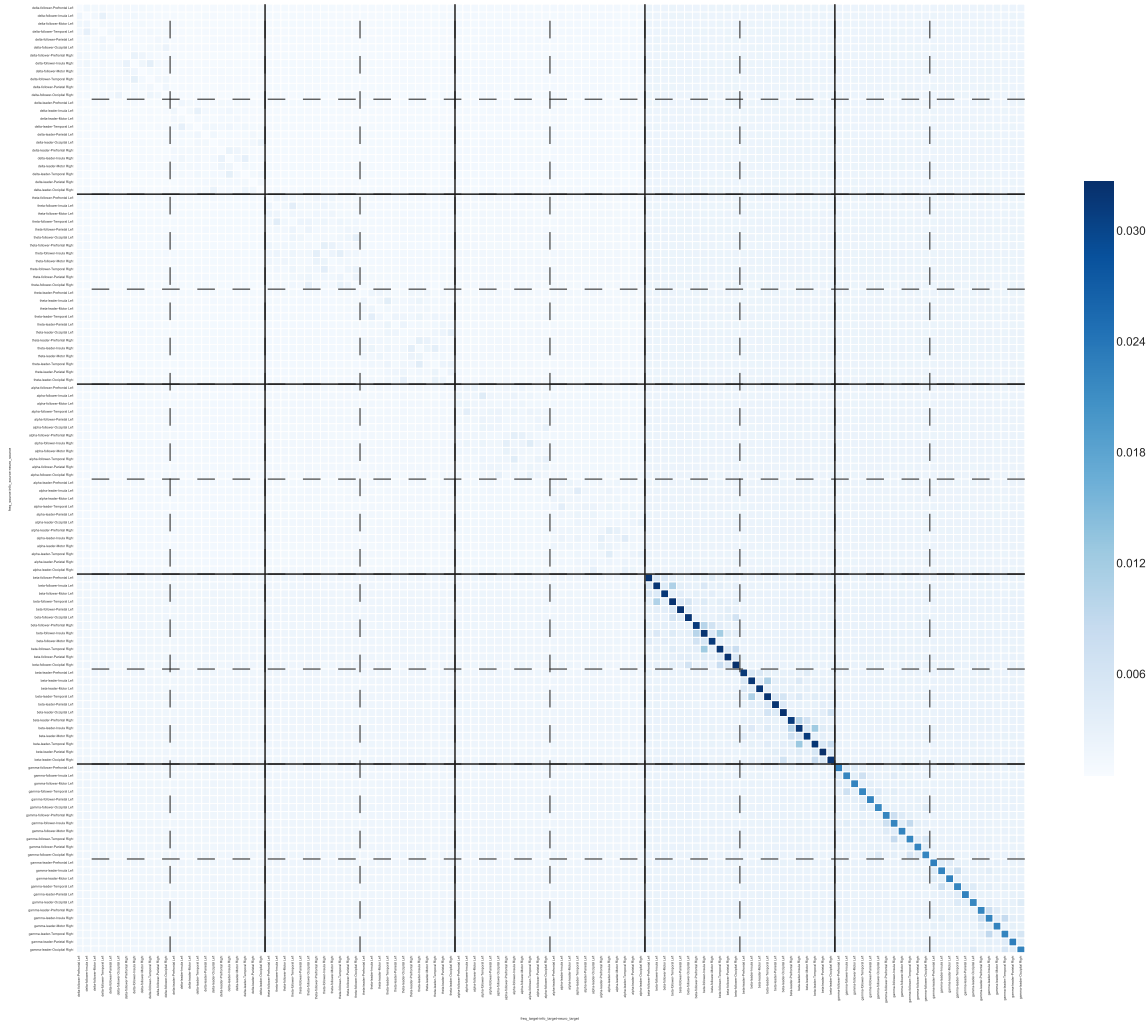

Figure 3.2: Full Hyperbrain networks at 20ms delay. Colorbar represents STE values. Each big quadrant (solid lines) represents a frequency interaction (gamma to gamma, alpha to beta, delta to delta, etc.). Note this matrix is not symmetrical and it has not been thresholded in any way. The matrix is ordered based on three hierarchical factors: frequency, leadership, and brain patch. Symbolic transfer entropy was calculated from row to column (i.e., source signals are on the x axis and target signals are on the y axis). Big quadrants (solid lines) represent frequency interactions (gamma, beta, alpha, delta, theta). Medium quadrants (dotted lines) represent leadership role and information flow (leader to leader, follower to leader, leader to follower, follower to follower). Each entry of the matrix represents the STE score originating at a given cortical patch, at a given frequency, from a given role in one person (x-axis), to a given cortical patch, at a given frequency, from a given role in the second person (y-axis).

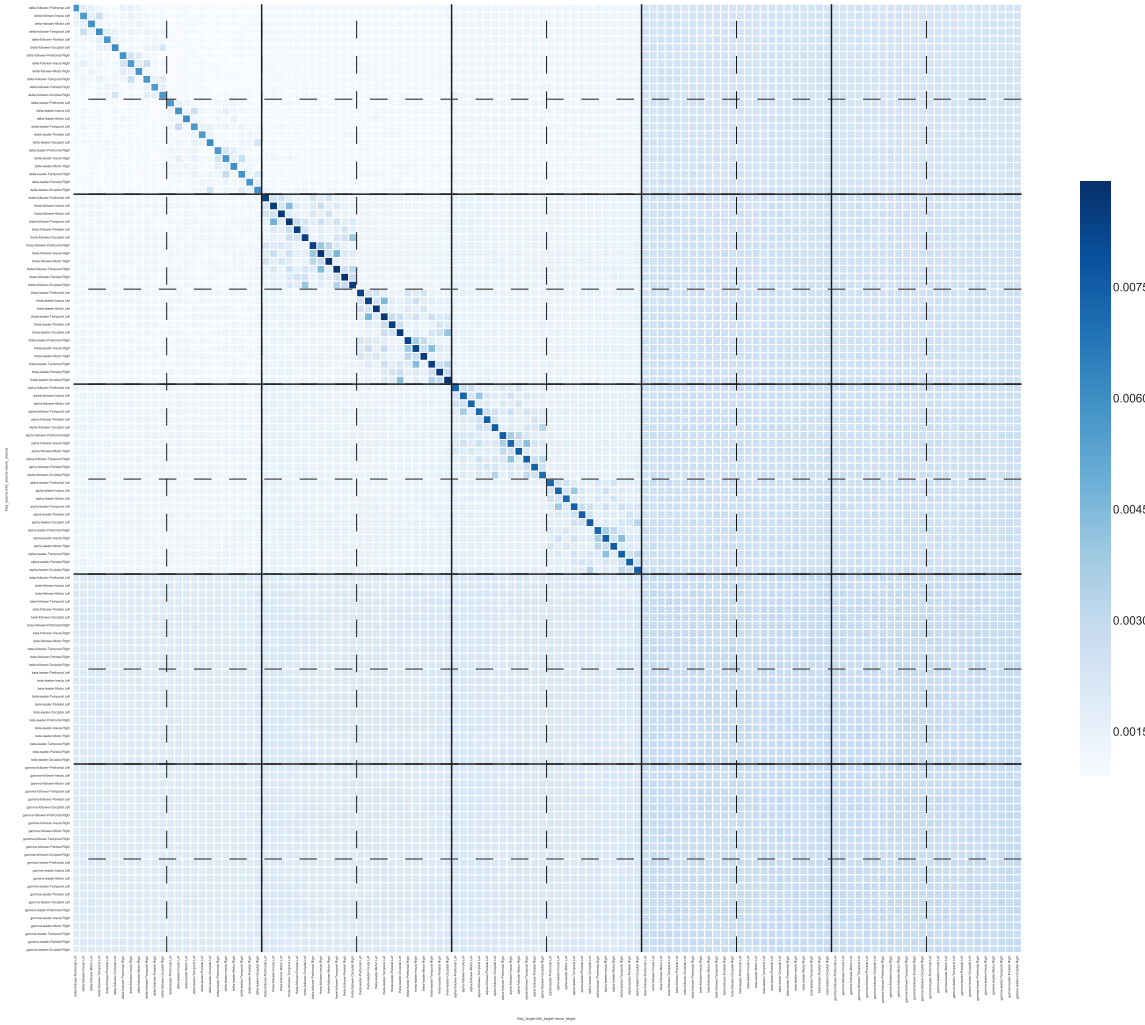

Figure 3.3: Full Hyperbrain networks at 200ms delay. Colorbar represents STE values. Each big quadrant (solid lines) represents a frequency interaction (gamma to gamma, alpha to beta, delta to delta, etc.). Note this matrix is not symmetrical and it has not been thresholded in any way. The matrix is ordered based on three hierarchical factors: frequency, leadership, and brain patch. Symbolic transfer entropy was calculated from row to column (i.e., source signals are on the x axis and target signals are on the y axis). Big quadrants (solid lines) represent frequency interactions (gamma, beta, alpha, delta, theta). Medium quadrants (dotted lines) represent leadership role and information flow (leader to leader, follower to leader, leader to follower, follower to follower). Each entry of the matrix represents the STE score originating at a given cortical patch, at a given frequency, from a given role in one person (x-axis), to a given cortical patch, at a given frequency, from a given role in the second person (y-axis).

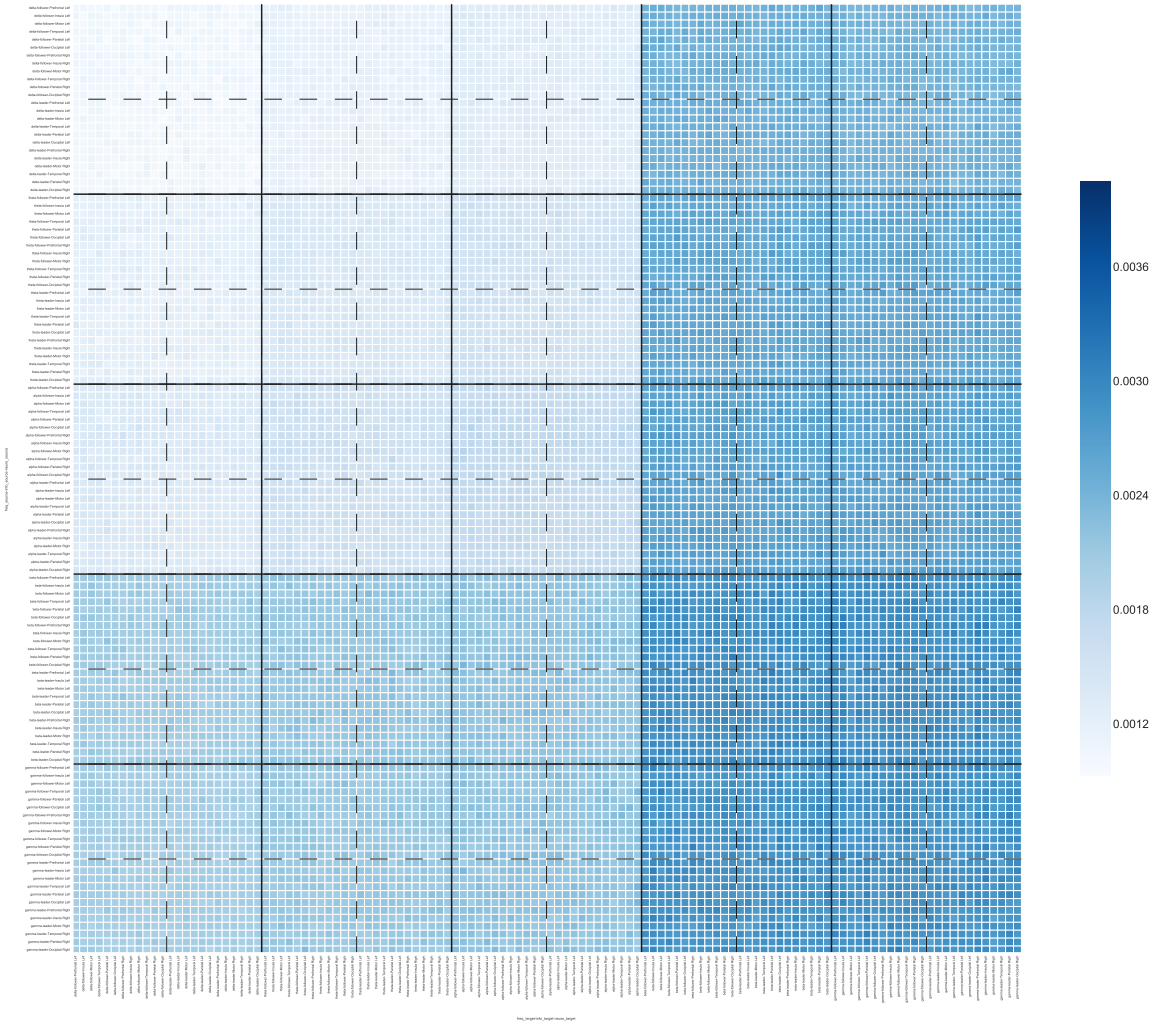

Figure 3.4: Full Hyperbrain networks at 1000ms delay. Colorbar represents STE values. Each big quadrant (solid lines) represents a frequency interaction (gamma to gamma, alpha to beta, delta to delta, etc.). Note this matrix is not symmetrical and it has not been thresholded in any way. The matrix is ordered based on three hierarchical factors: frequency, leadership, and brain patch. Symbolic transfer entropy was calculated from row to column (i.e., source signals are on the x axis and target signals are on the y axis). Big quadrants (solid lines) represent frequency interactions (gamma, beta, alpha, delta, theta). Medium quadrants (dotted lines) represent leadership role and information flow (leader to leader, follower to leader, leader to follower, follower to follower). Each entry of the matrix represents the STE score originating at a given cortical patch, at a given frequency, from a given role in one person (x-axis), to a given cortical patch, at a given frequency, from a given role in the second person (y-axis).

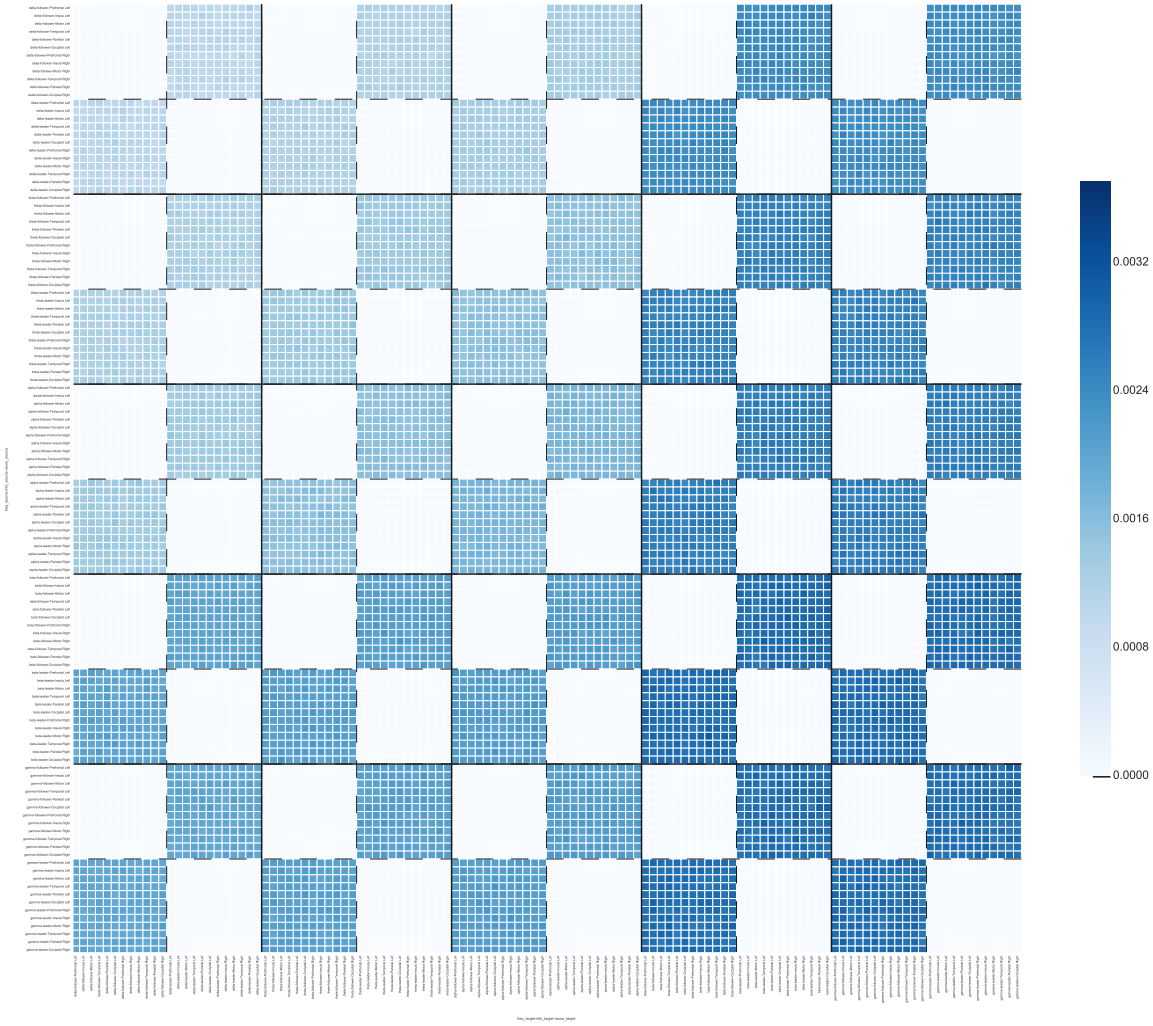

Figure 3.5: Between networks at 20ms delay (within connections have been set to zero). Colorbar represents STE values. Each big quadrant (solid lines) represents a frequency interaction (gamma to gamma, alpha to beta, delta to delta, etc.). Note this matrix is not symmetrical and it has not been thresholded in any way. The matrix is ordered based on three hierarchical factors: frequency, leadership, and brain patch. Symbolic transfer entropy was calculated from row to column (i.e., source signals are on the x axis and target signals are on the y axis). Big quadrants (solid lines) represent frequency interactions (gamma to beta, delta to theta, etc.). Medium quadrants (dotted lines) represent leadership role and information flow (leader to leader, follower to leader...). Each entry of the matrix represents the STE score originating at a given cortical patch, at a given frequency, from a given role in one person (x-axis), to a given cortical patch, at a given frequency, from a given role in the second person (y-axis).

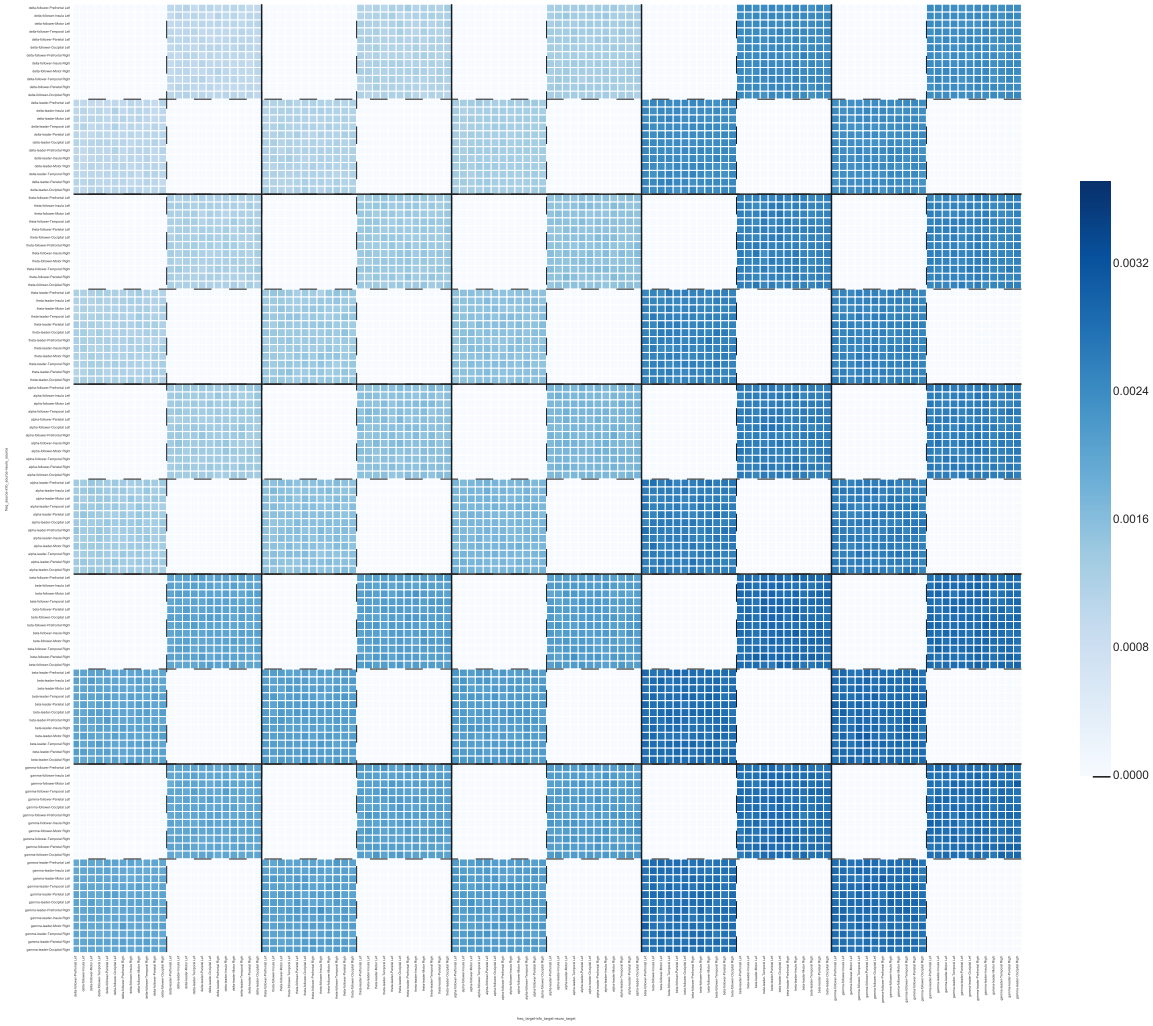

Figure 3.6: Between networks at 200ms delay (within connections have been set to zero). Colorbar represents STE values. Each big quadrant (solid lines) represents a frequency interaction (gamma to gamma, alpha to beta, delta to delta, etc.). Note this matrix is not symmetrical and it has not been thresholded in any way. The matrix is ordered based on three hierarchical factors: frequency, leadership, and brain patch. Symbolic transfer entropy was calculated from row to column (i.e., source signals are on the x axis and target signals are on the y axis). Big quadrants (solid lines) represent frequency interactions (gamma to beta, delta to theta, etc.). Medium quadrants (dotted lines) represent leadership role and information flow (leader to leader, follower to leader...). Each entry of the matrix represents the STE score originating at a given cortical patch, at a given frequency, from a given role in one person (x-axis), to a given cortical patch, at a given frequency, from a given role in the second person (y-axis).

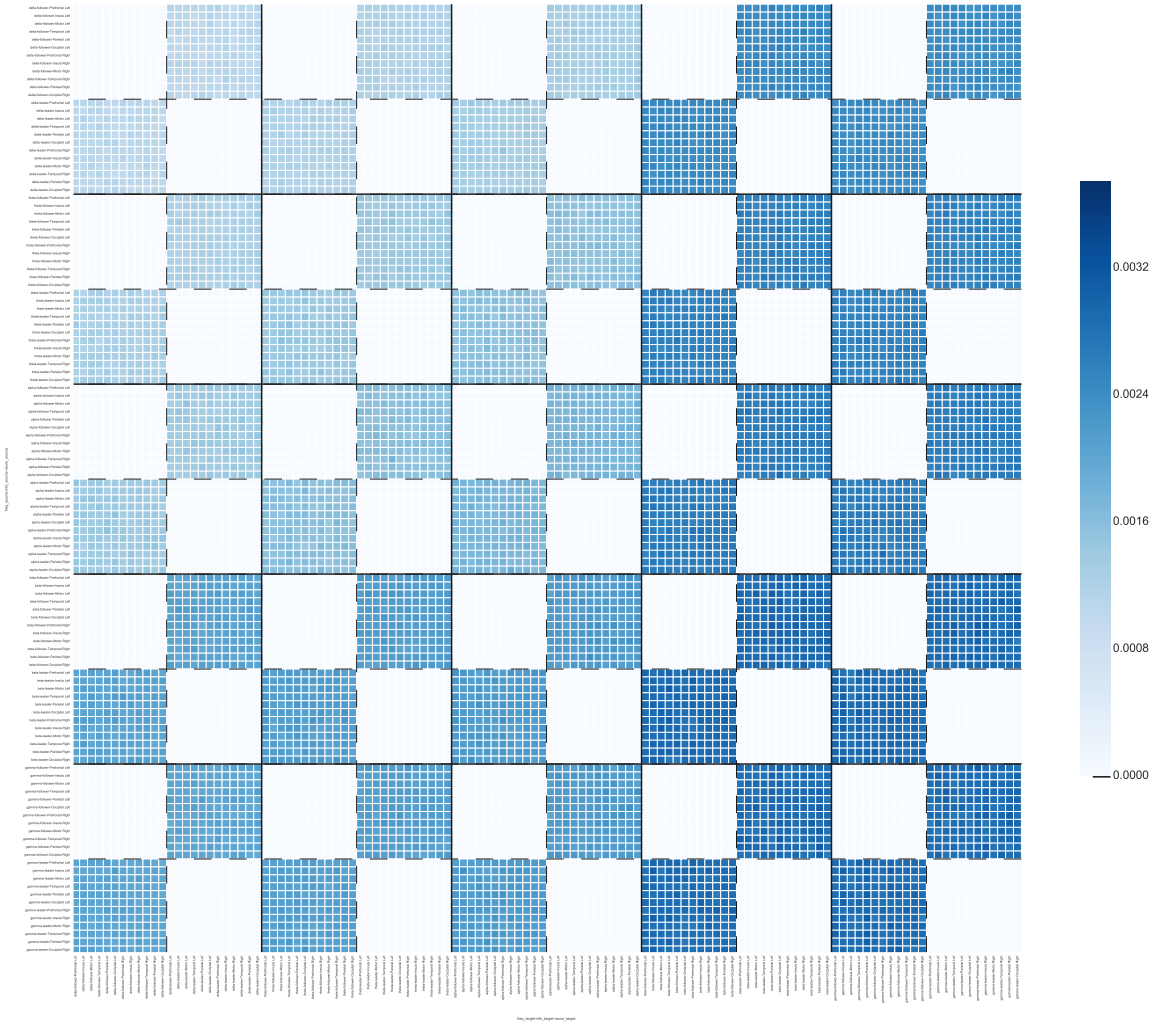

Figure 3.7: Between networks at 1000ms delay (within connections have been set to zero). Colorbar represents STE values. Each big quadrant (solid lines) represents a frequency interaction (gamma to gamma, alpha to beta, delta to delta, etc.). Note this matrix is not symmetrical and it has not been thresholded in any way. The matrix is ordered based on three hierarchical factors: frequency, leadership, and brain patch. Symbolic transfer entropy was calculated from row to column (i.e., source signals are on the x axis and target signals are on the y axis). Big quadrants (solid lines) represent frequency interactions (gamma to beta, delta to theta, etc.). Medium quadrants (dotted lines) represent leadership role and information flow (leader to leader, follower to leader...). Each entry of the matrix represents the STE score originating at a given cortical patch, at a given frequency, from a given role in one person (x-axis), to a given cortical patch, at a given frequency, from a given role in the second person (y-axis).

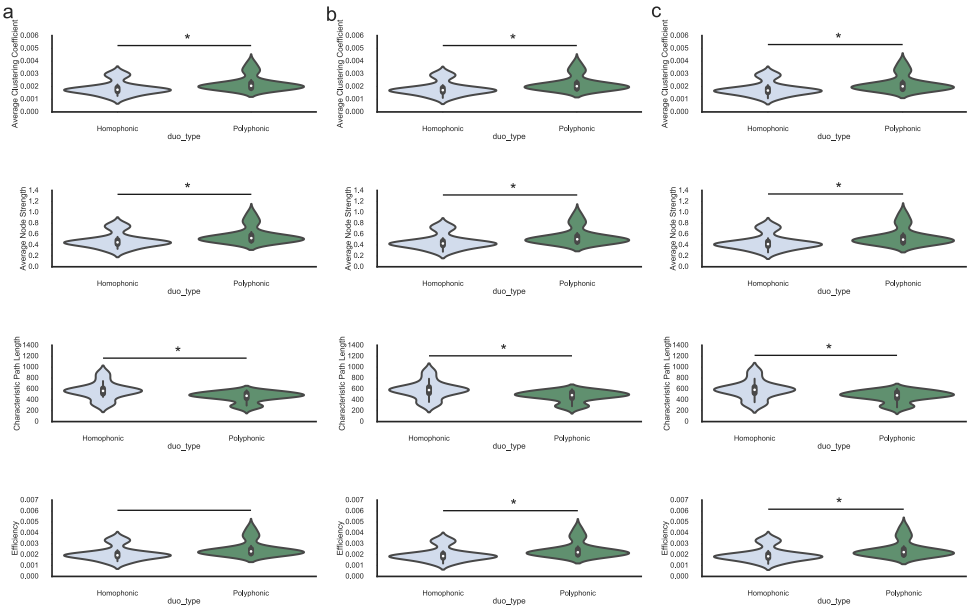

Figure 3.8: Comparison of graph theory statistics between polyphonic and homophonic pieces. Plotted here are violin plots. These are similar to box and whisker plots, but instead of showing actual data points, they show a kernel density estimation of the underlying data distribution. An asterisk signifies the difference is statistically significant at $\alpha = 0.05$. In this case, all statistics were significantly different between Homophonic and Polyphonic pieces. **(a)** Delay of 20ms. **(b)** Delay of 200ms. **(c)** Delay of 1000ms

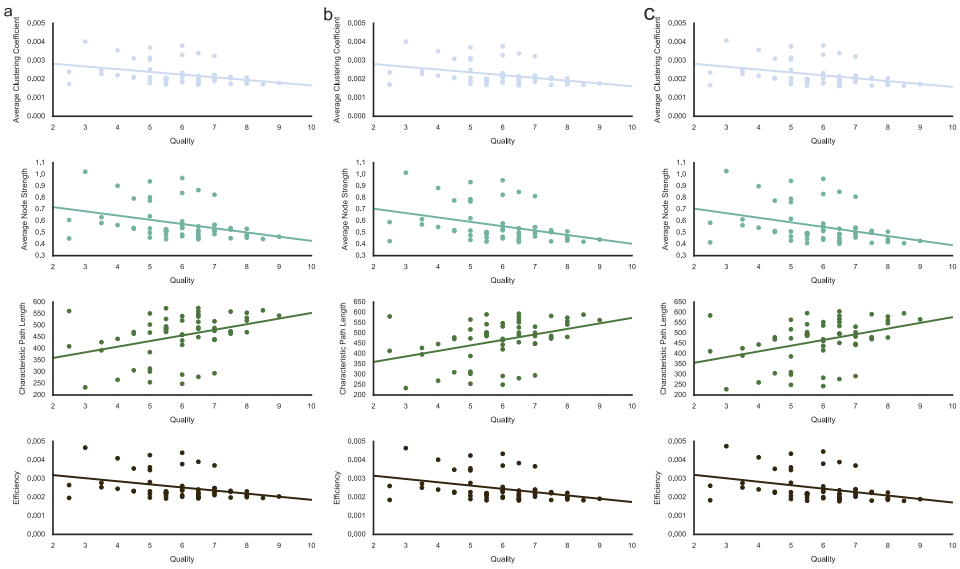

Figure 3.9: All graph theory statistics from polyphonic duos correlated significantly with the self report PMPQ measures. Shown here are scatter plots of each graph theory statistic by PMPQ measure at the trial level. The linear regression lines are shown as well. All correlations plotted here are statistically significant at $\alpha = 0.05$. **(a)** Delay of 20ms. **(b)** Delay of 200ms. **(c)** Delay of 1000ms

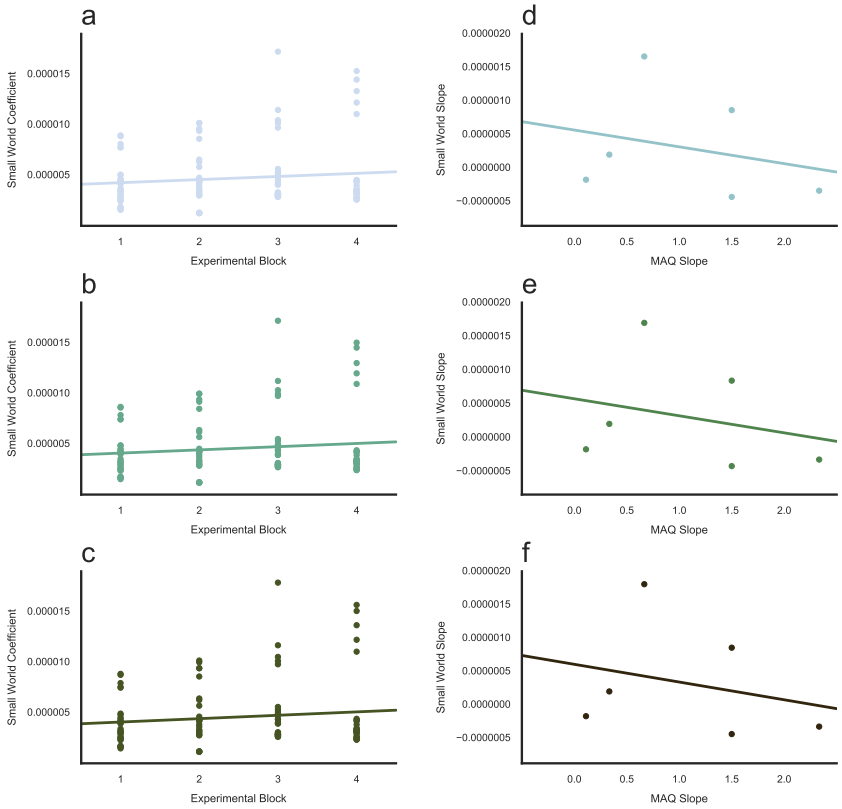

Figure 3.10: Small world coefficients as a function of time **(a, b, c)** and the difference score in music affiliation **(d, e, f)**. Scatter plots also include a linear regression. **(a, b, c).** Each individual point is the average of the five experimental trials for that experimental block position per duet pair at each delay (**(a)**: 20ms, **(b)**:200ms, **(c)**:1000ms). **(d, e, f).** Correlation between the difference score of affiliation before and after the experiment, and the rate of change between the first and last experimental blocks small world coefficients. Each individual point is one pair (**(a)**: 20ms, **(b)**:200ms, **(c)**:1000ms).

Chapter 4

Discussion

Using a complex dynamics framework, we did not find statistically significant hyperbrain networks during joint music playing. Characteristics of the grand hyperbrain networks, however, differentiated between experimental conditions. Furthermore, statistics related to polyphonic grand hyperbrain networks correlated with how good pianists thought their performance was. Here we discuss these results, acknowledge some limitations of this study, and provide some guidance for follow up analysis and future research.

4.1 Affiliation increases after experiment

The pianists in this study reported higher affiliation with their playing partners after compared to before the experimental procedure, even though they were explicitly forbidden to communicate verbally with each other. This is consistent with previous research showing that joint music making and synchronous movements promote pro-social behaviour and positive affect (Kirschner and Tomasello 2010; Cirelli et al. 2014; Mogan et al. 2017). We cannot conclude that music playing alone caused the increase in affiliation because we did not have proper control conditions. However, our results suggest that it is important to include self-report and behavioural measurements as they may

inform the interpretation of models of hyperbrain networks (Babiloni and Astolfi 2014; Hu et al. 2018; Goldstein et al. 2018). For more information on this, see Section 4.5

4.2 Top between-person connections are not distinguishable from noise

All of the top 1% between-person connections (0.33% per delay) were significantly different from the baseline levels, but not from the scrambled levels, suggesting that the Symbolic Transfer Entropy values reflected primarily noise. As Mu et al. (2018) suggests, having a proper baseline and control analyses is key when characterizing hyperbrain networks. None of the previous guitar ensemble studies (Lindenberger et al. 2009; Sänger et al. 2012; Sänger et al. 2013; Müller et al. 2018) included a scrambled analysis, nor a proper baseline, although they did threshold their hyperbrain networks using surrogate time series. Despite this, thresholding will only inform us of the significance of connections against noise, not of their interpretation—i.e., is it due to the perceptual stream or are these hyperconnections indexing other psychological mechanisms? We propose that using scrambled data (or other proper control conditions) allows us to correctly interpret these hyperbrain networks. Future hyperscanning studies should make use of experimental designs that manipulate variables to address this problem (Burgess 2013). For example, by introducing a perturbation in the system, we can then test whether the perturbation causes a change in between-person brain networks, indicating a real interaction rather than a potential coincidental synchrony (Weule et al. 1998). There are several possible reasons as to why we did not find the between connections we were looking for. These are discussed in the following paragraphs.

In the present study, we did take the approach of manipulating variables and choosing

an ecologically valid situation that required participants to be tightly synchronized—significant interaction is required to produce good quality music. However, it is possible that the pieces we chose were too difficult, and pianists concentrated more on playing their own part than interacting with each other. Using easier pieces would also have enabled less highly trained pianists to participate meaningfully, and could have enabled us to increase our sample size.

Toppi et al. (2016) also used an ecologically valid situation (Captain and First Officer in a flight simulation) and manipulated the task by having three phases: Take off, Cruising (control) and Landing. They used what they described as *interconnections density*—a graph theoretical statistic that quantifies how dense connections are between participants. Using this, they showed differences between both of their experimental conditions (Take off and Landing) and the control condition (Cruising). After shuffling the pairs and calculating the randomized Interconnections density, they found no difference between real and shuffled couples for Take off or Cruising, but they did find a significant difference for Landing against the shuffled statistics. The authors concluded that this was due to the Landing phase being the part of the experiment in which the pilots had to be the most synchronized. The approach taken by Toppi et al. (2016) may help inform future analysis of musical interactions. Specifically, they used graph theory statistics to determine information flow between leaders (Captain) and followers (First Officers) by thresholding their graphs and binarizing them (Bullmore and Sporns 2009; Sporns 2011) as opposed to looking at specific pairwise electrode (or brain region) relationships, as we did in the present study. They found direction of flow was affected by their experimental manipulation as indexed by the interconnections density. Given EEG's poor spatial resolution (Cohen 2014) and how coupling of the between-person networks seem to be consistently weaker than the within-person networks (Lindenberger et al. 2009; Sänger et al. 2013), perhaps it is better to use a graph theory approach for hypothesis testing (i.e. multivariate statistics to summarize the whole network into

one single scalar, or even look at every brain as a single vertex of a graph; Duan et al. 2015) as opposed to testing for differences at the pairwise interaction levels (i.e.. mass univariate testing framework).

Hyperbrain EEG has been used successfully in the past to characterize leader and follower dynamics (Jiang et al. 2015; Sänger et al. 2013; Konvalinka et al. 2014). In our case, we actively avoided the words "leader" and "follower" so as to not explicitly prime our participants to behave a certain way. Rather, we were expecting the music structure itself (homophonic vs. polyphonic) to provide enough context for leadership. We defined leadership as a high level construct embedded in the melody of the music—whoever has the melody, leads. Nevertheless, leadership in this context is probably mediated by a myriad of variables ranging from low level ones, such as who starts the piece, to high level ones, such as personality traits (e.g., people with more outgoing personalities may be more likely to lead) and context (e.g., the more experienced of the two pianists might be more likely to lead). Previous work has shown that *leadership emergence* is an empirical question in itself (Modlmeier et al. 2014; Smith and Foti 1998; Jiang et al. 2015) and future hyperscanning studies should take into account inherent asymmetries between people (Dumas 2011).

To date, no other Hyperscanning EEG study had tried to characterize networks at the source level (Burgess 2013). We chose a structural decomposition that included 12 major brain regions. This might have not been ideal: the event-related potential literature suggests that the activity measured at the scalp level is generated at specific neuroanatomical modules (as opposed to individual structures) when computational operations are performed (Näätänen and Picton 1987; Neuper and Pfurtscheller 2001; Luck 2014). Perhaps using a functional approach based on other kind of decompositions, such as Principal Component Analysis or Individual Component Analysis, might provide more insightful answers in future studies, although such approaches do not localize activity to

specific brain regions.

Symbolic Transfer Entropy provides a means of investigating very fine grain dynamics in complex systems. Nevertheless, the researcher has to choose the values of many parameters (delay, embedding dimension, etc). Out of these, two are of particular importance in the present context: delay and sampling rate. However, there is no one way to determine optimal values for these a priori (Weber et al. 2017; Wibral et al. 2014), so we chose to do a parameter space sweep. One factor that may have contributed to our null effects is that we tried to characterize too many relations (e.g., cross-frequency relations, relations between multiple brain regions) at the same time using a one-size-fits all approach of using the same parameter values in all cases (Jirsa and Müller 2013). Furthermore, we were exploring new territory as Symbolic Transfer Entropy had never been used previously to characterize this kind of network. We chose STE rather than Circular Correlation (Goldstein et al. 2018) and Partial Directed Coherence (Toppi et al. 2016), statistics slowly gaining popularity in the field, because the latter do not readily offer the possibility to investigate delays of the information transfer in the system under study (Burgess 2013). We hypothesized that a short, a medium, and a long delay would constitute a good start to characterizing EEG hyperscanning networks (Varela et al. 2001). However, our results suggest that Transfer Entropy is not a good statistic to use, at least for initial exploratory analysis.

In terms of sampling rate, previous work showed that Transfer Entropy is quite robust to common preprocessing steps (as opposed to Granger Causality and other connectivity methods; Weber et al. 2017). By decimating the signal (i.e., symbolizing windows of 20ms of data) we were trying to tap into relevant scales of neural activity (i.e., making the self prediction of Y optimal). Transfer Entropy is robust against Type II errors as long as we do not filter out or decimate out the effect we are looking for. Optimal sampling rate and delay then become empirical questions in and of themselves. Furthermore,

these two parameters interact with each other in complex manners, and the relevant time scales of the complex system under study (brains playing in concert) are unknown. To our knowledge, only one other research study has tried to characterize Hyperbrain connectivity between cooperating partners using Transfer Entropy, also with null results. It is important to note that they used a delay of 7.8ms, which might not be ideal to characterize between brain connectivity (Cha and Lee 2018). In sum, the optimal parameter space to use when employing transfer entropy remains a significant challenge for future work.

Finally, there is no information transfer without a causal interaction, but the reverse does not hold true—Transfer entropy can be zero even when there is causality involved between two signals (Wibral et al. 2014). This happens because TE quantifies information transfer, but information can be transfered immediately between the interacting parts of the system, or even stored for variable amounts of time. If this happens, then there is nothing to predict. Furthermore, Transfer Entropy is not able to differentiate a lack of information transfer from an inhibitory processes (Garofalo et al. 2009), and, despite its robustness, it is best at identifying strong connections (Ito et al. 2011), which might explain why we are not able to identify the between-person connections reported by (Sänger et al. 2012; Sänger et al. 2013). Certainly, we found between-person connections were considerably weaker than within-person connections.

4.3 Networks change as a function of music structure

Using different graph theory statistics (efficiency, characteristic path length, average node strength, average clustering coefficient) we demonstrated that grand hyperbrain networks do distinguish between musical structure when pianists play together. Because

none the top between-person connections were significantly different from noise, the differences we see at the whole network level might be driven largely by the within-person parts of the networks. Grand hyperbrain networks during the polyphonic pieces had a higher rate of information transfer (average node strength) and more complex structures (higher efficiency and average clustering coefficients; Bullmore and Sporns 2009) than homophonic pieces at every delay we investigated (short, medium, and long). Homophonic pieces provide a clear leadership scenario, where Piano I plays the melody while Piano II accompanies. Polyphonic pieces, on the other hand, provide an "ambiguous role" scenario, where both pianists are either playing the same melody at different delays (e.g., Hindemith's Kanon), or there is no melody at all (Ravel's Entre Cloche). Perhaps, the lack of a clear leader role rendered the participants to be more active in their interactions with each other, so they could meet the coordinative demands of these two pieces.

Role ambiguity provides opportunity for individuals to "rise to the occasion". In an organization setting, House and Rizzo (1972) found that the presence of role ambiguity provides an opportunity for a person to expansively define their role. Under these conditions, individuals are more likely to perform effective leadership, even if they were not explicitly designated as leaders. Emergent leaders posit positive influence on group performance and satisfaction when they establish functional structure. This might explain why we found significant correlations between quality and graph theory statistics only for polyphonic pieces (see below). Leaders are able to recognize, explore, and benefit from ambiguous situations (Wilkinson 2006), and these situations require leaders to more thoroughly define lines of communication between themselves and their followers for successful leadership in organizations (Omar 2016). Because we counterbalanced the roles, it is possible that, given the right conditions, any individual can rise to the occasion and take on a leadership role. Modlmeier et al. (2014) define the concept of "episodic keystone individuals", which are individuals who influence their group (or, in

this case, their peer) for restricted periods of time. Together, these ideas provide a plausible explanation as to why Polyphonic pieces might have led to higher synchronization through their role ambiguity.

4.4 Polyphonic network characteristics correlate with perceived quality of musical performance

All graph theory statistics from polyphonic pieces correlated significantly with participants' self reports of the quality of their musical performance at the trial level at each delay. In line with our results, Kitzbichler et al. (2011) found modulations in network topology (efficiency) that were associated with the difficulty of an n-back task. Global efficiency in beta band networks distinguished between fast and slow performing participants in an n-back test. Several studies in the Hyperscanning literature have successfully correlated behaviour and self reports with hyperbrain network characteristics: Dikker et al. (2017) used heuristic statistics that are very similar to average node strength (i.e., total and student-to-group interdependence) and correlated them with self reports of likeability and affiliation; Goldstein et al. (2018) correlated activity at hyperbrain clusters with the pain mitigating effect of social touch and the observer's empathic accuracy; Hu et al. (2018) correlated cooperation rate with mean Alpha phase locking value in human interactions; Ciaramidaro et al. (2018) showed that network topology (modularity, efficiency, interbrain density) was modulated as a function of the level of fairness in a "Third Party Punishment" game. We also looked at the correlation between amount of time they had played together (first vs. last experimental block) and change in small world properties; and the pre to post change in affiliation ratings with change in small world properties. Even though we did not have enough statistical power to draw conclusions in the later case, the former one did not show a clear pattern. We were not, however, the first to try to correlate network topology with some measurements

of affiliation: Müller and Lindenberger (2014) correlated subjectively assessed partner-oriented kissing satisfaction and immediate kissing quality with average node strength in hyperbrain networks, while Dikker et al. (2017) correlated student self-reported closeness with pairwise total interdependence. All in all, as Duan et al. (2015) suggested, collecting both self reports and behavioural data help us to establish a framework for how hyperbrain networks topology is related to real world dynamics and behaviour.

4.5 Limitations and future directions

Here we will discuss limitations of our study, starting from the particular choices that we made, all the way to general critiques of the fields of brain connectomics and network science. First, we were only able to recruit 6 pairs of participants. The recruitment process was quite cumbersome because we required a time commitment from the participants of about a month and a half. Professional pianists were reluctant to participate because they did not consider we were paying them enough. Future studies should still try to systematically manipulate the kind of music used, but choosing easier pieces would likely make recruitment easier. Consulting with professional musicians or musicologists would help enlighten us as to what kind of pieces we should use. It is also clear from our results that the definition of leadership should be established using low-level constructs and more explicit instructions for the participants (see Chang et al. 2017).

Given our naturalistic environment (the LIVELab), the EEG data we obtained were very noisy, especially because we avoided telling participants to be still. Despite employing thorough, state of the art preprocessing, even the best algorithms cannot substitute for clean data (Luck 2014; Bigdely-Shamlo et al. 2015). Source decompositions are sensitive to low levels of signal-to-noise ratio. On the other hand, the Cortical Patch Basis model is fairly robust against noisy data (Limpiti et al. 2006) and we defined patches that

were fairly large (e.g., temporal lobe or insular cortex). However, the "goodness" of the source decomposition is very hard to assess, specially because we used a head template for all experimental subjects in the absence of individual MRI scans. As we discussed in Section 4.2, there is common agreement that activity picked up at the scalp tends to be a complex combination of activity from different cortical structures (Näätänen and Picton 1987; Neuper and Pfurtscheller 2001; Luck 2014). Future hyperscanning studies should compare scalp level results with both anatomical (beamformer, dipole solutions) and functional (Independent Component Analysis, Principal Component Analysis) decompositions, as well as compare functional and anatomical with each other. This will provide very useful insights not only for the field of hyperscanning, but for the general field of advanced EEG processing and brain connectivity.

There are two basic types of statistics that can be used to determine dyadic relations between vertices (such as cortical patches, channels, neurons, etc.). On the one hand, there are statistics that measure coupling, or synchrony in the Huygens's sense (i.e. appearance of phase locking due to interaction; Pikovsky et al. 2003). These statistics posit that the adjustment of rhythms due to interaction is the essence of synchronization. Of these statistics, Burgess (2013) concludes that the two least biased are Circular Correlation and Kraskov's Mutual Information. This paper, however, failed to account for a second type of statistics—Wiener-based statistics. As discussed previously, Wiener-based statistics, such as Partial Directed Coherence, Granger Causality, and Transfer Entropy, measure how the prediction of signal Y is better by including the past of X in the model. Wiener-based statistics are not coupling measurements (Wibral et al. 2014), and they should be strictly interpreted as Predictive Information Transfer. This was actually inadvertently shown by Burgess (2013) (see Fig. 5C, D from their paper), where Partial Directed Coherence is shown to be insensitive to immediate couplings, but is actually able to pick up delayed interactions. Here, we examined Symbolic Transfer Entropy in an attempted proof of concept, but we found null results for between-person

connections. Future hyperscanning studies should not take the choice of statistic lightly; here we propose to use a multi-step process. Step zero is to truly define the psychological mechanism that is being indexed by the hyperbrain networks (see next paragraph). As a first analysis step, Circular Correlation and Kraskov's Mutual Information seem to be multi-purpose statistics that will fare well under different contexts (Goldstein et al. 2018). Then, if the experimental manipulation introduces asymmetries between the participants (such as leader-follower roles), Partial Directed Coherence will help determine asymmetrical interactions (Toppi et al. 2016), specially because simulations show that squared partial directed coherence more stable than Granger Causality (Florin et al. 2010). As a final step, Transfer Entropy can be used to characterize the delays of the interactions, as well as cross-frequency interactions (see below), allowing us to build and model the system (Dumas et al. 2014). The bottom line is that the researcher should be fully aware of the limitations and advantages of the statistic they are using in order to be able to interpret the results accordingly. For this, we need to lay down the groundwork of the neural processes these statistics are actually indexing.

The field of brain connectomics as a whole is at a very early stage. Currently, we characterize dyadic relationships between interacting entities of the system under study. This is not optimal, because simulations have shown the existence of "synergistic" systems; or systems with higher level interactions (three, four, five...) that cannot be accounted for by using naive dyadic approaches (James et al. 2016). Despite the current existence of methods to alleviate this, such as Conditional Granger Causality or conditioning Transfer Entropy on multiple signals' pasts, these methods have yet to be widely adopted by the community. Furthermore, the field needs to move from a mass-univariate framework (Groppe et al. 2011) towards a multivariate framework (McIntosh and Mišić 2013; Duan et al. 2015), exploiting the multivariate methods that already exist. Of special interest for us is Graph Theory, which allows us to summarize the characteristics of the networks under different conditions (Müller et al. 2018). Furthermore, when using statistics such

as PDC, we should binarize and threshold our graphs (Toppi et al. 2016). As a first step, dyadic-based interactions will keep the field busy in the near future, but we should monitor developments in the "hypergraph" literature (graphs that characterize higher order interactions—three, four, five...—as opposed to dyadic; James et al. 2016).

Hyperbrain studies have a particular problem: interpretation. Because most of the research published at this point has been very exploratory, a framework regarding the underlying mechanisms of synchronization still needs to be proposed (Liu et al. 2018). Dumas (2011) proposes these synchronies index sensory-motor loops influenced by a bi-directional coupling between participants with the behaviour of each one influencing the other's behaviour in complex and dynamical ways. Along these lines, Sänger et al. (2011) propose a forward model of action regulation to Interpersonal Action Coordination. Taking a step back and trying to make this framework more general, and following up on the proposed ideas of Dikker et al. (2017), Buehlmann and Deco (2010), and Dumas (2011), we propose to regard hyperbrain activity not as a mechanism in itself, but rather a way of operationalizing high level social constructs. As Toppi et al. (2016) concluded, there are interactions that go unnoticed when scanning only one person. Moving towards a two person neuroscience (Dumas 2011; Schilbach et al. 2013) will help us understand complex social mechanisms, such as joint attention (Dikker et al. 2017), empathy (Babiloni et al. 2012), and interactional synchroncy (Müller et al. 2018) in more naturalistic ways and indexed by objective metrics (multivariate statistics on hyperbrain networks). Both the field of brain connectomics and hyperscanning will greatly benefit from being able to draw lines between these high level constructs and the low-level brain activity supporting them (Mu et al. 2018).

In our definition of interactional synchrony, there is always a driver. The problem can potentially arise when the experiment itself becomes the driver, imposing a rhythm causing hyperconnnections to be spurious (e.g., the hyperconnections related to

the metronome frequency in Lindenberger et al. 2009). As Burgess (2013) concluded, spurious hyperconnections can be found under a broad range of experimental conditions. This happens because any systematic difference between conditions (movement, mentation, stimulus) will entrain the brain of the participants (be the driver) as opposed to the participants driving each other. Furthermore, the danger here is that these hyperconnections are not just Type-I errors that can be taken care of by using an appropriate statistical control. We propose here that using appropriate baseline and control conditions, such as a shuffled participant analysis, provides enough statistical power to conclude participants are driving each other (Burgess 2013).

Taking all of the information discussed so far, we propose this framework to approaching the hyperscanning endeavour:

1. Define the psychological mechanism under study (empathy, joint attention, interactional synchrony) and design an experiment with a good baseline and a good control conditions. (Goldstein et al. 2018; Jiang et al. 2015) provide good examples of proper experimental control.

2. Choose a statistic based on the psychological mechanism of interest. For most exploratory studies, either Kraskov's Mutual Information or Circular Coherence (Burgess 2013) should suffice. If there are reasons to believe there will be asymmetries in the way information is flowing between participants, or if such asymmetries are dictated through experimental manipulation, then exploratory studies should use Partial Directed Coherence (Florin et al. 2010). Transfer Entropy should be used to fully characterize and model the underlying system, not as a first step (Wibral et al. 2014).

3. Binarize and threshold the matrices (see Toppi et al. 2016). Matrices can be thresholded using surrogate time series. After this, graph theory (or any multivariate

approach can be used; see Bullmore and Sporns 2009; McIntosh and Mišić 2013; Sporns 2011) to determine the characteristics of the networks. Most importantly, choices need to relate to the hypotheses in question. One of the biggest issues of the guitar ensemble papers (Lindenberger et al. 2009; Sänger et al. 2013; Müller et al. 2018) is that they do several analysis without any real underlying hypotheses. Good studies using graph theory for hypothesis testing are: Toppi et al. 2016; Goldstein et al. 2018; Jiang et al. 2015.

4. For statistical testing, compare either the statistics (multivariate) or the individual connections (mass univariate) to both baseline and control condition/scrambled participants. This step is crucial: using surrogate time series to threshold the matrices will ensure choosing statistically relevant connections, but the interpretation of these will fall short if they are not compared to an appropriate control (see Burgess 2013).

5. To build stronger arguments, correlate either the individual vertices or the graph characteristics with self reports and measurements of behaviour related to the underlying psychological mechanisms (Duan et al. 2015; Jiang et al. 2015).

4.6 Conclusion

EEG Hyperscanning is a novel and promising avenue for the field of neuroscience as a whole. It has implications at a number of distinct levels. At the clinical level, understanding hyperbrain networks will allow us to objectively operationalize high level social constructs such as interactional synchrony and empathy, thus helping us to understand complex disorders such as Autism Spectrum Disorder (Wang et al. 2018; Liu et al. 2018; Dickten and Lehnertz 2014). Identifying brain areas and underlying mechanisms allow

us to both diagnose these disorders better, and measure progress and efficacy of therapies. At the research level, as we have discussed above, the study of hyperbrain networks allows us to operationalize high level constructs, such as joint attention, or even consciousness (Dumas 2011; Toppi et al. 2016; Dikker et al. 2017). As Dumas et al. (2014) mentions, we need to create a multiscale framework for social interaction, from neurobiological accounts of social cognition to its dynamical neural components. Hyperscanning can help elucidate and link these scales. Finally, Hyperscanning can be of interest even at the industry level: it can help us come up with educational settings to elicit better student engagement (Dikker et al. 2017), or even minimize errors in high stakes settings, such as nuclear reactors (Cha and Lee 2018). Here, we proposed for the first time a more unified multivariate framework on how to approach the study of hyperbrain networks in naturalistic settings as indexed by EEG. Despite our null results at the individual connection level, we were able to show differences in network topology due to ambiguity in music structure and roles. Furthermore, these network characteristics correlated with the participants' perceptions of the their performances, but only when there was ambiguity in leadership. In sum, the field of EEG hyperscanning is very fertile and it will benefit greatly from more holistic (both methodological and multidisciplinary) approaches.

Bibliography

Ackerman, J. M. and Bargh, J. A. (2010). Two to Tango: Automatic Social Coordination and the Role of Felt Effort. In: *Effortless Attention: A New Perspective in the Cognitive Science of Attention and Action*. Ed. by B. Bruya. MIT Press Scholarship Online. Chap. 14, 335–372.

Ahn, S., Cho, H., Kwon, M., Kim, K., Kwon, H., Kim, B. S., Chang, W. S., Chang, J. W., and Jun, S. C. (2018). Interbrain phase synchronization during turn-taking verbal interaction—a hyperscanning study using simultaneous EEG/MEG. *Human Brain Mapping* 39(1), 171–188.

Amodio, D. M. and Frith, C. D. (2006). Meeting of minds: the medial frontal cortex and social cognition. *Nature Reviews Neuroscience* 7(4), 268–277.

Astolfi, L., Toppi, J., Borghini, G., Vecchiato, G., Isabella, R., Fallani, F. D. V., Cincotti, F., Salinari, S., Mattia, D., He, B., et al. (2011). Study of the functional hyperconnectivity between couples of pilots during flight simulation: an EEG hyperscanning study. In: *2011 Annual International Conference of the IEEE Engineering in Medicine and Biology Society*. IEEE, 2338–2341.

Babiloni, C., Buffo, P., Vecchio, F., Marzano, N., Del Percio, C., Spada, D., Rossi, S., Bruni, I., Rossini, P. M., and Perani, D. (2012). Brains in concert: Frontal oscillatory alpha rhythms and empathy in professional musicians. *NeuroImage* 60(1), 105–116. ISSN: 1053-8119.

Babiloni, F. and Astolfi, L. (2014). Social neuroscience and hyperscanning techniques: past, present and future. *Neuroscience & Biobehavioral Reviews* 44, 76–93.

Babiloni, F., Astolfi, L., Cincotti, F., Mattia, D., Tocci, A., Tarantino, A., Marciani, M. G., Salinari, S., Gao, S., Colosimo, A., et al. (2007). Cortical activity and connectivity of human brain during the prisoner's dilemma: an EEG hyperscanning study. In: *Engineering in Medicine and Biology Society, 2007. EMBS 2007. 29th Annual International Conference of the IEEE*. IEEE, 4953–4956.

Balconi, M., Gatti, L., and Vanutelli, M. E. (2018). EEG functional connectivity and brain-to-brain coupling in failing cognitive strategies. en. *Consciousness and Cognition* 60, 86–97. ISSN: 10538100.

Bandt, C. and Pompe, B. (2002). Permutation entropy: a natural complexity measure for time series. *Physical Review Letters* 88(17), 174102.

Beard, D. and Gloag, K. (2004). *Musicology: the key concepts*. Routledge.

Ben-Ari, Y. (2001). Developing networks play a similar melody. *Trends in neurosciences* 24(6), 353–360.

Benjamini, Y. and Hochberg, Y. (1995). Controlling the false discovery rate: a practical and powerful approach to multiple testing. *Journal of the royal statistical society. Series B (Methodological)*, 289–300.

Bernier, R., Dawson, G., Webb, S., and Murias, M. (2007). EEG mu rhythm and imitation impairments in individuals with autism spectrum disorder. *Brain and Cognition* 64(3), 228–237.

Bernieri, F. J. and Rosenthal, R. (1991). Interpersonal coordination: Behavior matching and interactional synchrony.

Bigdely-Shamlo, N., Mullen, T., Kothe, C., Su, K.-M., and Robbins, K. A. (2015). The PREP pipeline: standardized preprocessing for large-scale EEG analysis. *Frontiers in Neuroinformatics* 9, 16.

Bilek, E., Ruf, M., Schäfer, A., Akdeniz, C., Calhoun, V. D., Schmahl, C., Demanuele, C., Tost, H., Kirsch, P., and Meyer-Lindenberg, A. (2015). Information flow between

interacting human brains: Identification, validation, and relationship to social expertise. *Proceedings of the National Academy of Sciences*. ISSN: 0027-8424.

Boker, S. M. (1996). Linear and nonlinear dynamical systems data analytic techniques and an application to developmental data. PhD thesis. Citeseer.

Buehlmann, A. and Deco, G. (2010). Optimal information transfer in the cortex through synchronization. *PLoS Computational Biology* 6(9), e1000934.

Bullmore, E. and Sporns, O. (2009). Complex brain networks: graph theoretical analysis of structural and functional systems. *Nature Reviews Neuroscience* 10(3), 186.

Burgess, A. P. (2013). On the interpretation of synchronization in EEG hyperscanning studies: a cautionary note. *Frontiers in Human Neuroscience* 7. ISSN: 1662-5161.

Cha, K.-M. and Lee, H.-C. (2018). A novel qEEG measure of teamwork for human error analysis: An EEG hyperscanning study. *Nuclear Engineering and Technology*. ISSN: 1738-5733.

Chang, A., Livingstone, S. R., Bosnyak, D. J., and Trainor, L. J. (2017). Body sway reflects leadership in joint music performance. *Proceedings of the National Academy of Sciences* 114(21), E4134–E4141. ISSN: 0027-8424.

Cheng, X., Li, X., and Hu, Y. (2015). Synchronous brain activity during cooperative exchange depends on gender of partner: A fNIRS-based hyperscanning study. *Human Brain Mapping* 36(6), 2039–2048.

Ciaramidaro, A., Toppi, J., Casper, C., Freitag, C., Siniatchkin, M., and Astolfi, L. (2018). Multiple-Brain Connectivity During Third Party Punishment: an EEG Hyperscanning Study. *Scientific Reports* 8(1), 6822.

Cirelli, L. K., Einarson, K. M., and Trainor, L. J. (2014). Interpersonal synchrony increases prosocial behavior in infants. *Developmental Science* 17(6), 1003–1011.

Cohen, M. X. (2017). Where does EEG come from and what does it mean? *Trends in neurosciences* 40(4), 208–218.

Cohen, M. X. (2014). *Analyzing neural time series data: theory and practice*. MIT press.

Cutini, S., Scatturin, P., and Zorzi, M. (2011). A new method based on ICBM152 head surface for probe placement in multichannel fNIRS. *Neuroimage* 54(2), 919–927.

Dai, B., Chen, C., Long, Y., Zheng, L., Zhao, H., Bai, X., Liu, W., Zhang, Y., Liu, L., Guo, T., et al. (2018). Neural mechanisms for selectively tuning in to the target speaker in a naturalistic noisy situation. *Nature Communications* 9(1), 2405.

D'Ausilio, A., Novembre, G., Fadiga, L., and Keller, P. E. (2015). What can music tell us about social interaction? *Trends in Cognitive Sciences* 19(3), 111–114.

Davis, M. H. et al. (1980). A multidimensional approach to individual differences in empathy. *JSAS Catalog of Selected Documents in Psychology* 10.

Decety, J., Jackson, P. L., Sommerville, J. A., Chaminade, T., and Meltzoff, A. N. (2004). The neural bases of cooperation and competition: an fMRI investigation. *Neuroimage* 23(2), 744–751.

Delorme, A. and Makeig, S. (2004). EEGLAB: an open source toolbox for analysis of single-trial EEG dynamics including independent component analysis. *Journal of Neuroscience Methods* 134(1), 9–21.

Dickten, H. and Lehnertz, K. (2014). Identifying delayed directional couplings with symbolic transfer entropy. *Physical Review E* 90(6), 062706.

Dikker, S., Wan, L., Davidesco, I., Kaggen, L., Oostrik, M., McClintock, J., Rowland, J., Michalareas, G., Bavel, J. J. V., Ding, M., and Poeppel, D. (2017). Brain-to-Brain Synchrony Tracks Real-World Dynamic Group Interactions in the Classroom. English. *Current Biology* 27 (9), 1375–1380. ISSN: 0960-9822.

Duan, L., Dai, R., Xiao, X., Sun, P., Li, Z., and Zhu, C. (2015). Cluster imaging of multi-brain networks (CIMBN): a general framework for hyperscanning and modeling a group of interacting brains. *Frontiers in Neuroscience* 9, 267.

Duane, T. D. and Behrendt, T. (1965). Extrasensory electroencephalographic induction between identical twins. *Science* 150(3694), 367.

Dumas, G. (2011). Towards a two-body neuroscience. *Communicative & Integrative Biology* 4(3), 349–352.

Dumas, G., Kelso, J., and Nadel, J. (2014). Tackling the social cognition paradox through multi-scale approaches. *Frontiers in Psychology* 5, 882.

Dumas, G., Nadel, J., Soussignan, R., Martinerie, J., and Garnero, L. (2010). Inter-brain synchronization during social interaction. *PLOS ONE* 5(8), e12166.

Ernst, M. D. et al. (2004). Permutation methods: a basis for exact inference. *Statistical Science* 19(4), 676–685.

Florin, E., Gross, J., Pfeifer, J., Fink, G. R., and Timmermann, L. (2010). The effect of filtering on Granger causality based multivariate causality measures. *Neuroimage* 50(2), 577–588.

Fonov, V., Evans, A. C., Botteron, K., Almli, C. R., McKinstry, R. C., Collins, D. L., Group, B. D. C., et al. (2011). Unbiased average age-appropriate atlases for pediatric studies. *Neuroimage* 54(1), 313–327.

Frith, C. D. and Frith, U. (2006). The neural basis of mentalizing. *Neuron* 50(4), 531–534.

Funane, T., Kiguchi, M., Atsumori, H., Sato, H., Kubota, K., and Koizumi, H. (2011). Synchronous activity of two people's prefrontal cortices during a cooperative task measured by simultaneous near-infrared spectroscopy. *Journal of Biomedical Optics* 16(7), 077011-1–077011-10.

Garofalo, M., Nieus, T., Massobrio, P., and Martinoia, S. (2009). Evaluation of the Performance of Information Theory-Based Methods and Cross-Correlation to Estimate the Functional Connectivity in Cortical Networks. *PLoS ONE* 4(8). Ed. by O. Sporns, e6482. ISSN: 1932-6203.

Goldstein, P., Weissman-Fogel, I., Dumas, G., and Shamay-Tsoory, S. G. (2018). Brain-to-brain coupling during handholding is associated with pain reduction. *Proceedings of the National Academy of Sciences* 115(11), E2528–E2537.

Gosling, S. D., Rentfrow, P. J., and Swann Jr, W. B. (2003). A very brief measure of the Big-Five personality domains. *Journal of Research in Personality* 37(6), 504–528.

Groppe, D. M., Urbach, T. P., and Kutas, M. (2011). Mass univariate analysis of event-related brain potentials/fields I: A critical tutorial review. *Psychophysiology* 48(12), 1711–1725.

Hargreaves, D. J. and North, A. C. (1999). The functions of music in everyday life: Redefining the social in music psychology. *Psychology of Music* 27(1), 71–83.

Hari, R. and Kujala, M. V. (2009). Brain basis of human social interaction: from concepts to brain imaging. *Physiological Reviews* 89(2), 453–479.

Hirsch, J., Zhang, X., Noah, J. A., and Ono, Y. (2017). Frontal temporal and parietal systems synchronize within and across brains during live eye-to-eye contact. *NeuroImage* 157, 314–330. ISSN: 1053-8119.

Honey, C. J., Kötter, R., Breakspear, M., and Sporns, O. (2007). Network structure of cerebral cortex shapes functional connectivity on multiple time scales. *Proceedings of the National Academy of Sciences* 104(24), 10240–10245.

House, R. J. and Rizzo, J. R. (1972). Role conflict and ambiguity as critical variables in a model of organizational behavior. *Organizational Behavior and Human Performance* 7(3), 467–505.

Hu, Y., Pan, Y., Shi, X., Cai, Q., Li, X., and Cheng, X. (2018). Inter-brain synchrony and cooperation context in interactive decision making. *Biological Psychology* 133, 54–62.

Iacoboni, M. and Dapretto, M. (2006). The mirror neuron system and the consequences of its dysfunction. *Nature Reviews Neuroscience* 7(12), 942–951.

Iacoboni, M., Woods, R. P., Brass, M., Bekkering, H., Mazziotta, J. C., and Rizzolatti, G. (1999). Cortical mechanisms of human imitation. *Science* 286(5449), 2526–2528.

Ito, S., Hansen, M. E., Heiland, R., Lumsdaine, A., Litke, A. M., and Beggs, J. M. (2011). Extending Transfer Entropy Improves Identification of Effective Connectivity in a Spiking Cortical Network Model. *PLOS ONE* 6(11), 1–13.

James, R. G., Barnett, N., and Crutchfield, J. P. (2016). Information Flows? A Critique of Transfer Entropies. *Physical Review Letters* 116(23). ISSN: 0031-9007, 1079-7114.

Jiang, J., Chen, C., Dai, B., Shi, G., Ding, G., Liu, L., and Lu, C. (2015). Leader emergence through interpersonal neural synchronization. *Proceedings of the National Academy of Sciences* 112(14), 4274–4279. ISSN: 0027-8424.

Jirsa, V. and Müller, V. (2013). Cross-frequency coupling in real and virtual brain networks. *Frontiers in Computational Neuroscience* 7, 78.

Kirschner, S. and Tomasello, M. (2010). Joint music making promotes prosocial behavior in 4-year-old children. *Evolution and Human Behavior* 31(5), 354–364.

Kitzbichler, M. G., Henson, R. N., Smith, M. L., Nathan, P. J., and Bullmore, E. T. (2011). Cognitive effort drives workspace configuration of human brain functional networks. *Journal of Neuroscience* 31(22), 8259–8270.

Koike, T., Tanabe, H. C., Okazaki, S., Nakagawa, E., Sasaki, A. T., Shimada, K., Sugawara, S. K., Takahashi, H. K., Yoshihara, K., Bosch-Bayard, J., et al. (2016). Neural substrates of shared attention as social memory: A hyperscanning functional magnetic resonance imaging study. *NeuroImage* 125, 401–412.

Konvalinka, I., Bauer, M., Stahlhut, C., Hansen, L. K., Roepstorff, A., and Frith, C. D. (2014). Frontal alpha oscillations distinguish leaders from followers: multivariate decoding of mutually interacting brains. *NeuroImage* 94, 79–88.

LaPlante, R. (2018). *Brain Connectivity Toolbox for Python*. `https://github.com/aestrivex/bctpy`.

Lee, U., Blain-Moraes, S., and Mashour, G. A. (2015). Assessing levels of consciousness with symbolic analysis. *Philosophical Transactions of the Royal Society A: Mathematical, Physical and Engineering Sciences* 373(2034), 20140117.

Limpiti, T., Van Veen, B. D., and Wakai, R. T. (2006). Cortical patch basis model for spatially extended neural activity. *IEEE Transactions on Biomedical Engineering* 53(9), 1740–1754.

Lindenberger, U., Li, S.-C., Gruber, W., and Müller, V. (2009). Brains swinging in concert: cortical phase synchronization while playing guitar. *BMC Neuroscience* 10(1), 22.

Liu, D., Liu, S., Liu, X., Zhang, C., Li, A., Jin, C., Chen, Y., Wang, H., and Zhang, X. (2018). Interactive Brain Activity: Review and Progress on EEG-Based Hyperscanning in Social Interactions. *Frontiers in Psychology* 9, 1862.

Lizier, J. T. JIDT: An Information-Theoretic Toolkit for Studying the Dynamics of Complex Systems. *Frontiers in Robotics and AI* 1, 11. ISSN: 2296-9144.

Luck, S. J. (2014). *An introduction to the event-related potential technique*. MIT press.

Lungarella, M. and Sporns, O. (2006). Mapping information flow in sensorimotor networks. *PLoS Computational Biology* 2(10), e144.

MacKay, D. J. and Mac Kay, D. J. (2003). *Information theory, inference and learning algorithms*. Cambridge University Press.

McIntosh, A. R. and Mišić, B. (2013). Multivariate statistical analyses for neuroimaging data. *Annual Review of Psychology* 64, 499–525.

Merriam, A. P. and Merriam, V. (1964). *The Anthropology of Music*. Northwestern University Press. ISBN: 978-0-8101-3309-9.

Modlmeier, A. P., Keiser, C. N., Watters, J. V., Sih, A., and Pruitt, J. N. (2014). The keystone individual concept: an ecological and evolutionary overview. *Animal Behaviour* 89, 53–62.

Mogan, R., Fischer, R., and Bulbulia, J. A. (2017). To be in synchrony or not? A meta-analysis of synchrony's effects on behavior, perception, cognition and affect. *Journal of Experimental Social Psychology* 72, 13–20.

Molenberghs, P., Cunnington, R., and Mattingley, J. B. (2012). Brain regions with mirror properties: a meta-analysis of 125 human fMRI studies. *Neuroscience & Biobehavioral Reviews* 36(1), 341–349.

Montague, P. R., Berns, G. S., Cohen, J. D., McClure, S. M., Pagnoni, G., Dhamala, M., Wiest, M. C., Karpov, I., King, R. D., Apple, N., and Fisher, R. E. (2002). Hyperscanning: Simultaneous fMRI during Linked Social Interactions. *NeuroImage* 16(4), 1159–1164. ISSN: 1053-8119.

Mu, Y., Cerritos, C., and Khan, F. (2018). Neural mechanisms underlying interpersonal coordination: A review of hyperscanning research. *Social and Personality Psychology Compass* 12(11), e12421.

Mullen, T., Kothe, C., Chi, Y. M., Ojeda, A., Kerth, T., Makeig, S., Cauwenberghs, G., and Jung, T.-P. (2013). Real-time modeling and 3D visualization of source dynamics and connectivity using wearable EEG. In: *Engineering in Medicine and Biology Society (EMBC), 2013 35th Annual International Conference of the IEEE*. IEEE, 2184–2187.

Müllensiefen, D., Gingras, B., Musil, J., and Stewart, L. (2014). The musicality of non-musicians: an index for assessing musical sophistication in the general population. *PLOS ONE* 9(2), e89642.

Müller, V. and Lindenberger, U. (2014). Hyper-brain networks support romantic kissing in humans. *PLOS ONE* 9(11), e112080.

Müller, V., Sänger, J., and Lindenberger, U. (2018). Hyperbrain network properties of guitarists playing in quartet. *Annals of the New York Academy of Sciences* 1423(1), 198–210.

Näätänen, R. and Picton, T. (1987). The N1 wave of the human electric and magnetic response to sound: a review and an analysis of the component structure. *Psychophysiology* 24(4), 375–425.

Neuper, C. and Pfurtscheller, G. (2001). Event-related dynamics of cortical rhythms: frequency-specific features and functional correlates. *International Journal of Psychophysiology* 43(1), 41–58.

Newman, M. E. and Girvan, M. (2004). Finding and evaluating community structure in networks. *Physical Review E* 69(2), 026113.

Novembre, G., Sammler, D., and Keller, P. E. (2016). Neural alpha oscillations index the balance between self-other integration and segregation in real-time joint action. en. *Neuropsychologia* 89, 414–425. ISSN: 00283932.

Oliphant, T. E. (2006). *A guide to NumPy*. Vol. 1. Trelgol Publishing USA.

Oliphant, T. E. (2007). Python for scientific computing. *Computing in Science & Engineering* 9(3), 10–20.

Omar, K. M. (2016). Ambiguity: A Critical Factor that Affect Leadership. *Human Resource Management Research* 6(3), 73–81.

Oostendorp, T. F. and Van Oosterom, A. (1989). Source parameter estimation in inhomogeneous volume conductors of arbitrary shape. *IEEE Transactions on Biomedical Engineering* 36(3), 382–391.

Oostenveld, R., Fries, P., Maris, E., and Schoffelen, J.-M. (2011). FieldTrip: open source software for advanced analysis of MEG, EEG, and invasive electrophysiological data. *Computational Intelligence and Neuroscience* 2011, 1.

Osaka, N., Minamoto, T., Yaoi, K., Azuma, M., Shimada, Y. M., and Osaka, M. (2015). How two brains make one synchronized mind in the inferior frontal cortex: fNIRS-based hyperscanning during cooperative singing. *Frontiers in Psychology* 6, 1811.

Pesquita, A., Corlis, T., and Enns, J. T. (2014). Perception of musical cooperation in jazz duets is predicted by social aptitude. *Psychomusicology: Music, Mind, and Brain* 24(2), 173–183.

Pikovsky, A., Rosenblum, M., and Kurths, J. (2003). *Synchronization: a universal concept in nonlinear sciences*. Vol. 12. Cambridge University Press.

Rizzolatti, G. and Craighero, L. (2004). The mirror-neuron system. *Annu. Rev. Neurosci.* 27, 169–192.

Roelfsema, P. R., Engel, A. K., Singer, W., et al. (1997). Visuomotor integration is associated with zero time-lag synchronization among cortical areas. *Nature* 385(6612), 157–161.

Saito, D. N., Tanabe, H. C., Izuma, K., Hayashi, M. J., Morito, Y., Komeda, H., Uchiyama, H., Kosaka, H., Okazawa, H., Fujibayashi, Y., et al. (2010). "Stay tuned": inter-individual neural synchronization during mutual gaze and joint attention. *Frontiers in Integrative Neuroscience* 4, 127.

Sanes, J. N. and Donoghue, J. P. (1993). Oscillations in local field potentials of the primate motor cortex during voluntary movement. *Proceedings of the National Academy of Sciences* 90(10), 4470–4474.

Sänger, J., Lindenberger, U., and Müller, V. (2011). Interactive brains, social minds. *Communicative & Integrative Biology* 4(6), 655–663.

Sänger, J., Müller, V., and Lindenberger, U. (2012). Intra- and interbrain synchronization and network properties when playing guitar in duets. *Frontiers in Human Neuroscience* 6, 312. ISSN: 1662-5161.

Sänger, J., Müller, V., and Lindenberger, U. (2013). Directionality in hyperbrain networks discriminates between leaders and followers in guitar duets. *Frontiers in Human Neuroscience* 7, 234.

Saxe, R. (2006). Uniquely human social cognition. *Current Opinion in Neurobiology* 16(2), 235–239.

Schilbach, L., Timmermans, B., Reddy, V., Costall, A., Bente, G., Schlicht, T., and Vogeley, K. (2013). Toward a second-person neuroscience. en. *Behavioral and Brain Sciences* 36(04), 393–414. ISSN: 0140-525X, 1469-1825.

Schilbach, L., Wilms, M., Eickhoff, S. B., Romanzetti, S., Tepest, R., Bente, G., Shah, N. J., Fink, G. R., and Vogeley, K. (2010). Minds made for sharing: initiating joint attention recruits reward-related neurocircuitry. *Journal of Cognitive Neuroscience* 22(12), 2702–2715.

Schreiber, T. (2000). Measuring information transfer. *Physical Review Letters* 85(2), 461–464.

Shannon, C. E. (1948). A mathematical theory of communication. *Bell System Technical Journal* 27(3), 379–423.

Shannon, C. E. (2001). A mathematical theory of communication. *ACM SIGMOBILE Mobile Computing and Communications Review* 5(1), 3–55.

Smith, J. A. and Foti, R. J. (1998). A pattern approach to the study of leader emergence. *The Leadership Quarterly* 9(2), 147–160.

Soares, J. M., Magalhães, R., Moreira, P. S., Sousa, A., Ganz, E., Sampaio, A., Alves, V., Marques, P., and Sousa, N. (2016). A hitchhiker's guide to functional magnetic resonance imaging. *Frontiers in Neuroscience* 10, 515.

Sperduti, M., Guionnet, S., Fossati, P., and Nadel, J. (2014). Mirror Neuron System and Mentalizing System connect during online social interaction. *Cognitive Processing* 15(3), 307–316.

Sporns, O. (2011). The non-random brain: efficiency, economy, and complex dynamics. *Frontiers in Computational Neuroscience* 5, 5.

Staniek, M. and Lehnertz, K. (2007). Parameter selection for permutation entropy measurements. *International Journal of Bifurcation and Chaos* 17(10), 3729–3733.

Staniek, M. and Lehnertz, K. (2008). Symbolic Transfer Entropy. *Phys. Rev. Lett.* 100 (15), 158101.

Tang, H., Mai, X., Wang, S., Zhu, C., Krueger, F., and Liu, C. (2015). Interpersonal brain synchronization in the right temporo-parietal junction during face-to-face economic exchange. *Social Cognitive and Affective Neuroscience* 11(1), 23–32.

Tognoli, E., Lagarde, J., DeGuzman, G. C., and Kelso, J. S. (2007). The phi complex as a neuromarker of human social coordination. *Proceedings of the National Academy of Sciences* 104(19), 8190–8195.

Toppi, J., Borghini, G., Petti, M., He, E. J., De Giusti, V., He, B., Astolfi, L., and Babiloni, F. (2016). Investigating cooperative behavior in ecological settings: an EEG hyperscanning study. *PLOS ONE* 11(4), e0154236.

Travers, J. and Milgram, S. (1967). The small world problem. *Phychology Today* 1(1), 61–67.

Tzourio-Mazoyer, N., Landeau, B., Papathanassiou, D., Crivello, F., Etard, O., Delcroix, N., Mazoyer, B., and Joliot, M. (2002). Automated anatomical labeling of activations in SPM using a macroscopic anatomical parcellation of the MNI MRI single-subject brain. *Neuroimage* 15(1), 273–289.

Van Overwalle, F. (2011). A dissociation between social mentalizing and general reasoning. *Neuroimage* 54(2), 1589–1599.

Van Overwalle, F. and Baetens, K. (2009). Understanding others' actions and goals by mirror and mentalizing systems: a meta-analysis. *Neuroimage* 48(3), 564–584.

Van Veen, B. D., Van Drongelen, W., Yuchtman, M., and Suzuki, A. (1997). Localization of brain electrical activity via linearly constrained minimum variance spatial filtering. *IEEE Transactions on Biomedical Engineering* 44(9), 867–880.

Varela, F., Lachaux, J.-P., Rodriguez, E., and Martinerie, J. (2001). The brainweb: phase synchronization and large-scale integration. *Nature Reviews Neuroscience* 2(4), 229–239.

Wang, M.-Y., Luan, P., Zhang, J., Xiang, Y.-T., Niu, H., and Yuan, Z. (2018). Concurrent mapping of brain activation from multiple subjects during social interaction by hyperscanning: a mini-review. *Quantitative Imaging in Medicine and Surgery* 8(8), 819–837.

Weber, I., Florin, E., Papen, M. von, and Timmermann, L. (2017). The influence of filtering and downsampling on the estimation of transfer entropy. *PLOS ONE* 12(11). Ed. by J. Ma, e0188210. ISSN: 1932-6203.

Weule, J. et al. (1998). Detection of n: m phase locking from noisy data: application to magnetoencephalography. *Physical Review Letters* 81(15), 3291–3294.

Wibral, M., Pampu, N., Priesemann, V., Siebenhühner, F., Seiwert, H., Lindner, M., Lizier, J. T., and Vicente, R. (2013). Measuring information-transfer delays. *PLOS ONE* 8(2), e55809.

Wibral, M., Vicente, R., and Lizier, J. T. (2014). *Directed information measures in neuroscience*. Berlin Heidelberg. Springer.

Wiener, N. F. (2013). The theory of prediction. In: *Modern Mathematics for the Engineer: First Series*. Ed. by B. Edwin. First. New York: Courier Corporation, 165–191. ISBN: 978-0-486-49746-4.

Wilkinson, D. (2006). *The ambiguity advantage: What great leaders are great at*. New York. Springer.

Appendix A

LIVELab study: Screening Questionnaire (On-line)

Hello! Thank you for taking the time to answer this questionnaire. It will take you about five minutes to complete. We aim to determine your eligibility for our study with these questions. Please take your time to read them carefully. Note that this information will remain anonymous and it won't be shared with anyone. We will get back to you as soon as possible regarding next steps. Should you have any question, please do not hesitate to contact us (orozcoph@mcmaster.ca). -Hector

1. Email address
2. First name
3. Last name
4. Are you right handed or left handed?
5. Do you have any neurological disorders?
    (a) If so, please specify

6. Do you have any hearing problems that you are aware of?

    (a) If so, please specify

7. How many years of musical training do you have?

8. Have you played in any kind of music ensemble before?

    (a) If so, how many years?

    (b) Please specify what kind of ensemble

Appendix B

Music Sheet

Here you can find the four music sheets used for this experiment. For details, see the section 2.3 in chapter 2

3
Canon

Slow (♪=50)

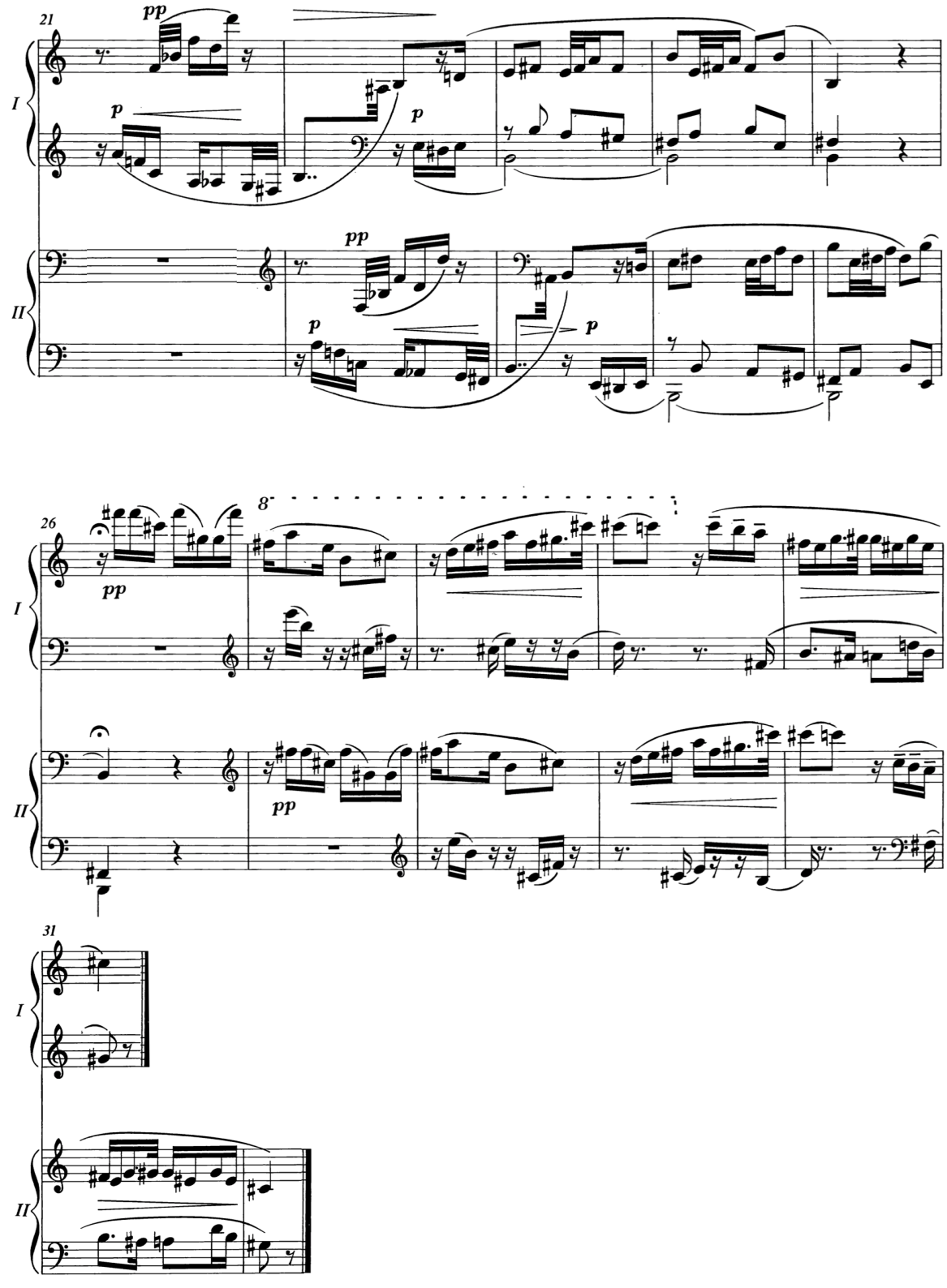

Caprice mélancolique

Reynaldo Hahn
(1874–1947)

Andantino poétique; presque allegretto *(almost allegretto)*

rêveusement, sans beaucoup de nuances
(dreamily, without many nuances)

I

II

rêveusement, sans beaucoup de nuances
(dreamily, without many nuances)

RH

LH

6

rit.

léger *(lightly)*

12

espressivo

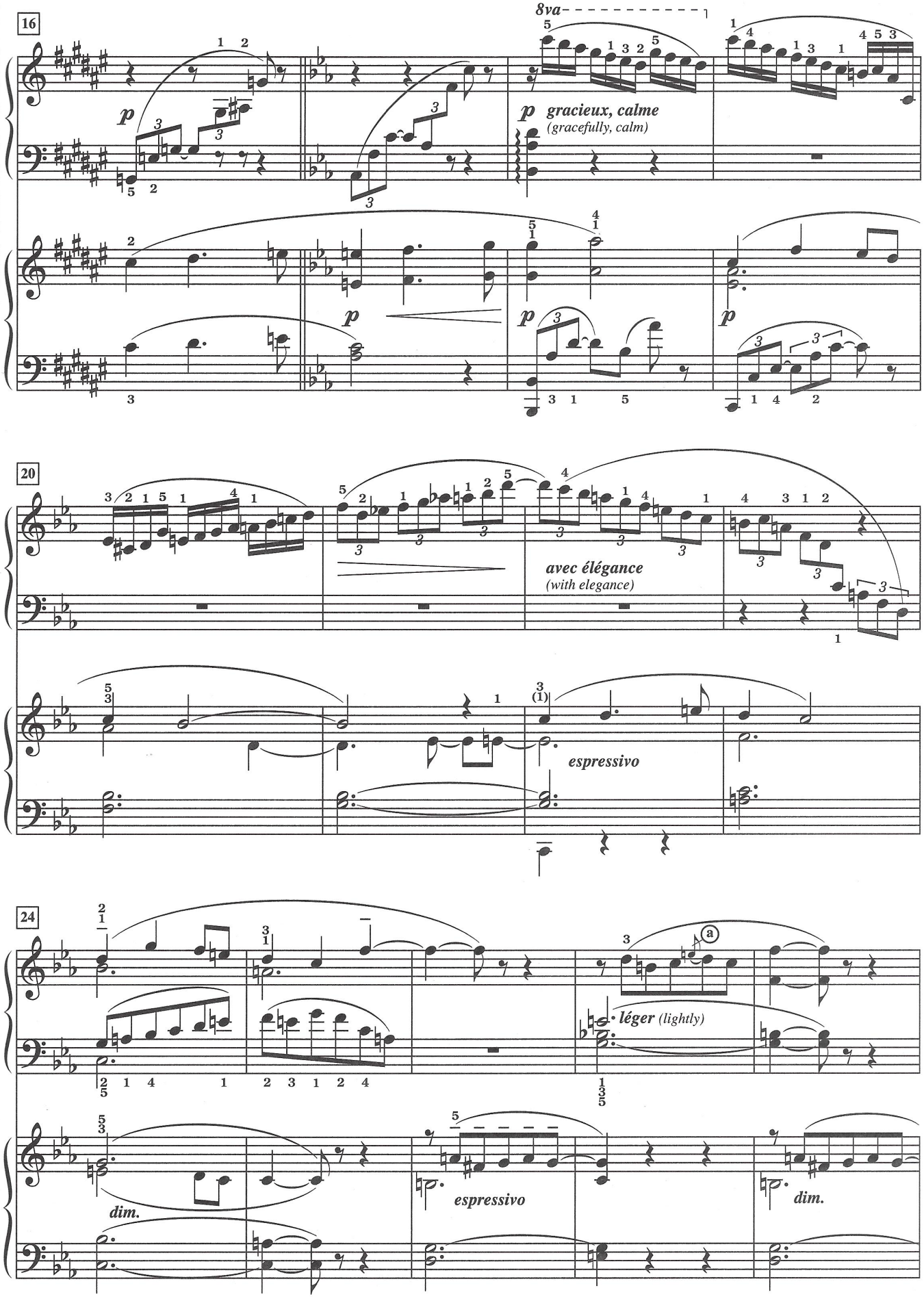

ⓐ Play the grace note slightly before the beat.

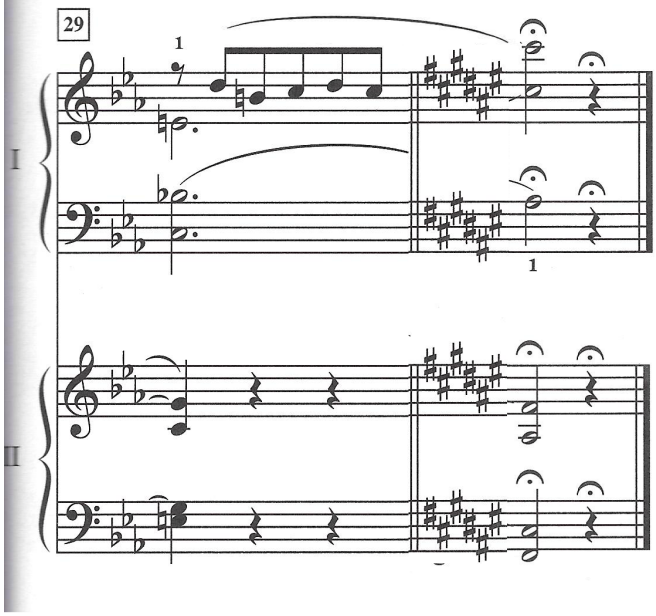
29
1
1
I
II

2.

Entre cloches

(1897)

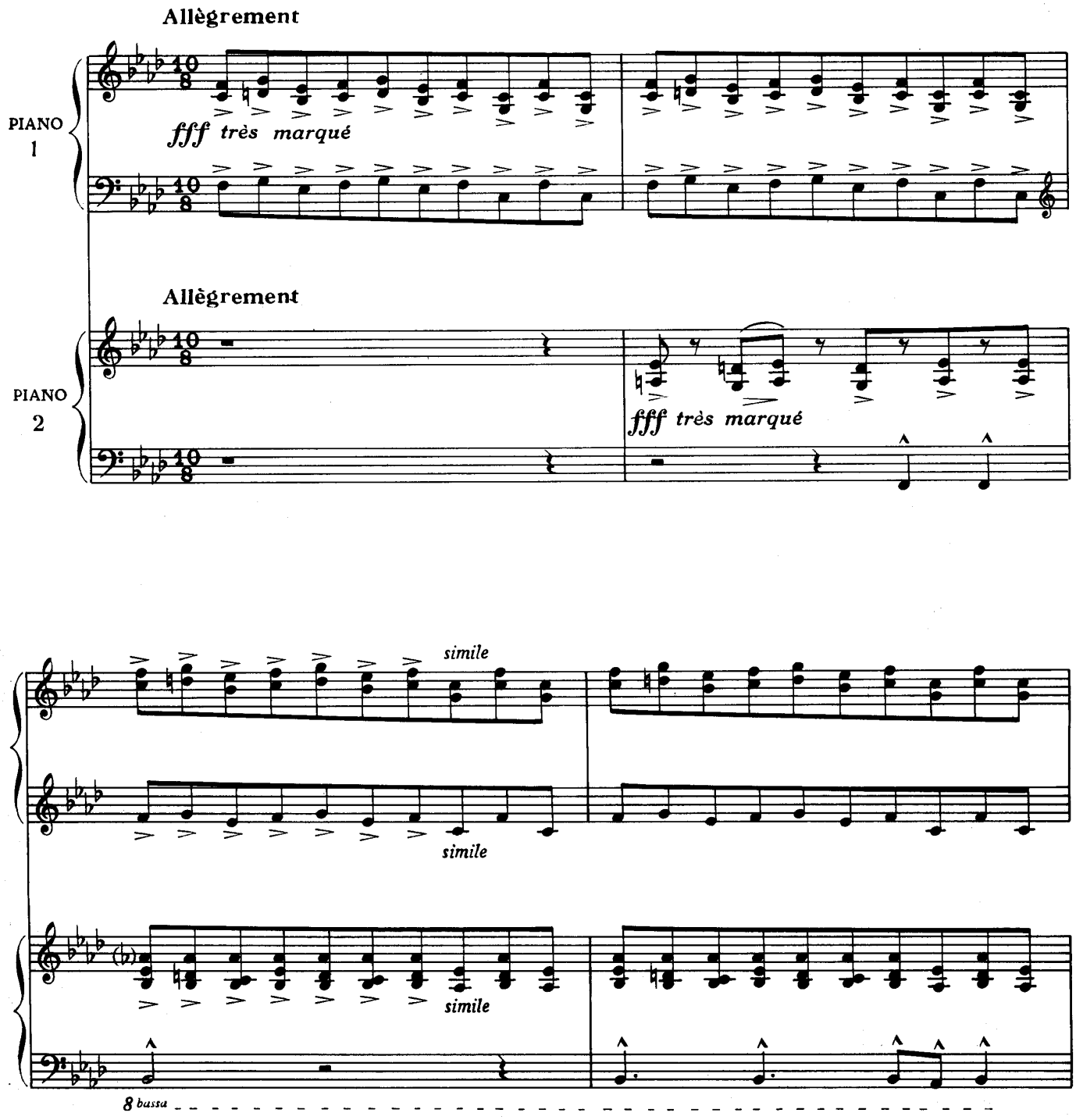

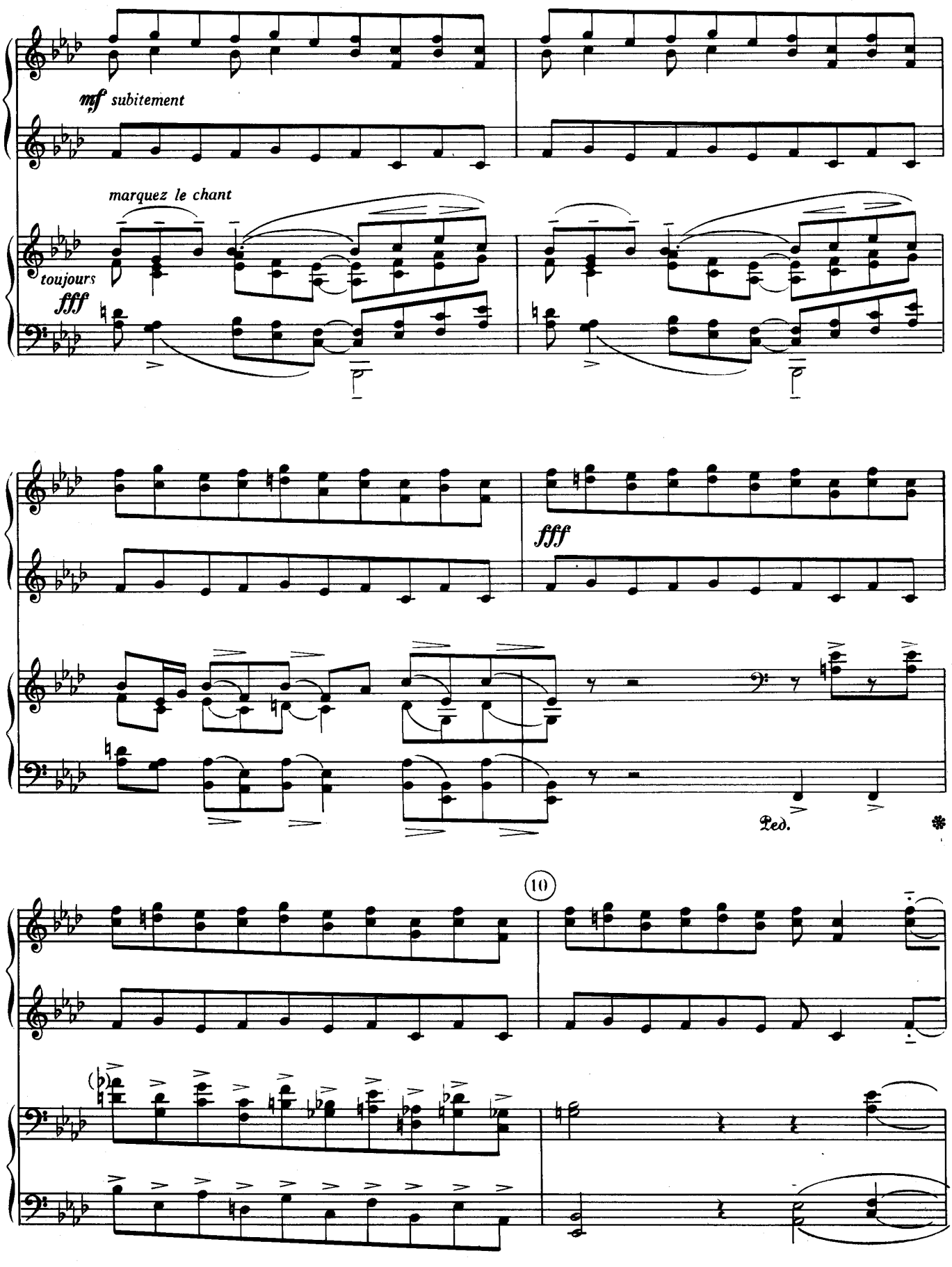
mf subitement
marquez le chant
toujours
fff
fff
Ped.
10

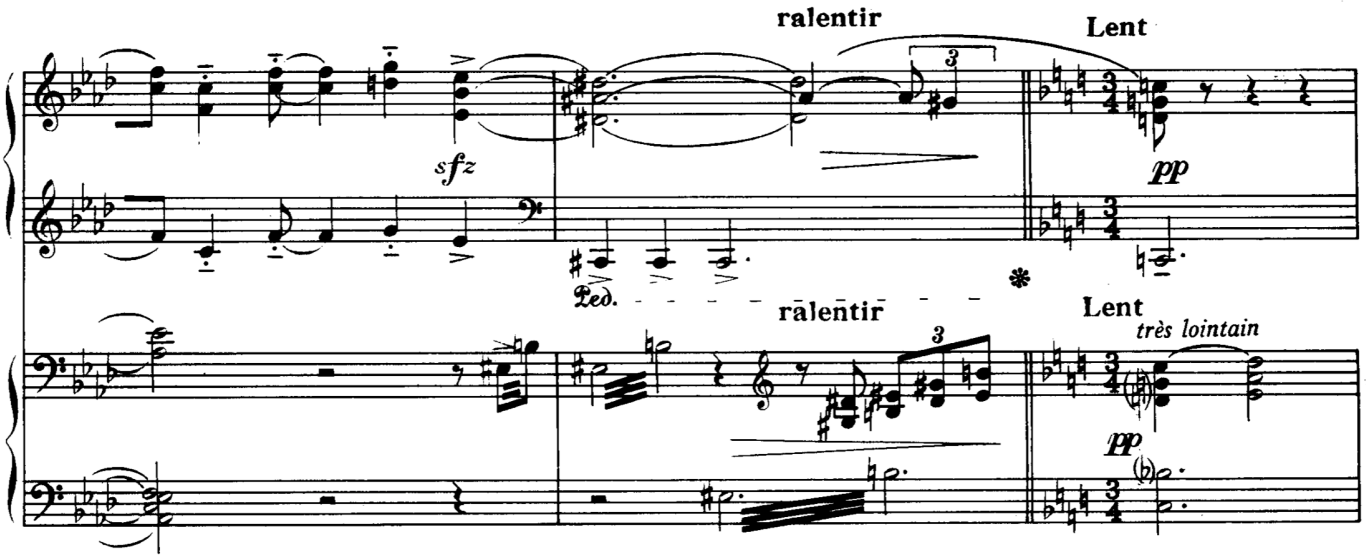
ralentir
Lent
sfz
pp
Ped.
ralentir
Lent
très lointain
pp

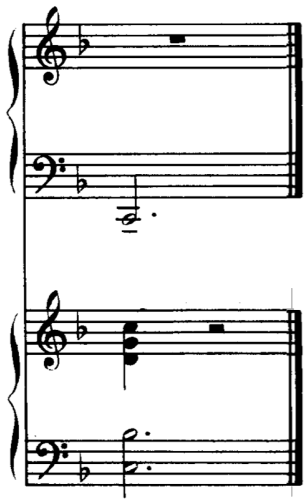

Waltz
from *Suite No. 1*

Anton Arensky (1861–1906)
Op. 15, No. 2

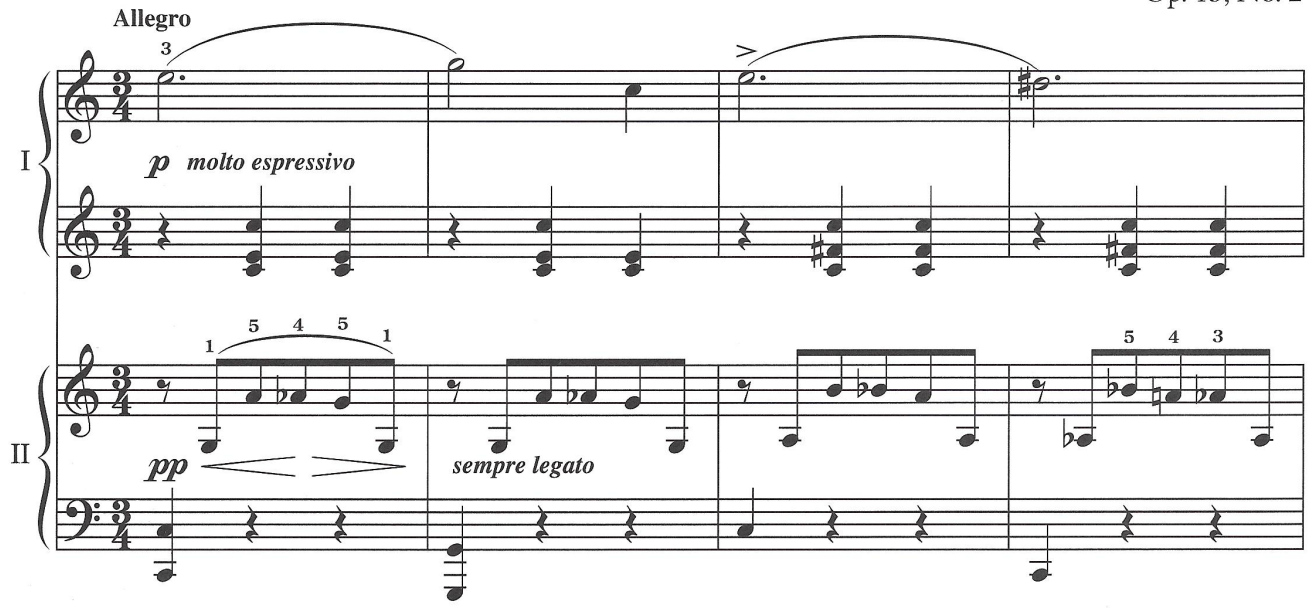

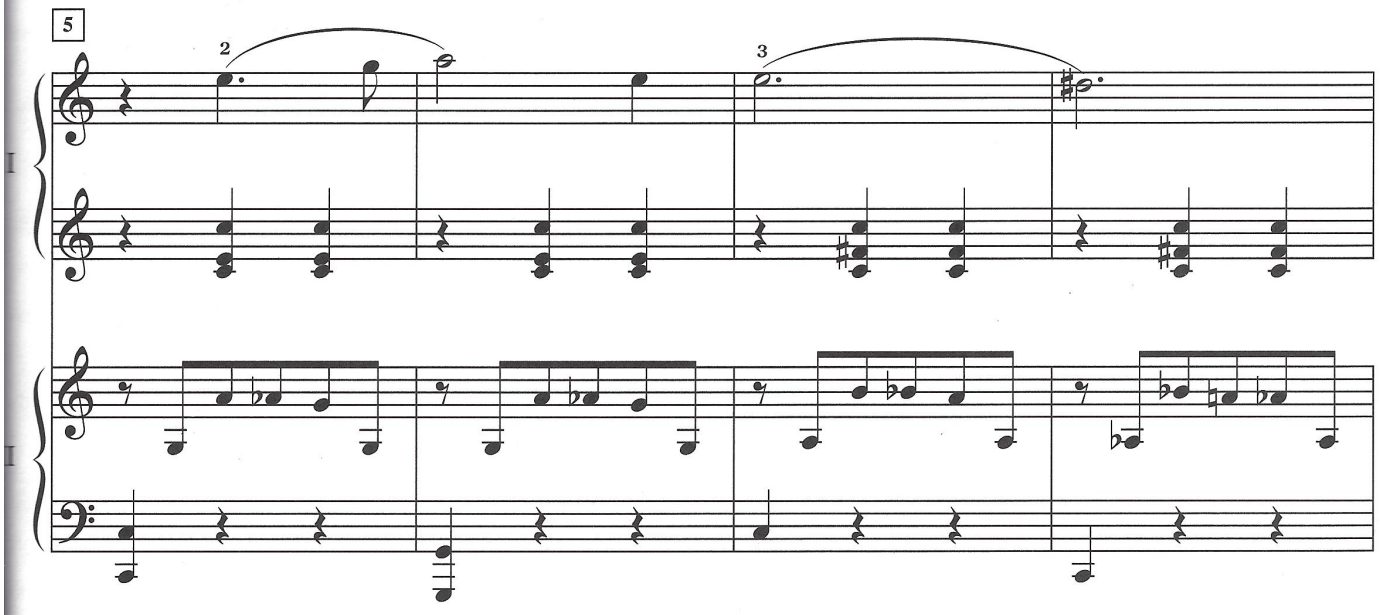

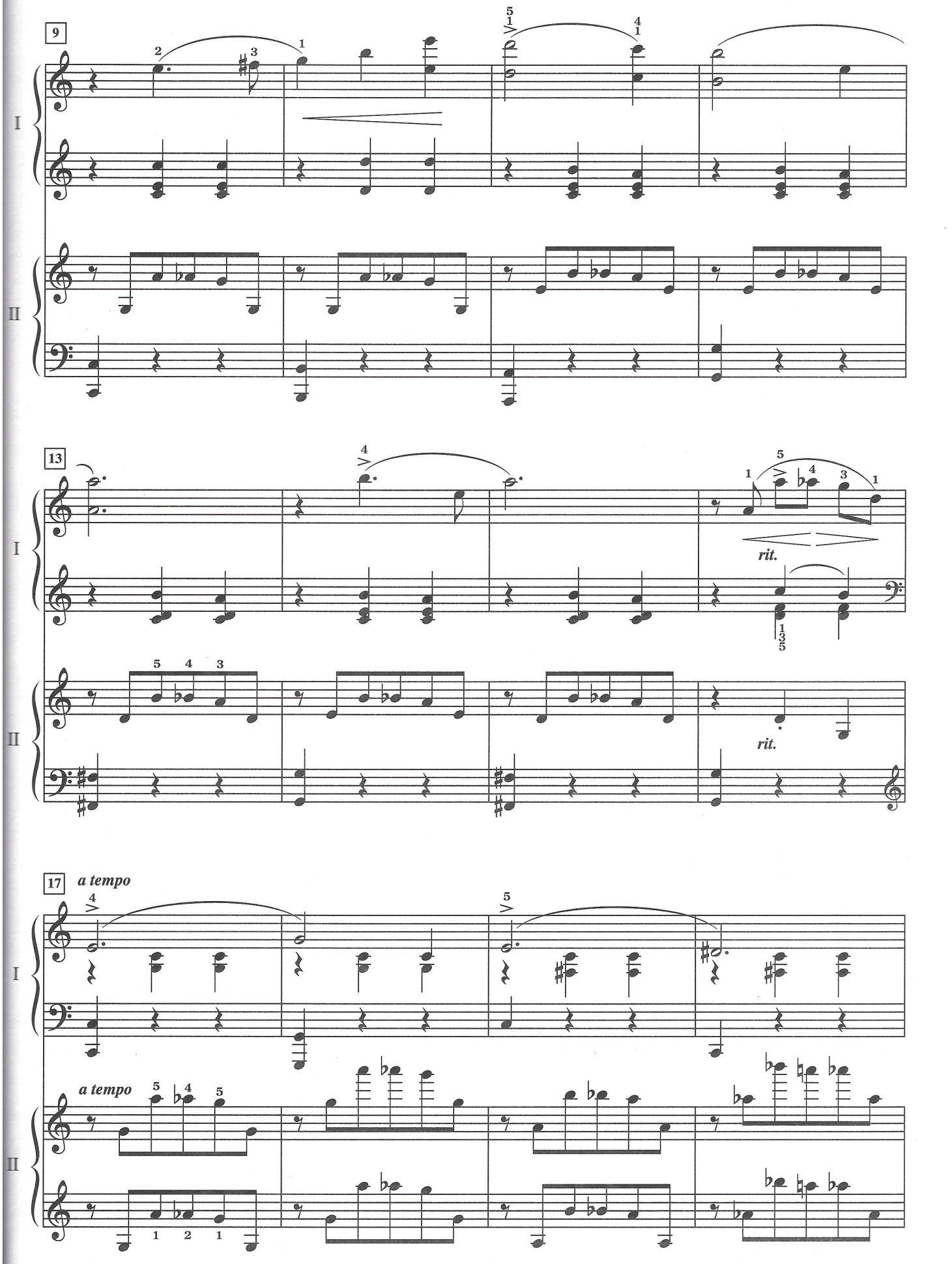
9
I
II
13
rit.
rit.
17
a tempo
a tempo

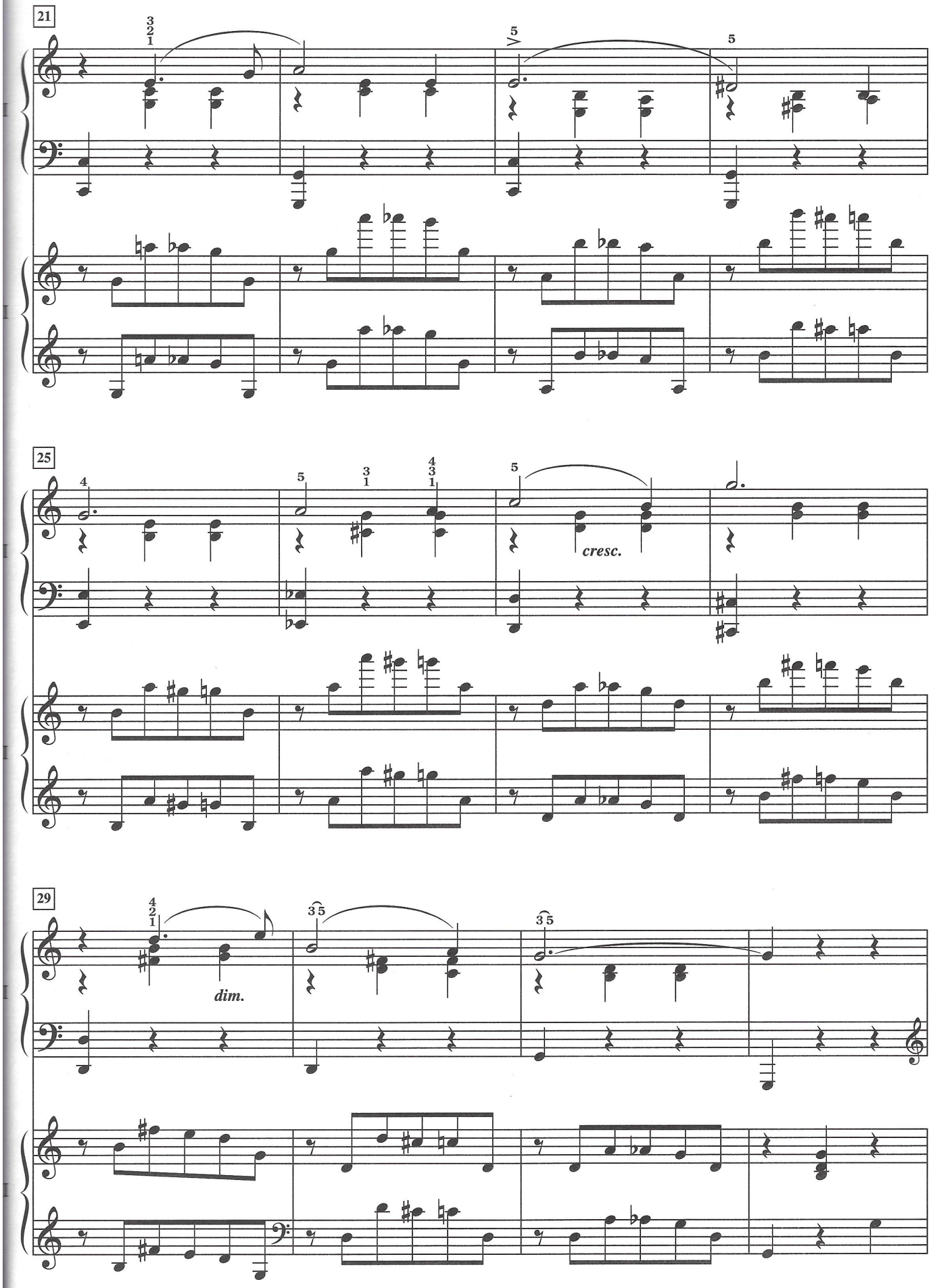
21
25
cresc.
29
dim.

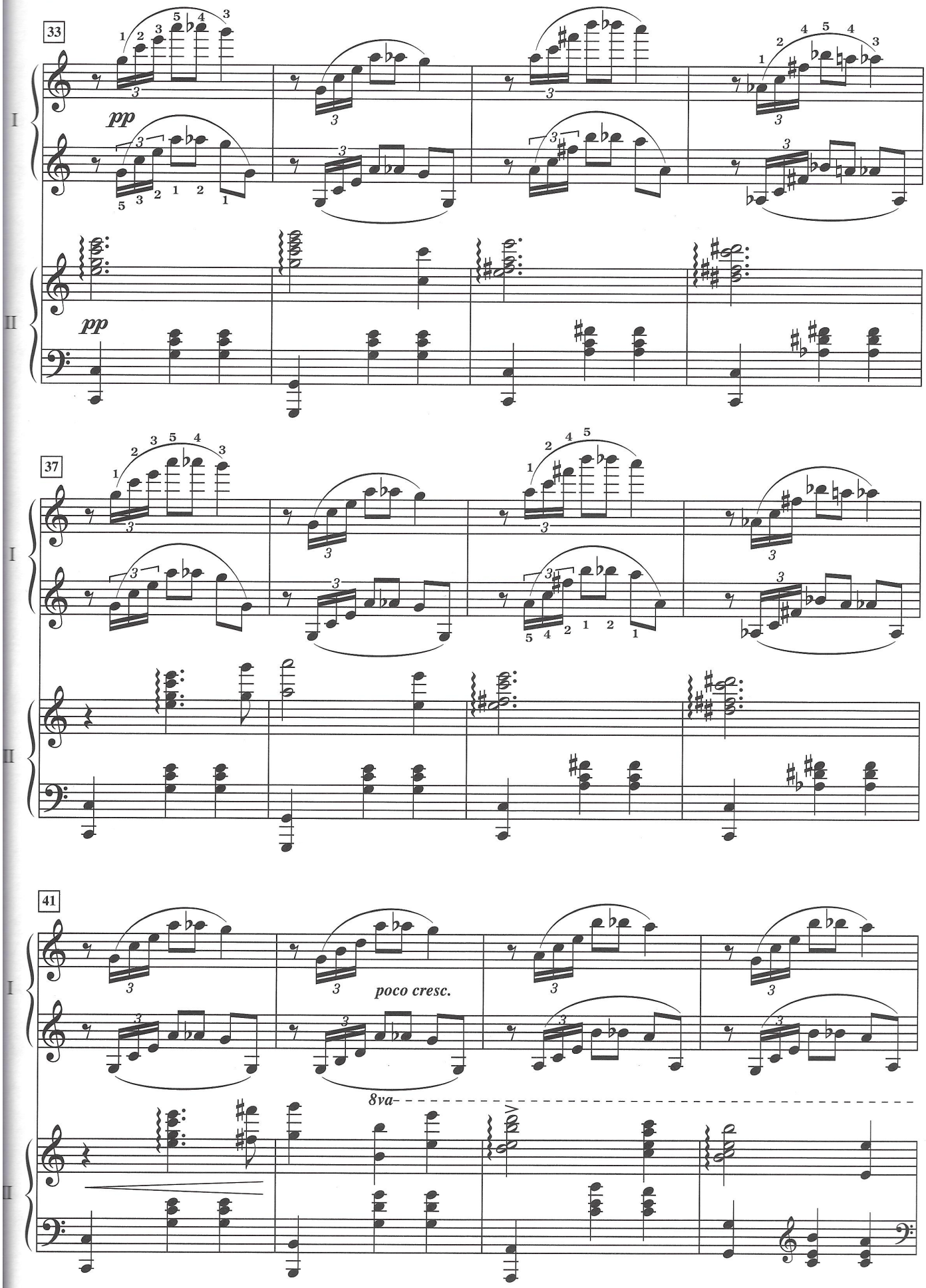
33
pp
pp
37
41
poco cresc.
8va

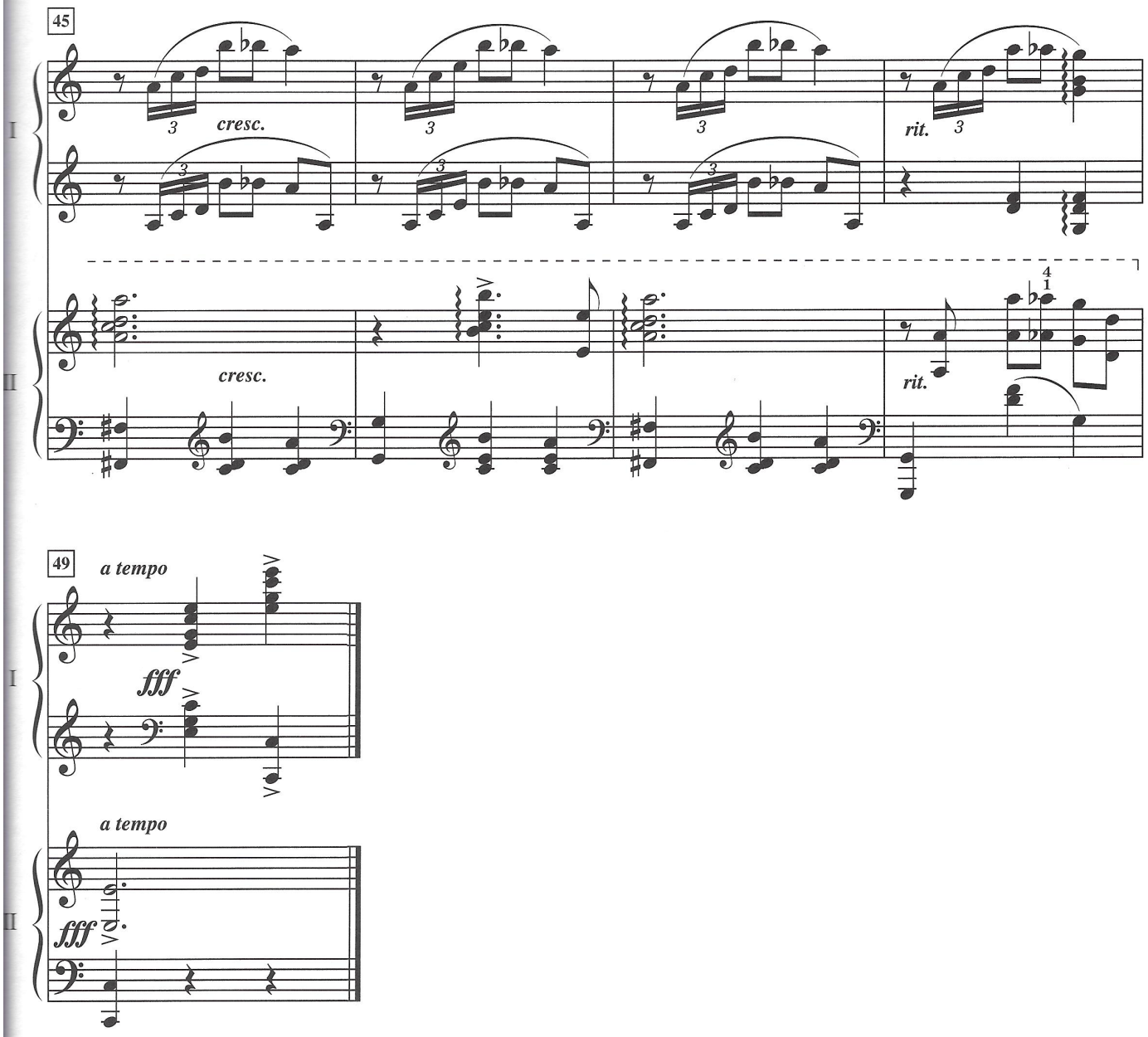
45
I
II
cresc.
cresc.
rit.
rit.
49
a tempo
fff
a tempo
fff

Appendix C

Music Affiliation Questionnaire

The following statements inquire about your thoughts and feelings regarding your music partner. For each item, indicate how well it describes how you currently feel by choosing the appropriate number on the scale. When you have decided on your answer, circle the number on the scale. READ EACH ITEM CAREFULLY BEFORE RESPONDING. Answer as honestly as you can. Know that this answers are anonymous and will not be shown to your music partner. Thank you.

1. I enjoyed playing music with my music partner

Totally Disagree	Mostly Disagree	Slightly Disagree	Slightly Agree	Mostly Agree	Totally Agree
1	2	3	4	5	6

2. I would like to play again with my music partner

Totally Disagree	Mostly Disagree	Slightly Disagree	Slightly Agree	Mostly Agree	Totally Agree
1	2	3	4	5	6

3. When I played Secondo, I had no trouble musically accompanying my music partner

Totally Disagree 1	Mostly Disagree 2	Slightly Disagree 3	Slightly Agree 4	Mostly Agree 5	Totally Agree 6

4. I would like to become friends with my music partner

Totally Disagree 1	Mostly Disagree 2	Slightly Disagree 3	Slightly Agree 4	Mostly Agree 5	Totally Agree 6

5. If my music partner needed help, I would help them

Totally Disagree 1	Mostly Disagree 2	Slightly Disagree 3	Slightly Agree 4	Mostly Agree 5	Totally Agree 6

6. I would trust my music partner with a secret

Totally Disagree 1	Mostly Disagree 2	Slightly Disagree 3	Slightly Agree 4	Mostly Agree 5	Totally Agree 6

Appendix D

LIVELab Experimental Setup

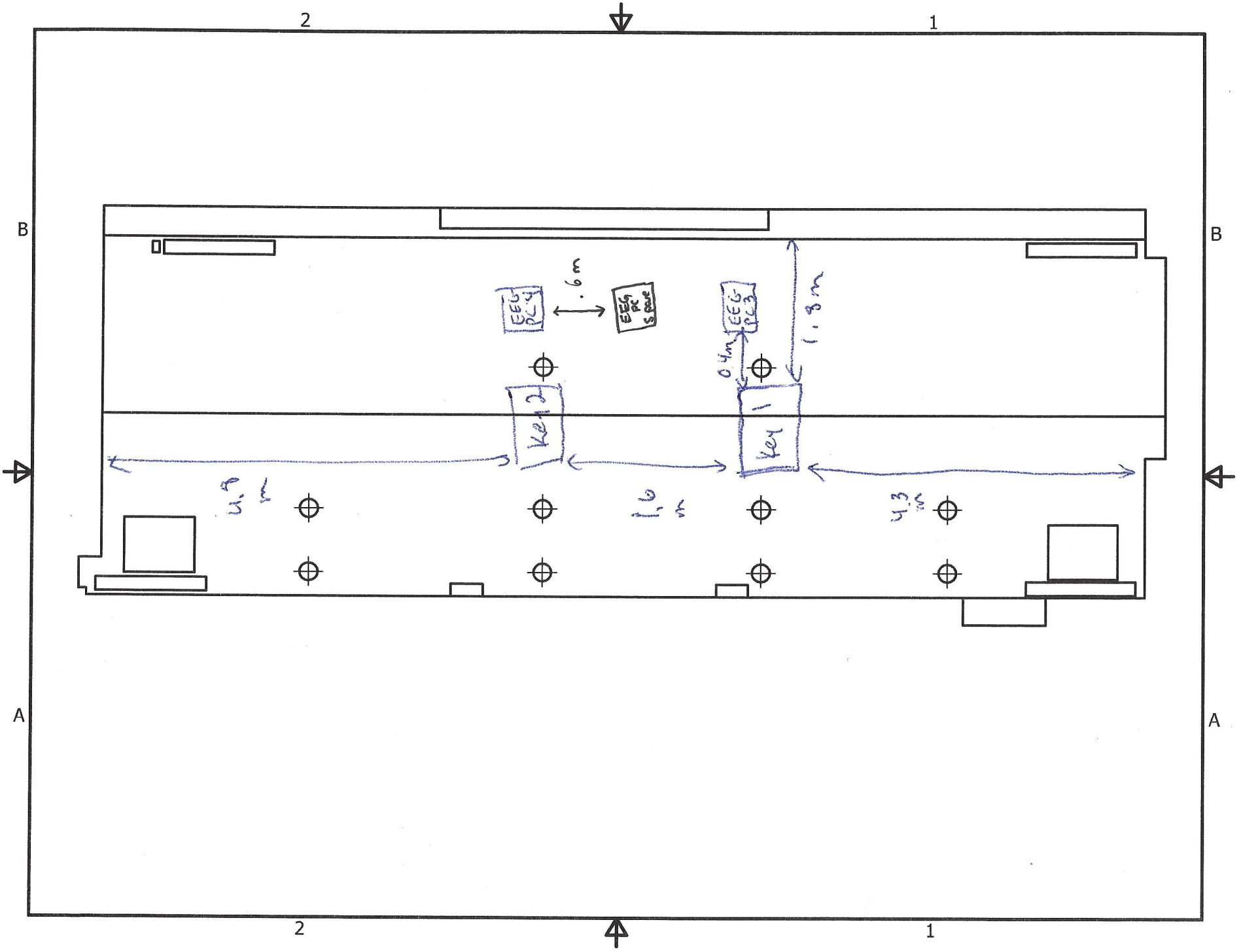
2
1
B
A
EEG PC4
EEG PC Space
EEG C3
0.4m
1.8m
Key 2
Key 1
1.9 m
1.6 m
1.3 m

Appendix E

Perception of Music Performance Questionnaire

Perception of Music Performance Questionnaire (PMPQ)

The following statements inquire about different aspects of the last piano performance. Rate each scale using a small vertical line. READ EACH ITEM CAREFULLY BEFORE RESPONDING. Answer as honestly as you can. Know that this answers are anonymous and will not be shown to your music partner. Thank you.

SYNERGY

Synergy refers to the notion that a "whole" is greater than the sum of the individual parts. That is, **there is added value derived from cooperating and playing together.**

SYNCHRONY

Synchrony refers to the notion of temporal coordination. That is, **when playing synchronized, each note of the music is temporally precise.**

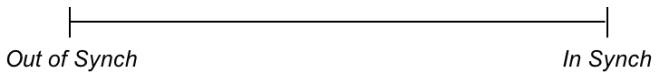

QUALITY

Quality refers to how good or bad the performance was.

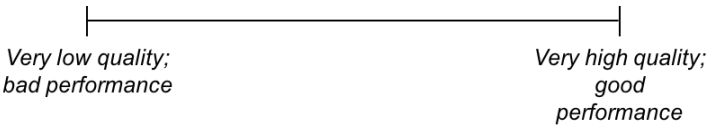

ANXIETY

Anxiety refers to an emotional state of inner turmoil and apprehension. It includes feelings of tension, nervousness and worry.

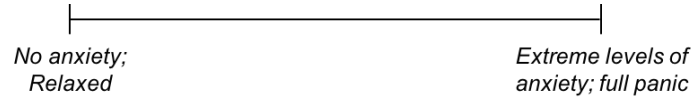

Appendix F

Participant Information Form

PARTICIPANT INFORMATION FORM

The following information will be kept confidential.

First Name: _____ Age: _____ Sex: _____

1. Do you **currently** play a musical instrument (including voice)?
   _____ Yes (go to question #2) _____ No (skip to question #3)

2. Please provide the following information for each instrument you **currently** play, starting with the one that you consider your primary instrument.

Instrument	**Ages during which you have played this instrument**	**Ages during which you took music lessons on this instrument**	**Hours per week that you play this instrument** currently

Please describe the situations in which you play (e.g., alone, in a small ensemble or band, in a large orchestra or choir, etc.)

_____

_____

3. Have you **previously** played an instrument (including voice) that you no longer play (e.g., as a child)?
   ____ Yes (go to question #4) _____ No (skip to question #5)

4. Please provide the following information for each instrument that you **used to play.**

Instrument	**Ages during which you played this instrument**	**Ages during which you took lessons on this instrument**	**Hours per week that you played this instrument**

Please describe the situations in which you played (e.g., alone, in a small ensemble or band, in a large orchestra or choir, etc.)

_____

_____

5. Do you have **dance** experience (lessons, amateur or professional experience)?
   _____ Yes (go to question #6) _____ No (skip to question #7)

6. Please provide the following information for each **dance style** you are familiar with.

Style of dance	Ages during which you danced this style	Ages during which you took lessons in this style	Hours per week that you dance(d) this style

Please describe the situations in which you dance(d) (e.g. alone, with family, in group classes)

_____

7. Please indicate the highest formal music levels (instrumental/vocal performance, dance or theory) that you have achieved (e.g. Royal Conservatory, Theory, Suzuki Books, etc).

Instrument/Course/Subject	Level

8. Do you play music professionally? If so, please describe the situations in which you are paid to play music (e.g. performance, teaching, playing in bands, DJ, etc):

_____

9. Have you played music in an ensemble? If so, please specify the number of years, type of ensemble and your role (melodist, accompanist, leader…)

_____

10. Describe your **current** recreational music and dance activities (e.g., "jam sessions" with friends, singing karaoke, dancing at nightclubs, etc.):

_____

_____

11. For how many years have you played any instrument (including voice) or danced regularly and consistently (e.g. at least 3x per week, most weeks of the year?)
    _____

12. How often do you attend musical or dance concerts or performances?
    _____

13. Have you had any formal ear training*? ___ Yes (____ years) ___ No
    ___ Not sure

*** In ear training or "aural skills" lessons, musicians learn to identify musical elements such as intervals, chords and rhythms, simply by hearing them.**

14. Do you play by ear*? ____Yes ____ No

*** playing or learning to play a piece of music by listening to a musical rendition, without the aid of printed material**

15. Do you have absolute/"perfect" pitch*? ___Yes ___ No ___ Not sure

*** absolute pitch is the ability to name notes without a reference, e.g. to hear a tone and immediately know it was a "C"**

16. Can you name a note if you are given a reference*? ___ Yes ____No ___NS

*** e.g., if you heard two notes on the piano and were told the first one was a "C", could you name the other note?**

17. To the best of your knowledge, are you tone deaf*? ___ Yes ____No ___NS

*** tone deafness is when you are unable to perceive differences of musical pitch accurately**

18. How many hours per week do you spend listening to music? _____ hours/week

19. Please describe your regular listening habits (e.g., listen to mp3/iPod on the bus, play stereo at home, etc.):

_____

_____

20. Do you pay close attention when listening to music? Please rank from 1 to 5 (music is background only) 1 2 3 4 5 (always pay close attention)

21. What styles of music do you listen to (e.g., rock, r&b, classical, traditional/folk, etc.)

_____

_____

22. Do any of your close friends or family members play a musical instrument (or did so in the past)? If so, please provide the following information.

Their relation to you	**Instrument that they play(ed)**	**How old were you (age range) when you heard them play?**	**Number of hours per week that you hear/heard them play**

23. Please briefly describe your other main activities or interests (e.g., sports, outdoor activities, art, reading, video game playing, etc.).

_____

_____

24. What is the highest level of education you have completed, or are currently completing?

____ High school / High school equivalency

____ College / skilled trade training program

____ University undergraduate (e.g. B.Sc., H.B.A, etc)

____ Graduate school – professional or academic (e.g. LLD, MD, Ph.D)

____ Other (please specify) _____

____ Prefer not to say

24. What is your current employment status?

____ Student

____ Employed – Full time

____ Employed – Part time

____ Unemployed

____ Retired

____ Other

____ Prefer not to say

25. Please indicate the range that reflects your annual household income

____ less than $30,000

____ $30,000 - $60,000

____ $60,000 - $90,000

____ $90,000 - $120,000

____ $120,000 - $150,000

____ greater than $150,000

____ Prefer not to say

24. Do you **currently** speak any other languages besides English? ___ Yes ___ No
If yes, please indicate which language(s) including English, the percentage of time that you use them, and the situations in which you speak each language.

Language	**Percentage (%) of time that you use this language**	**Situations in which you use the language**

25. Did you **previously** speak any languages other than English that you no longer speak? If yes, please list and describe the ages and situations in which you used these languages:

_____

_____

26. Have you lived in North America for all your life? ____Yes ____No
If not, please describe where else you have lived, and for how long.

Location	**How old were you (age range) when you lived there?**

27. Do you have any hearing problems that you are aware of? If yes, please specify.

_____

28. Please indicate whether you are left or right handed when performing the following tasks:

	Left	Right	Both
Writing	_____	_____	_____

Drawing	_____	_____	_____
Using a Spoon	_____	_____	_____
Throwing	_____	_____	_____
Kicking	_____	_____	_____

29. Do you wear glasses or contacts? ____Yes ____No

30. Do you currently have a cold? ____Yes ____No

31. Do you have any major neurological disorders? If yes, please specify.

_____

32. Do you take any medications regularly? If yes, please specify.

_____

33. Have you lost consciousness in the past 6 months? ____Yes ____No

34. How anxious did you feel last month?

35. How stressed did you feel last month?

Thank you for your assistance!

Appendix G

Top Hyperbrain Network Connections - Values and Significance

Here you will find all the top 48 between connections at each delay for the playing STE (average of all pieces) and their comparison to baseline and scrambled-pairs values. See Section 2.7.5 for more information.

Table A7.1: Top Between Connections: Comparison between baseline, playing, and scrambled conditions

Neuro Source	Neuro Target	Frequency Source	Frequency Target	Info Source	Infor Target	STE	Baseline STE	Scrambled STE	Baseline P Value (FDR)	Scrambled P Value (FDR)
Insula Left	Motor Right	beta	gamma	leader	follower	0.003040272	0.000980372	0.003632281	0.0002	0.921875
Insula Left	Occipital Left	beta	gamma	leader	follower	0.002959146	0.001031336	0.003624427	0.0002	0.921875
Insula Left	Occipital Right	beta	beta	follower	leader	0.003012067	0.001096499	0.003642387	0.0002	0.921875
Insula Left	Parietal Right	gamma	gamma	leader	follower	0.002969122	0.001108114	0.003638136	0.0002	0.921875
Insula Left	Prefrontal Right	beta	gamma	follower	leader	0.003018758	0.001206983	0.003617069	0.0002	0.921875
Insula Right	Insula Right	gamma	beta	follower	leader	0.002979424	0.000919886	0.003544427	0.0002	0.921875
Insula Right	Motor Right	beta	beta	leader	follower	0.002965014	0.001021114	0.003553263	0.0002	0.921875
Insula Right	Parietal Left	gamma	gamma	follower	leader	0.003003705	0.00115268	0.003497809	0.0002	0.921875
Insula Right	Prefrontal Right	beta	gamma	follower	leader	0.00298087	0.001193992	0.003609673	0.0002	0.921875
Insula Right	Temporal Left	gamma	beta	follower	leader	0.002977074	0.001229784	0.003627144	0.0002	0.921875
Insula Right	Temporal Right	beta	beta	follower	leader	0.002952373	0.001078044	0.003530927	0.0002	0.921875
Motor Left	Insula Left	beta	beta	leader	follower	0.002963739	0.001241239	0.003518466	0.0002	0.921875
Motor Left	Insula Left	gamma	gamma	leader	follower	0.002996402	0.001086011	0.003781679	0.0002	0.921875
Motor Left	Motor Right	beta	beta	follower	leader	0.002974058	0.001126291	0.003603986	0.0002	0.921875
Motor Left	Occipital Left	gamma	gamma	leader	follower	0.00297787	0.001146408	0.003653625	0.0002	0.921875
Motor Right	Motor Right	beta	beta	leader	follower	0.003083236	0.001171066	0.003560303	0.0002	0.921875
Motor Right	Occipital Right	gamma	beta	leader	follower	0.002973556	0.001073613	0.003630668	0.0002	0.921875
Motor Right	Parietal Right	beta	beta	leader	follower	0.002974547	0.001053261	0.003607427	0.0002	0.921875
Motor Right	Temporal Left	beta	beta	follower	leader	0.003030856	0.001118911	0.00352188	0.0002	0.921875
Motor Right	Temporal Left	gamma	beta	leader	follower	0.002985521	0.001113232	0.003463593	0.0002	0.921875
Occipital Left	Insula Left	gamma	beta	leader	follower	0.002957041	0.00116908	0.003569297	0.0002	0.921875
Occipital Left	Occipital Right	beta	beta	follower	leader	0.002972493	0.001160671	0.003526414	0.0002	0.921875
Occipital Left	Occipital Right	gamma	beta	follower	leader	0.003006376	0.001024407	0.003551011	0.0002	0.921875
Occipital Left	Parietal Right	gamma	beta	follower	leader	0.002971591	0.001004361	0.003515268	0.0002	0.921875
Occipital Left	Prefrontal Right	beta	beta	follower	leader	0.003022301	0.001016072	0.003702606	0.0002	0.921875
Occipital Right	Parietal Right	beta	gamma	leader	follower	0.003018189	0.001199198	0.003783888	0.0002	0.921875
Occipital Right	Prefrontal Left	beta	gamma	leader	follower	0.002953732	0.00114599	0.003591014	0.0002	0.921875
Occipital Right	Prefrontal Left	gamma	gamma	follower	leader	0.00297155	0.001125158	0.003435529	0.0002	0.921875
Occipital Right	Temporal Left	gamma	gamma	leader	follower	0.003012323	0.001217606	0.003481963	0.0002	0.921875
Parietal Left	Occipital Right	beta	beta	follower	leader	0.002982212	0.001082189	0.00371512	0.0002	0.921875
Parietal Left	Prefrontal Right	beta	gamma	leader	follower	0.002989087	0.001063419	0.003700664	0.0002	0.921875
Parietal Right	Insula Left	gamma	gamma	leader	follower	0.002963067	0.0010778	0.003689513	0.0002	0.921875
Parietal Right	Prefrontal Left	beta	beta	follower	leader	0.00295183	0.001124522	0.003793934	0.0002	0.921875
Parietal Right	Temporal Right	beta	beta	follower	leader	0.002969092	0.001090707	0.003602164	0.0002	0.921875
Prefrontal Left	Occipital Right	beta	beta	follower	leader	0.002961046	0.001061782	0.003773848	0.0002	0.921875
Prefrontal Left	Occipital Right	beta	gamma	follower	leader	0.002980375	0.000979618	0.003475608	0.0002	0.921875
Prefrontal Left	Parietal Right	gamma	gamma	follower	leader	0.003030231	0.001171279	0.003736824	0.0002	0.921875
Prefrontal Left	Prefrontal Left	beta	beta	leader	follower	0.002960907	0.001132514	0.003651269	0.0002	0.921875
Prefrontal Left	Temporal Right	beta	beta	leader	follower	0.002963054	0.001119733	0.003760432	0.0002	0.921875
Prefrontal Right	Insula Right	beta	beta	follower	leader	0.002964989	0.001146298	0.003784285	0.0002	0.921875
Prefrontal Right	Parietal Left	gamma	gamma	leader	follower	0.003003778	0.001094844	0.003724828	0.0002	0.921875
Temporal Left	Occipital Left	beta	beta	follower	leader	0.002965645	0.001012058	0.003588308	0.0002	0.921875
Temporal Right	Insula Right	gamma	beta	follower	leader	0.002981493	0.000846547	0.003635822	0.0002	0.921875
Temporal Right	Motor Right	beta	beta	leader	follower	0.003020787	0.001056804	0.003478411	0.0002	0.921875
Temporal Right	Parietal Left	gamma	beta	follower	leader	0.002977759	0.000922063	0.003602728	0.0002	0.921875
Temporal Right	Parietal Right	beta	gamma	follower	leader	0.002981327	0.001087813	0.003727172	0.0002	0.921875
Temporal Right	Prefrontal Right	beta	beta	follower	leader	0.002954769	0.000963123	0.003564896	0.0002	0.921875

Table A7.2: Top Between Connections: Comparison between baseline, playing, and scrambled conditions

Neuro Source	Neuro Target	Frequency Source	Frequency Target	Info Source	Infor Target	STE	Baseline STE	Scrambled STE	Baseline P Value (FDR)	Scrambled P Value (FDR)
Insula Left	Prefrontal Right	beta	gamma	follower	leader	0.002999391	0.001204265	0.003629189	0.0002	0.953125
Insula Right	Insula Left	gamma	gamma	leader	follower	0.002978422	0.00102134	0.003761068	0.0002	0.953125
Insula Right	Insula Right	beta	beta	follower	leader	0.003046495	0.001191505	0.003528944	0.0002	0.953125
Insula Right	Parietal Right	gamma	gamma	leader	follower	0.002978145	0.001136874	0.003745295	0.0002	0.953125
Insula Right	Prefrontal Left	gamma	gamma	follower	leader	0.003018378	0.001108302	0.003731528	0.0002	0.953125
Insula Right	Temporal Left	beta	gamma	leader	follower	0.002996987	0.001002847	0.003475908	0.0002	0.953125
Motor Left	Occipital Right	gamma	gamma	follower	leader	0.003082347	0.001024668	0.003739867	0.0002	0.953125
Motor Left	Prefrontal Right	gamma	gamma	leader	follower	0.00308726	0.000967844	0.003741555	0.0002	0.953125
Motor Right	Occipital Left	gamma	beta	follower	leader	0.003029309	0.001162975	0.003456079	0.0002	0.953125
Motor Right	Parietal Left	beta	gamma	leader	follower	0.003092132	0.001032539	0.003657281	0.0002	0.953125
Motor Right	Prefrontal Left	gamma	beta	leader	follower	0.003018181	0.001158428	0.003652448	0.0002	0.953125
Motor Right	Temporal Left	beta	gamma	leader	follower	0.003046021	0.001131517	0.003694131	0.0002	0.953125
Occipital Left	Insula Left	beta	gamma	leader	follower	0.002997861	0.000999288	0.003772402	0.0002	0.953125
Occipital Left	Insula Right	beta	beta	follower	leader	0.002981653	0.000954629	0.003562519	0.0002	0.953125
Occipital Left	Insula Right	gamma	gamma	leader	follower	0.003005361	0.001122752	0.003797451	0.0002	0.953125
Occipital Right	Motor Left	beta	beta	leader	follower	0.002985073	0.001027626	0.003516614	0.0002	0.953125
Occipital Right	Occipital Left	beta	beta	follower	leader	0.003023075	0.001050218	0.003702876	0.0002	0.953125
Occipital Right	Parietal Right	beta	beta	leader	follower	0.003000253	0.001089686	0.003691025	0.0002	0.953125
Occipital Right	Prefrontal Right	beta	gamma	follower	leader	0.003002899	0.001223112	0.003606374	0.0002	0.953125
Occipital Right	Temporal Left	gamma	beta	leader	follower	0.002974388	0.001148914	0.003725321	0.0002	0.953125
Occipital Right	Temporal Right	gamma	gamma	follower	leader	0.002978132	0.001105087	0.00365284	0.0002	0.953125
Parietal Left	Insula Left	beta	gamma	leader	follower	0.002971563	0.000931402	0.003815394	0.0002	0.953125
Parietal Left	Insula Right	beta	beta	follower	leader	0.002998322	0.001084889	0.003749758	0.0002	0.953125
Parietal Left	Occipital Left	beta	beta	follower	leader	0.002982567	0.00115068	0.003728851	0.0002	0.953125
Parietal Left	Prefrontal Left	beta	gamma	leader	follower	0.002983246	0.001235827	0.003527103	0.0002	0.953125
Parietal Right	Motor Left	beta	beta	follower	leader	0.002987238	0.001075413	0.003618097	0.0002	0.953125
Parietal Right	Occipital Right	beta	beta	leader	follower	0.002976138	0.001024913	0.003584249	0.0002	0.953125
Parietal Right	Occipital Right	gamma	gamma	follower	leader	0.00297624	0.001171395	0.003672592	0.0002	0.953125
Parietal Right	Parietal Right	beta	gamma	follower	leader	0.002981823	0.001096937	0.003876748	0.0002	0.953125
Parietal Right	Temporal Left	beta	beta	follower	leader	0.002996637	0.001145114	0.003418663	0.0002	0.953125
Parietal Right	Temporal Left	beta	gamma	leader	follower	0.002972348	0.001189259	0.003890871	0.0002	0.953125
Parietal Right	Temporal Right	beta	beta	follower	leader	0.00298225	0.000978129	0.003689299	0.0002	0.953125
Prefrontal Left	Insula Right	beta	beta	follower	leader	0.003005655	0.00107364	0.003725372	0.0002	0.953125
Prefrontal Left	Parietal Right	beta	gamma	leader	follower	0.002974844	0.001097633	0.003548547	0.0002	0.953125
Prefrontal Left	Prefrontal Right	beta	gamma	follower	leader	0.002990569	0.001258409	0.003719448	0.0002	0.953125
Prefrontal Left	Temporal Left	gamma	gamma	follower	leader	0.002988293	0.001107563	0.003639251	0.0002	0.953125
Prefrontal Right	Insula Right	beta	gamma	follower	leader	0.002991835	0.001067296	0.003504421	0.0002	0.953125
Prefrontal Right	Parietal Right	beta	gamma	leader	follower	0.003017599	0.001157522	0.00355408	0.0002	0.953125
Prefrontal Right	Temporal Right	beta	gamma	leader	follower	0.002973816	0.001030615	0.003780362	0.0002	0.953125
Temporal Left	Motor Right	beta	beta	leader	follower	0.003009715	0.001141358	0.003757684	0.0002	0.953125
Temporal Left	Occipital Left	beta	gamma	leader	follower	0.003010744	0.00125037	0.003749379	0.0002	0.953125
Temporal Left	Parietal Left	gamma	gamma	leader	follower	0.003006685	0.001093488	0.003883738	0.0002	0.953125
Temporal Left	Temporal Left	beta	beta	follower	leader	0.002977035	0.001222485	0.003693375	0.0002	0.953125
Temporal Right	Insula Left	beta	gamma	follower	leader	0.003006287	0.000975038	0.003737431	0.0002	0.953125
Temporal Right	Motor Right	beta	beta	leader	follower	0.002971778	0.001008415	0.003578285	0.0002	0.953125
Temporal Right	Occipital Left	gamma	beta	follower	leader	0.003022461	0.001167828	0.00390102	0.0002	0.953125
Temporal Right	Parietal Left	beta	gamma	leader	follower	0.003003434	0.001091453	0.003935257	0.0002	0.953125
Temporal Right	Prefrontal Right	beta	gamma	follower	leader	0.002993582	0.001281078	0.003593987	0.0002	0.953125

Table A7.3: Top Between Connections: Comparison between baseline, playing, and scrambled conditions

Neuro Source	Neuro Target	Frequency Source	Frequency Target	Info Source	Infor Target	STE	Baseline STE	Scrambled STE	Baseline P Value (FDR)	Scrambled P Value (FDR)
Insula Left	Insula Left	gamma	beta	leader	follower	0.00308078	0.001117731	0.003719518	0.0002	0.953125
Insula Left	Insula Left	gamma	gamma	follower	leader	0.003032599	0.001077881	0.004042105	0.0002	0.953125
Insula Left	Insula Left	gamma	gamma	leader	follower	0.003019333	0.001077881	0.003826624	0.0002	0.953125
Insula Left	Insula Right	gamma	gamma	leader	follower	0.003038927	0.001143675	0.003620703	0.0002	0.953125
Insula Left	Prefrontal Right	beta	beta	leader	follower	0.003046188	0.001035406	0.003676983	0.0002	0.953125
Insula Right	Insula Left	gamma	beta	leader	follower	0.00304149	0.001125623	0.003669134	0.0002	0.953125
Insula Right	Motor Left	beta	beta	leader	follower	0.003109616	0.001076546	0.003883486	0.0002	0.953125
Insula Right	Occipital Right	beta	beta	leader	follower	0.003042566	0.001081511	0.00380457	0.0002	0.953125
Insula Right	Parietal Left	gamma	gamma	leader	follower	0.003089728	0.00101102	0.003695029	0.0002	0.953125
Insula Right	Prefrontal Right	beta	gamma	follower	leader	0.003092756	0.001134048	0.003781879	0.0002	0.953125
Insula Right	Temporal Left	gamma	beta	leader	follower	0.003030979	0.001247712	0.003701372	0.0002	0.953125
Insula Right	Temporal Right	gamma	beta	follower	leader	0.00303013	0.001142153	0.003778542	0.0002	0.953125
Motor Left	Motor Right	beta	gamma	leader	follower	0.003030024	0.001085536	0.00372159	0.0002	0.953125
Motor Left	Occipital Left	beta	gamma	leader	follower	0.003032775	0.00115854	0.003690713	0.0002	0.953125
Motor Left	Parietal Left	beta	beta	follower	leader	0.003046352	0.001124473	0.003804971	0.0002	0.953125
Motor Left	Temporal Left	beta	beta	leader	follower	0.003074446	0.001066287	0.003811086	0.0002	0.953125
Motor Right	Insula Right	gamma	gamma	leader	follower	0.003045382	0.001131913	0.003708664	0.0002	0.953125
Motor Right	Parietal Right	gamma	beta	follower	leader	0.003026069	0.00105018	0.003666913	0.0002	0.953125
Occipital Left	Insula Left	beta	gamma	leader	follower	0.003028665	0.00121261	0.003568265	0.0002	0.953125
Occipital Left	Occipital Right	beta	beta	leader	follower	0.0030343	0.001124001	0.003732246	0.0002	0.953125
Occipital Left	Parietal Right	gamma	beta	follower	leader	0.003022475	0.001113949	0.003486181	0.0002	0.953125
Occipital Left	Prefrontal Left	beta	beta	follower	leader	0.003070503	0.001391377	0.003596826	0.0002	0.953125
Occipital Left	Temporal Left	beta	gamma	leader	follower	0.003027178	0.001120043	0.003904257	0.0002	0.953125
Occipital Right	Insula Left	beta	gamma	leader	follower	0.003092216	0.001043577	0.003766231	0.0002	0.953125
Occipital Right	Insula Right	gamma	gamma	leader	follower	0.003032878	0.00107705	0.003962663	0.0002	0.953125
Occipital Right	Motor Right	beta	gamma	leader	follower	0.003052219	0.001203555	0.00375187	0.0002	0.953125
Occipital Right	Motor Right	gamma	gamma	leader	follower	0.003114923	0.001106273	0.00363238	0.0002	0.953125
Parietal Left	Insula Left	beta	gamma	leader	follower	0.003036032	0.001072044	0.003906933	0.0002	0.953125
Parietal Left	Occipital Right	beta	gamma	follower	leader	0.003060483	0.001036245	0.003767569	0.0002	0.953125
Parietal Left	Parietal Left	gamma	gamma	leader	follower	0.00304063	0.001110726	0.00375724	0.0002	0.953125
Parietal Right	Insula Right	gamma	gamma	follower	leader	0.003039331	0.00119321	0.003562287	0.0002	0.953125
Parietal Right	Occipital Right	beta	gamma	leader	follower	0.003101998	0.001056787	0.003611238	0.0002	0.953125
Parietal Right	Parietal Left	gamma	gamma	leader	follower	0.003032929	0.001216377	0.003935561	0.0002	0.953125
Parietal Right	Parietal Right	gamma	beta	follower	leader	0.003072936	0.001019325	0.003663953	0.0002	0.953125
Prefrontal Left	Occipital Left	gamma	beta	follower	leader	0.003049473	0.001184939	0.00367605	0.0002	0.953125
Prefrontal Left	Prefrontal Right	gamma	gamma	follower	leader	0.003063154	0.001100629	0.003758926	0.0002	0.953125
Prefrontal Right	Insula Right	beta	beta	follower	leader	0.003035235	0.001012138	0.003751357	0.0002	0.953125
Prefrontal Right	Insula Right	beta	gamma	follower	leader	0.003104124	0.001132703	0.003661267	0.0002	0.953125
Prefrontal Right	Parietal Left	beta	beta	follower	leader	0.003056288	0.001009226	0.00364136	0.0002	0.953125
Prefrontal Right	Parietal Right	beta	beta	leader	follower	0.003022376	0.001052177	0.003521849	0.0002	0.953125
Prefrontal Right	Prefrontal Right	gamma	gamma	follower	leader	0.003062216	0.001182596	0.003942406	0.0002	0.953125
Prefrontal Right	Prefrontal Right	beta	gamma	follower	leader	0.003095918	0.001129153	0.003860626	0.0002	0.953125
Prefrontal Right	Temporal Left	beta	beta	leader	follower	0.003038089	0.001236614	0.003685499	0.0002	0.953125
Temporal Left	Occipital Left	beta	beta	follower	leader	0.00305009	0.001213975	0.003690327	0.0002	0.953125
Temporal Left	Temporal Right	beta	gamma	follower	leader	0.003037601	0.001160023	0.003714544	0.0002	0.953125
Temporal Right	Occipital Left	beta	beta	follower	leader	0.003049889	0.001131032	0.003768896	0.0002	0.953125
Temporal Right	Occipital Left	gamma	beta	follower	leader	0.003067738	0.001009131	0.003604576	0.0002	0.953125
Temporal Right	Parietal Left	gamma	gamma	leader	follower	0.003065476	0.001037207	0.003848992	0.0002	0.953125

Appendix H

Graph Theory Statistics: Detailed Statistical Description

Here you will find a detailed description of the statistical values used for the statistical comparison of homophonic vs polyphonic duos and the correlations between these values and the PMPQ scales. See Section 2.7.7 for more information.

TABLE A8.1: Comparison of Homophonic and Polyphonic pieces using graph theory (20ms)

Graph Statistic	P Value (FDR)	Homophonic	Polyphonic	T Test
Average Clustering Coefficient	0	0.001869524	0.002254327	2.989822895
Average Node Strength	0	0.479907906	0.57542127	3.006609666
Characteristic Path Length	0	563.943702	453.8268615	-2.112409787
Efficiency	0	0.002098883	0.002537704	2.993939107

TABLE A8.2: Comparison of Homophonic and Polyphonic pieces using graph theory (200ms)

Graph Statistic	P Value (FDR)	Homophonic	Polyphonic	T Test
Average Clustering Coefficient	0	0.001836987	0.002225507	3.011748115
Average Node Strength	0	0.459004868	0.556318783	3.03092332
Characteristic Path Length	0	580.1421138	463.8955691	-2.137330821
Efficiency	0	0.002015942	0.00246426	3.053698503

Table A8.3: Comparison of Homophonic and Polyphonic pieces using graph theory (1000ms)

Graph Statistic	P Value (FDR)	Homophonic	Polyphonic	T Test
Average Clustering Coefficient	0	0.001816607	0.002214234	3.008713225
Average Node Strength	0	0.45050908	0.550549187	3.019747503
Characteristic Path Length	0	582.7493852	463.3260307	-2.133029853
Efficiency	0	0.002011337	0.002475265	3.03413717

Table A8.4: Correlations between graph theory statistics and the PMPQ at 20ms delay

Correlation	Duo Type	Graph Statitistics	PMPQ Scale	P Value (FDR)
-0.357642722	p	Average Clustering Coefficient	quality	0.048904494
0.15719801	h	Average Clustering Coefficient	quality	0.290942418
-0.353881525	p	Average Node Strength	quality	0.048904494
0.161197297	h	Average Node Strength	quality	0.290942418
0.3735079	p	Characteristic Path Length	quality	0.048904494
-0.060000689	h	Characteristic Path Length	quality	0.64882348
-0.344212269	p	Efficiency	quality	0.048904494
0.166649151	h	Efficiency	quality	0.28680161
-0.28533732	p	Average Clustering Coefficient	synchrony	0.076620346
0.17881686	h	Average Clustering Coefficient	synchrony	0.274590944
-0.282090186	p	Average Node Strength	synchrony	0.076620346
0.182889035	h	Average Node Strength	synchrony	0.274590944
0.291669839	p	Characteristic Path Length	synchrony	0.076620346
-0.105653318	h	Characteristic Path Length	synchrony	0.44006592
-0.273525055	p	Efficiency	synchrony	0.082363647
0.189412663	h	Efficiency	synchrony	0.271761336
-0.135663922	p	Average Clustering Coefficient	synergy	0.370862932
0.308373917	h	Average Clustering Coefficient	synergy	0.05665157
-0.131670596	p	Average Node Strength	synergy	0.370862932
0.313631975	h	Average Node Strength	synergy	0.05665157
0.170189328	p	Characteristic Path Length	synergy	0.28680161
-0.197012278	h	Characteristic Path Length	synergy	0.262710603
-0.121154011	p	Efficiency	synergy	0.398146986
0.320780232	h	Efficiency	synergy	0.05665157

Table A8.5: Correlations between graph theory statistics and the PMPQ at 200ms delay

Correlation	Duo Type	Graph Statitistics	PMPQ Scale	P Value (FDR)
-0.361613898	p	Average Clustering Coefficient	quality	0.03442548
0.15479648	h	Average Clustering Coefficient	quality	0.30015006
-0.36025942	p	Average Node Strength	quality	0.03442548
0.156810114	h	Average Node Strength	quality	0.30015006
0.388330455	p	Characteristic Path Length	quality	0.03442548
-0.053464769	h	Characteristic Path Length	quality	0.684952065
-0.358389953	p	Efficiency	quality	0.03442548
0.161359511	h	Efficiency	quality	0.30015006
-0.288244115	p	Average Clustering Coefficient	synchrony	0.063926473
0.176825386	h	Average Clustering Coefficient	synchrony	0.264779726
-0.287236838	p	Average Node Strength	synchrony	0.063926473
0.178912956	h	Average Node Strength	synchrony	0.264779726
0.304922197	p	Characteristic Path Length	synchrony	0.0598332
-0.098719149	h	Characteristic Path Length	synchrony	0.472694156
-0.286384169	p	Efficiency	synchrony	0.063926473
0.182942531	h	Efficiency	synchrony	0.264779726
-0.140271005	p	Average Clustering Coefficient	synergy	0.329015646
0.304574904	h	Average Clustering Coefficient	synergy	0.0598332
-0.138843655	p	Average Node Strength	synergy	0.329015646
0.30706804	h	Average Node Strength	synergy	0.0598332
0.189170779	p	Characteristic Path Length	synergy	0.264779726
-0.188348028	h	Characteristic Path Length	synergy	0.264779726
-0.137995002	p	Efficiency	synergy	0.329015646
0.31180484	h	Efficiency	synergy	0.0598332

Table A8.6: Correlations between graph theory statistics and the PMPQ at 1000ms delay

Correlation	Duo Type	Graph Statitistics	PMPQ Scale	P Value (FDR)
-0.361907219	p	Average Clustering Coefficient	quality	0.034101385
0.153593169	h	Average Clustering Coefficient	quality	0.304838228
-0.36095025	p	Average Node Strength	quality	0.034101385
0.155297064	h	Average Node Strength	quality	0.304838228
0.388605136	p	Characteristic Path Length	quality	0.034101385
-0.048236922	h	Characteristic Path Length	quality	0.714368928
-0.358763413	p	Efficiency	quality	0.034101385
0.157715243	h	Efficiency	quality	0.304838228
-0.290351059	p	Average Clustering Coefficient	synchrony	0.062065855
0.173941638	h	Average Clustering Coefficient	synchrony	0.275692168
-0.289678336	p	Average Node Strength	synchrony	0.062065855
0.175461347	h	Average Node Strength	synchrony	0.275692168
0.306031106	p	Characteristic Path Length	synchrony	0.058428999
-0.093007407	h	Characteristic Path Length	synchrony	0.500539403
-0.287848196	p	Efficiency	synchrony	0.062065855
0.177989123	h	Efficiency	synchrony	0.275692168
-0.142230447	p	Average Clustering Coefficient	synergy	0.323440866
0.303938703	h	Average Clustering Coefficient	synergy	0.058428999
-0.141440395	p	Average Node Strength	synergy	0.323440866
0.305959749	h	Average Node Strength	synergy	0.058428999
0.192602624	p	Characteristic Path Length	synergy	0.275692168
-0.183953115	h	Characteristic Path Length	synergy	0.275692168
-0.139447759	p	Efficiency	synergy	0.323440866
0.309297415	h	Efficiency	synergy	0.058428999

Appendix I

Small World Coefficients: Detailed Statistical Description

Here you will find a detailed description of the statistical values, both correlation coefficients and pvalues, for the small world coefficient analysis. See Section 2.7.8 and 2.7.9 for more information.

TABLE A9.1: Pearson Correlation Coefficient and significance of Small world as a function of time and music affiliation

Correlation	Delay	P Value (FDR)	Scale
0.113129977	20ms	0.445123704	Small world as a funtion of time
0.116885965	200ms	0.445123704	Small world as a funtion of time
0.118306012	1000ms	0.445123704	Small world as a funtion of time
-0.259322736	20ms	0.6197354	Small world correlated with music affiliation change
-0.259330569	200ms	0.6197354	Small world correlated with music affiliation change
-0.26007884	1000ms	0.6197354	Small world correlated with music affiliation change